UNCLASSIFIED

AD NUMBER

AD815390

NEW LIMITATION CHANGE

TO

Approved for public release, distribution unlimited

FROM

Distribution authorized to U.S. Gov't. agencies and their contractors; Critical Technology; MAR 1967. Other requests shall be referred to Air Force Materials Laboratory, Metals and Ceramics Division [MAM], Wright-Patterson AFB, OH 45433.

AUTHORITY

usafml ltr, 29 mar 1972

THIS PAGE IS UNCLASSIFIED

AFML-TR-66-228

AD815390

AN EXPERIMENTAL STUDY OF THE WEIBULL VOLUME THEORY

C. D. PEARS
H. STUART STARRETT

SOUTHERN RESEARCH INSTITUTE

TECHNICAL REPORT No. AFML-TR-66-228

MARCH 1967

This document is subject to special export controls and each transmittal to foreign governments or foreign naticnals may be made only with prior approval of the Metals and Ceramics Division (MAM), Air Force Materials Laboratory, Wright-Patterson AFB, Ohio 45433.

AIR FORCE MATERIALS LABORATORY
RESEARCH AND TECHNOLOGY DIVISION
AIR FORCE SYSTEMS COMMAND
WRIGHT-PATTERSON AIR FORCE BASE, OHIO

DISCLAIMER NOTICE

THIS DOCUMENT IS BEST QUALITY PRACTICABLE. THE COPY FURNISHED TO DTIC CONTAINED A SIGNIFICANT NUMBER OF PAGES WHICH DO NOT REPRODUCE LEGIBLY.

NOTICES

When Government drawings, specifications, or other data are used for any purpose other than in connection with a definitely related Government procurement operation, the United States Government thereby incurs no responsibility nor any obligation whatsoever; and the fact that the Government may have formulated, furnished, or in any way supplied the said drawings, specifications, or other data, is not to be regarded by implication or otherwise as in any manner licensing the holder or any other person or corporation, or conveying any rights or permission to manufacture, use, or sell any patented invention that may in any way be related thereto.

Copies of this report should not be returned to the Research and Technology Division unless return is required by security considerations, contractual obligations, or notice on a specific document.

500 - April 1967 - CO192 - 30-733

AN EXPERIMENTAL STUDY OF THE WEIBULL VOLUME THEORY

C. D. PEARS

H. STUART STARRETT

This document is subject to special export controls and each transmittal to foreign governments or foreign nationals may be made only with prior approval of the Metals and Ceramics Division (MAM), Air Force Materials Laboratory, Wright-Patterson AFB, Ohio 45433.

FOREWORD

This work was performed by Southern Research Institute under USAF Contract No. AF 33(615)-1690. This contract was initiated under Project No. 7350, "Refractory Inorganic Nonmetallic Materials," Task No. 735003, "Theory and Mechanical Phenomena." The work was administered under the direction of the Air Force Materials Laboratory, Research and Technology Division, Air Force Systems Command, Wright-Patterson Air Force Base, Ohio, with Mr. G. R. Atkins acting as project engineer.

This report covers work conducted from 28 May 1964 to 31 December 1965.

This program was under the direction of H. Stuart Starrett, Project Leader, and the general management of C. D. Pears, Head, Mechanical Engineering Division.

L. L. Fehrenbacher, Captain, USAF and R. E. Pence of the Air Force Materials Laboratory, Research and Technology Division, Air Force Systems Command, Wright-Patterson Air Force Base, Ohio, conducted and reported the fractography study.

The manuscript of this report was released by the authors June 1966 for publication as an RTD Technical Report.

This technical report has been reviewed and is approved.

W. J. TRAPP
Chief, Strength and Dynamics Branch
Metals and Ceramics Division
Air Force Materials Laboratory

ABSTRACT

Using a gas-bearing tensile test facility, an experimental program was conducted to provide clarification of Weibull's volume effect theory. The facility provides uniaxial loading with a uniform tensile field thus permitting a study of the Weibull theory in its simplest form. The primary material used for this investigation was hot pressed alumina made by AVCO. Graphite was used to explore effects as a guide to the general program. As a result, quite useful data are available on the graphite as well as alumina.

The program verified the general conclusions of the theory of decreasing strength and standard deviation with increasing volume, but a single set of material constants to describe the total results was not obtained. Criteria are presented that will assist in both material understanding and design with brittle materials with more confidence.

Evidence indicates that sample sizes should include at least 60 coupons for an optimum analysis of material constants and as few as 10 coupons for some values such as average strength.

Strength correlated with density and there was evidence that the fracture location, whether transgranular or in the grain boundaries, is dependent on grain size and/or the structure.

Unfortunately, the strengths between different discs of the material from which the specimens were machined varied more than desired and even more than some of the variables being measured.

This abstract is subject to special export controls and each transmittal to foreign governments or foreign nationals may be made only with prior approval of the Metals and Ceramics Division (MAM), Air Force Materials Laboratory, Wright-Patterson AFB, Ohio 45433.

PAGES NOT FILMED ARE BLANK

TABLE OF CONTENTS

	PAGE
1. Introduction	1
2. Gas-Bearing Facility	2
Load Frame	2
Gas-Bearings	2
Load Train	3
Mechanical Drive System	4
Instrumentation	5
Operating Procedure	5
3. Specimen Material and Preparation	6
ATJ Graphite	6
Alumina	7
4. Application of Weibull's Volume Effect Theory to the Ultimate Strength Data	10
Synopsis of Weibull's Theory	10
Methods of Determining Weibull's Constants	13
5. Data and Results	15
Graphite	15
Alumina	16
Influence of Large Flaws	16
Fractures Out of Gage Section	17
General Test Conditions	17
Grain Size Effect	17
Density Effect	18
Average Properties	18
Volume Effect and Fracture Probability	18
Minimum Samples for Various Properties	24

TABLE OF CONTENTS (continued)

	PAGE
6. Fractography Study of the Alumina Tensile Specimens	26
Experimental Procedures	26
Fracture Surface Replicas	26
Polished Surface Replicas	26
Results and Discussion of Results	27
Fracture Mechanisms	29
Conclusions	30
7. Conclusions	30
8. References	32

ILLUSTRATIONS

FIGURE		PAGE
1.	Gas-Bearing Tensile Facility	34
2.	Schematic Arrangement of Gas-Bearing Universals, Specimen, and Load Train	35
3.	Schematic of Collet-Type Specimen Grip	36
4.	Schematic of Precision Sleeve-Type Grips	37
5.	Cutting Plan for Block 1 of the ATJ Graphite	38
6.	Cutting Plan for Block 2 of the ATJ Graphite	39
7.	Typical Graphite Specimen Locations within the Slabs	40
8.	Dimensions of the Graphite Specimens Types I through IX and Type XI for the Phase I Study	41
9.	Configuration of the Type X Graphite Specimens for the Phase I Study	42
10.	Ultimate Strength versus Tile Number Indicating Variation of Strength Between Tiles	43
11.	Configuration of Alumina Sample Blanks Supplied by Avco	44
12.	Cutting Plans for Alumina Tiles 700, 746, 758, 764, 766, and 768	45
13.	Cutting Plans for Alumina Tiles 770, 774, 788, 790, 792, and 794	46
14.	Cutting Plans for Alumina Tiles 796, 798, 800, 806 808, and 810	47
15.	Cutting Plans for Alumina Tiles 826, 830, 832, 858, and 866	48

ILLUSTRATIONS (continued)

FIGURE		PAGE
16.	Configuration of the Type I Alumina Specimen	49
17.	Configuration of the Type II Alumina Specimen	50
18.	Configuration of the Type III Alumina Specimen	51
19.	Configuration of the Type IV Alumina Specimen	52
20.	Configuration of the Type V Alumina Specimen	53
21.	Ultimate Tensile Strength versus Gage Volume and Gage Surface Area for With Grain ATJ Graphite	54
22.	Ultimate Tensile Strength versus Gage Surface Area to Volume Ratio for With Grain ATJ Graphite	55
23.	Ultimate Tensile Strength versus Gage Length for With Grain ATJ Graphite	56
24.	Ultimate Tensile Strength versus Gage Diameter for With Grain ATJ Graphite	56
25.	Difference between Average Ultimate Tensile Strength for Specimens without Flaws and Specimens with Flaws versus Cross-Sectional Area for Alumina Specimens	57
26.	Difference between Average Ultimate Tensile Strength for Specimens without Flaws and Specimens with Flaws versus Volume for Alumina Specimens	58
27.	Ultimate Tensile Strength versus Percent Theoretical Density for All Alumina Data	59
28.	Average Ultimate Tensile Strength versus Volume, also Showing Standard Deviations for the Culled Alumina Data	60
29.	Frequency Plot for Alumina Type II Specimens	61

ILLUSTRATIONS (continued)

FIGURE		PAGE
30.	Frequency Plot for Alumina Type IV Specimens	62
31.	Log Log $\left[\frac{N+1}{N+1-n}\right]$ versus Log $(\sigma - \sigma_u)$ with σ_u = 9350 for Type II Alumina Specimens	63
32.	Log Log $\left[\frac{N+1}{N+1-n}\right]$ versus Log $(\sigma - \sigma_u)$ with σ_u = 0 for Type II Alumina Specimens	64
33.	Log Log $\left[\frac{N+1}{N+1-n}\right]$ versus Log $(\sigma - \sigma_u)$ with σ_u = 20,000 psi for Type II Alumina Specimens	65
34.	Log Log $\left[\frac{N+1}{N+1-n}\right]$ versus Log $(\sigma - \sigma_u)$ with σ_u = 15,000 psi for Type II Alumina Specimens	66
35.	Log Log $\left[\frac{N+1}{N+1-n}\right]$ versus Log $(\sigma - \sigma_u)$ with σ_u = 21,500 psi for Type IV Alumina Specimens	67
36.	Log Log $\left[\frac{N+1}{N+1-n}\right]$ versus Log $(\sigma - \sigma_u)$ with σ_u = 0 for Type IV Alumina Specimens	68
37.	Log Log $\left[\frac{N+1}{N+1-n}\right]$ versus Log $(\sigma - \sigma_u)$ with σ_u = 9350 psi for Type IV Alumina Specimens	69
38.	Log Log $\left[\frac{N+1}{N+1-n}\right]$ versus Log $(\sigma - \sigma_u)$ with σ_u = 15,000 psi for Type IV Alumina Specimens	70
39.	σ_u versus m for Type II and Type IV Alumina Specimens	71
40.	σ_o versus m for Type II and Type IV Alumina Specimens	72
41.	Tensile Stress versus the Probability of Fracture	73
42.	Probability of Fracture versus $\frac{\sigma - \sigma_m}{a}$ for Various Values of m	74
43.	Standard Deviation versus Subset Size N	75
44.	m versus Subset Size N	76

ILLUSTRATIONS (continued)

FIGURE PAGE

45. σ_u versus Subset Size N 77

46. Schematic of Tensile Specimen Showing Areas Examined 78

47. Photomicrograph of Specimen 858-A Showing Inhomogeneous Microstructure (70X) 79

48. Electron Micrograph of a Replicated Polished Surface of Specimen 858-AA Showing the Three Microstructural Variations 79

49. Electron Micrograph of a Replicated Fracture Surface of Specimen 858-AA Showing the Three Microstructural Variations 80

50. Electron Micrograph of a Replicated Polished Surface of Specimen 858-AA Showing the Small, Rounded, "Dimpled", Grains 80

51. Electron Micrograph of a Replicated Fracture Surface of Specimen 858-A Showing the Microstructure Transition from Small, Rounded Grains to Large, Equiaxed Grains 81

52. Electron Micrograph of a Replicated Fracture Surface of Specimen 858-AA Showing the Microstructure Transition from Small, Rounded Grains to Large Equiaxed Grains 81

53. Electron Micrograph of a Replicated Fracture Surface of Specimen 858-L Showing the Microstructural Transition from Small, Rounded Grains to Equiaxed Grains 82

54. Electron Micrograph of a Replicated Fracture Surface of Specimen 858-L Showing the Large, Elongated Grains as Flat, Featureless Areas 82

55. Electron Micrograph of a Replicated Polished Surface of Specimen 826-44A Showing the Equiaxed Grain Structure 83

56. Electron Micrograph of a Replicated Fracture Surface of Specimen 826-44A Showing Equiaxed Grain Structure and Intergranular Fracture 83

ILLUSTRATIONS (continued)

FIGURE PAGE

57. Electron Micrograph of a Replicated Fracture Surface of Specimen 826-44A Showing Intergranular Fracture Surfaces 84

58. Electron Micrograph of a Replicated Polished Surface of Specimen 806-QA Showing Uniform Grain Structure 84

59. Electron Micrograph of a Replicated Fracture Surface of Specimen 806-QA Showing Uniform Grain Structure and Intergranular Fracture Characteristics 85

60. Electron Micrograph of a Replicated Fracture Surface of Specimen 806-QA Showing Transgranular and Cleavage Fracture Areas. . . . 85

61. Electron Micrograph of a Replicated Fracture Surface of Specimen 806-QA Showing Transgranular and Cleavage Fracture Areas. . . . 86

62. Electron Micrograph of a Replicated Fracture Surface of Specimen 830-13 Showing a Representative White Area 86

63. Electron Micrograph of a Replicated Fracture Surface of Specimen 830-13 Showing a Representative Gray Area 87

TABLES

TABLE		PAGE
1.	Ultimate Tensile Strength Values for the Phase I ATJ Graphite Specimens	88
2.	A Comparison of Parameters for the Phase I ATJ Graphite Specimens	91
3.	Average Percent Theoretical Density and Average Grain Size for the Alumina Tiles	92
4.	Ultimate Tensile Strength Values for the Phase II Alumina Specimens	93
5.	Ultimate Tensile Strength and Approximate Flaw Size for Alumina Specimens Containing Visible Flaws	98
6.	Average Grain Size and Average Ultimate Strength for Type II Alumina Specimens	99
7.	Fracture Strength Frequency Distribution for Type IV Alumina Specimens Using Culled Data Only	100
8.	Average Fracture Stress, Standard Deviation, Coefficient of Variation, and Weibull Material Constants for Subsets of Size N	101
9.	Physical Properties of Alumina Tensile Specimens Selected for Fractography	102

INTRODUCTION

This is the final summary report under Contract No. AF 33(615)-1690 for research to provide an experimental clarification of Weibull's volume effect on brittle materials under uniform tensile stress. The major material under study was a hot pressed alumina prepared by AVCO. ATJ graphite was used to study preliminary effects.

The program was divided into two phases. Phase I was a limited parameter study using ATJ graphite to establish the effects of some general parameters on strength. The parameters considered were surface area, surface area to volume ratio, volume, gage length, and gage diameter. The results of this study showed that the only parameter which affected the strength significantly was volume. Although volume did affect the strength of the graphite, the effect was not properly described by a Weibull analysis. This possibly could be accounted for by the fact that graphite is only a semi-brittle material.

Phase II of this program was a study of the effects of volume on specimen strength using a more brittle material, alumina. A study of the Weibull material constants was included in this phase. To accomplish this, five different groups of test specimens were used, each group containing geometrically identical specimens of a given volume. Two groups contained 120 specimens each, two groups contained 20 specimens each, and the other group contained 15 specimens. Due to nonuniformity of the material, radius breaks, visible flaws and improper control of surface finish, approximately 40% of the original specimens could not be used in the final analyses. For example, 59 specimens were rejected because they came from nonrepresentative tiles and 17 were rejected because large inclusions were observed in the fracture. Only 12, or 4.1%, of the specimens broke out of the gage section for no apparent reason.

Results of Phase II showed that volume did affect the strength of alumina in a manner similar to that predicted by Weibull. Also the standard deviations, except for one group of specimens, decreased for increasing volume as predicted by Weibull. Unfortunately the calculation of a single set of Weibull material constants was not successful. Material constants were calculated for both of the large groups of specimens, but the two sets of constants were significantly different, and neither set could be used to give a strength versus volume relation that closely approximated the data over the entire range of volumes. Thus these results cast some doubt on the usefulness of Weibull constants as rigid material parameters.

A limited study also was made on the number of specimens needed to determine accurately certain characteristics, such as average fracture strength, standard deviation, coefficient of variation, and the Weibull constants, for a brittle material. The alumina data were used for this study. The indications were that as few as 10 test specimens could be used to predict the average breaking strength reasonably accurately, but that this number was not sufficient to determine the standard deviation, the coefficient of variation, or the Weibull constants. For these about 40, 40, and 60 coupons respectively were required for reasonably good definition; for more precise numbers more specimens would be necessary. Prior work of this type performed here for the Air Force was reported in ASD-TDR 63-245.

GAS-BEARING FACILITY

The gas-bearing facility is shown in Figure 1. The facility consisted primarily of the load frame, gas-bearings, load train, mechanical drive system, and instruments for the measurement of load-time to failure.

Load Frame

The load frame was similar to most standard tensile frames with some modifications to accommodate the gas-bearings. Four steel columns supported the top and bottom base plates. These base plates contained sleeves and journals to align the upper and lower crossheads. A centrally located journal in each base plate accepted a partially threaded column of a precision mechanical screw jack which was secured to the base plate and imparted motion to the crossheads. The crossheads supported the gas-bearings and the load train.

Gas-Bearings

A spherical and a flat gas-bearing were used for pulling the smaller specimens. For the larger specimens, trouble was encountered when the bottom flat bearing bottomed at high loads. In order to correct this, the flat bearing was replaced with a spherical bearing. This proved to be a satisfactory arrangement for pulling the larger specimens, although bottoming still occurred on some of the higher strength specimens. In order to determine what effect, if any, this bottoming had on the test specimen, a continuous check of the alignment was made during the runs using dial gages. At no time was more than 0.0005 inches motion detected and generally there was no motion during the runs.

Each spherical bearing had a diameter of about 9 inches. This size bearing is sufficient to provide a load capacity of 15,000 lbs when an effective pressure of approximately 1200 psig is maintained within the annulus supplying the bearing nozzles. The construction of the flat bearing is similar to that of the spherical bearing; however, an effective pressure of over 1200 psig has to be maintained to support the same load. Pressure gradients within the contact area for the flat bearing cause an effective pressure within the gas film substantially less than the supply pressure, requiring that the supply pressure be maintained higher. Gas is supplied by means of a manifold of eight commerical nitrogen cylinders controlled by a high capacity regulator.

This gas was metered by a conventional orifice run that incorporated flange taps and a differential pressure gage. In order to control flow, a hand-operated valve to each bearing was provided downstream of the meter run. Bleed valves also were provided to release the pressure on the gas lines and to float the bearing with a maximum control sensitivity. Flexible hoses were used as the link from the piping to the gas bearings. These hoses imposed no external force on the specimen since they were not attached to the floating part (ball).

Flow meters, pressure gages, electrical indicators to warn of bearing contact, and other instruments were provided as necessary and were chosen for their ability to provide accurate data while not encumbering the facility.

Load Train

The load train, see Figure 2, consisted of pull rods, load cell, and specimen grips. A standard 1000 pound SR-4 Baldwin, type U-1 load cell, stated by the manufacturer to be accurate within $\pm \frac{1}{4}$% of capacity was used for testing the smaller specimens. This load cell, as received from the manufacturer, caused misalignments within the load train and bending stresses within the specimen. These misalignments were caused by an off-center weight in the load cell and by the failure of the threaded holes in each end to align on a common centerline. The off-center weight was balanced by a counter-weight and the misalignment of the centerlines of the holes was corrected by machining special adapters for the holes.

The load cell for the larger specimens was made by placing strain gages on the steel pull rod from the upper gas bearing. These strain gages were calibrated in a standard Tinius Olsen facility using also a standard Baldwin SR-4 5000 pound load cell as a check up to 5000 pounds.

Two types of grips were used on this program. For the graphite and small alumina specimens, a collet-type grip was used; see Figure 3. As the compression nut was advanced, the three-piece compression ring performed two functions. It moved into the groove in the test specimen providing the gripping force required and uniaxial alignment while also forcing together the ground end faces of the test specimen and extension rod to provide parallel axial alignment. Consideration of this grip design and observation of the performance confirmed that alignment was a function only of the precision to which the parts were machined.

Because of the large forces required to pull the large Type I, II, and III alumina specimens, special grips were designed. These grips, shown in Figure 4, were sleeve-type precision grips. Those ends of the grips which accepted the pull rods from the gas bearings were machined to within 0.0005 in. of the diameters of the individual pull rods, and the connections between the pull rods and the grips were made with $\frac{1}{4}$ in. steel pins. The other ends of the grips accepted sleeves that had been epoxyed onto the shanks of the specimen. These sleeves were machined to concentricity with the specimen within 0.0005 in. The connections between each sleeve and the grip were made with $\frac{5}{8}$ in. steel pins. This grip design provided the load carrying capacity needed and gave good alignment.

Mechanical Drive System

Separate mechanical drive systems were provided for the upper and lower crossheads. The mechanical drive system for the upper crosshead consisted of a simple reversible electric motor coupled to the mechanical screw jack. The electric motor can be seen on the top base plate of the load frame; see Figure 1. Push-button control switches (jog or non-holding) were mounted on the load frame. This system had a rather fast rate of travel and was normally used in positioning the load train for installation of the specimen.

The mechanical drive system for the lower crosshead consisted of a precision mechanical screw jack chain driven by a gear reducer. The gear reducer was driven by an Allispede unit (300-3000 rpm). With a 1025/1 gear reducer and different sprocket ratios, this system was capable of providing crosshead rates of from 0.006 in./min to 0.70 in./min. Different crosshead rates within this range were obtained by varying the speed setting on the Allispede Unit. By substituting another gear reducer, a different range of crosshead rates could be obtained.

The mechanical drive system for the lower crosshead had a relatively short travel and was used normally for applying the load or for making small changes in positioning the load train. The control switches for this system were mounted on the panel board and were the push-button (holding) type.

Both mechanical drive systems had limit switches to prevent over-travel of the crossheads. The upper crosshead also had positive stops to prevent the crosshead from falling should the limit switches fail to operate.

Instrumentation

Instrumentation consisted of the load cell, a constant d. c. voltage power supply, and a Moseley "Autograf" X-Y-time recorder.

The load cell received a constant d. c. voltage input from the power supply and transmitted a millivolt signal directly proportional to the load to the recorder, thus providing a continuous plot of stress-time to failure.

Prior to beginning the initial run of this program, the small load cell was calibrated to dead weights. The load measuring system was calibrated in place periodically thereafter, again by hanging dead weights from the load cell.

Operating Procedure

Because of the wide range of specimen sizes and the two types of grips used, the procedures for placing the large and small specimens in the testing machine were somewhat different.

The small specimens first were placed within the grips. The grips were then attached to the upper and lower extension rods after the upper gas-bearing had been "floated". The size of the larger specimens and the size of the grips for these specimens made this procedure impractical for them. To place these specimens in the machine, the upper gas-bearing was "floated", the grips were attached to the extension rods, and then the specimens were placed within the grips.

Load was applied at a predetermined crosshead rate by electrical engagement of the Allispede motor, and the load-time curves were plotted automatically by the X-Y time recorder through fracture. The fractured specimen was removed and final inspections were made.

SPECIMEN MATERIAL AND PREPARATION

The two materials which were studied under this program were ATJ graphite and high purity alumina. The ATJ graphite was employed for the brief preliminary study while the alumina was used to provide the basic data for the analysis. In order to study Weibull's theory and any other parameters affecting the strengths of these two materials, it was desired to obtain materials that were extremely pure and consistent. Therefore, an extensive study was made of the materials. Identification of specimen location and orientation also was maintained in order to evaluate the data in these terms.

ATJ Graphite

The ATJ graphite specimens for the preliminary phase were machined from two billets 13" in diameter by 14" long prepared by the National Carbon Company. A billet of this size was selected since they felt that it would be the most reproducible and the best quality that could be obtained.

The average density of the billets was 1.73 gm/cc. The density of each specimen was checked to confirm the consistency of the material. This was done by cutting from the billets constant diameter rods from which the specimens would be machined and measuring the density of these rods. The density values for each specimen are shown in Table 1 which also includes the tensile strength data discussed later. As can be seen, the values were very consistent ranging from 1.74 gm/cc to 1.78 gm/cc, illustrating the good quality of the billets employed.

The graphite specimens were machined from the $\frac{1}{4}$ diameter portion of the billets to insure the best consistency from specimen to specimen. The cutting plans for the graphite specimens from the two billets are shown in Figures 5, 6, and 7. A specimen number was devised to identify each specimen as to the bulk billet from which it was taken as well as location within the billet. For example, consider the number 1-A-i-I

1 - bulk billet number (two billets were used)
A - slab designation (Figures 5 and 6)
i - location with respect to a circle of radius equal to one-fourth of the billet diameter; i = inside, o = outside (Figure 7)
I - specimen type (discussed in the following paragraphs)

Under the preliminary phase eleven types of graphite specimens, identified as Type I through Type XI, were evaluated providing a very broad range for the parameters investigated. The parameters were gage volume, gage surface area, gage diameter, gage length, ratio of gage surface area to volume, and surface roughness. Originally only nine types were to be investigated; however, after an initial review of the data, it was decided to broaden the range further; therefore, Types X and XI represented the largest and smallest gage volume respectively.

The specimen configurations for the eleven types are shown in Figures 8 and 9. The values of the parameters for each type are shown in Table 2. Notice the large range of volumes, from 0.0013 in.^{3} to 0.2540 in.^{3}, that was evaluated.

Alumina

The alumina specimens employed for the major evaluation under this program were hot pressed by AVCO Corporation from Linde "A" grade powder. The alumina body (square tiles) was prepared by a hot pressing technique using graphite dies at a temperature of 1525°C and a pressure of 2000 psi. The typical analyses reported by AVCO were as follows:

	Linde A Powder	Hot Pressed Material
Fe	trace .001%	.01
Si	.01	.01
Ti	.002	.002
Mg	.002	.002
Cu	.001	.001
Ni	not detected	.0005
Ca	.0002	.0002
Cr	not detected	not detected
Mn	not detected	.0008
Carbon	.03	.02

The test specimens were prepared from the 12" x 12" x $1\frac{1}{8}$" thick hot pressed tiles. A total of 24 tiles were made and each was checked for grain size and density from strips cut from the center. These values and the identity of the tiles have been included in Table 3. According to AVCO the grain size for most of the tiles averaged from 1 to 2 microns

and the density ranged from 98.0% to 99.5% of theoretical density. AVCO also reported that the density within any tile could vary by approximately 0.5%. Although this point will be discussed in a subsequent section of this report, it is appropriate to mention the discrepancy noted between the grain size as reported by AVCO and those measurements made by this laboratory. A wide spread in tensile strength values motivated a cursory examination of the microstructure near the point of fracture. A fairly uniform grain size averaging 1 to 3 microns was found in specimens of high strength; however, with the lower strength specimens it was found that in the area near the fracture exaggerated grain growth had occurred. Grains as large as 50 microns were found. In addition, islands of unbonded grains were found in the weaker tiles. The results of additional microstructure and fractology studies will be discussed later.

Upon receipt and visual inspection of the specimen material, a wide range of color from white to dark gray was noted; also many of the specimen blanks contained gray striations and spots. This condition spurred an investigation into the reasons for the color variation and any consequential physical variations in the material. AVCO reported that the carbon, or graphite content, that might have caused the color variations, averaged approximately 200 parts per million. This contamination presumedly was introduced by the graphite dies employed in the hot pressing processing. However, AVCO believed that this concentration was not critical as far as the strength was concerned. The striations or two tone colors of gray to white were studied at AVCO. No significant chemical variation was noted and the grain size variation on the tiles was less than $\frac{1}{2}$ microns. AVCO concluded that the two tone colors and the variation in color from specimen to specimen were results of slight density variations of less than 0.5%. It generally was observed by AVCO that the striations and two tone colors occurred after repressing which was necessary to obtain the adequate density in some tiles. It also was observed generally that the whiter tiles and specimens exhibited lower density.

As can be seen from the above discussion, no exact conclusions could be drawn as to the reasons for the color variations since the extensive analysis that would be required was not within the scope of the program. However, the data obtained were scrutinized closely to determine if the variation in appearance did indicate sufficient physical differences to influence the tensile strength. An effort was made to correlate strength and color. However, the fact that the colors varied almost continuously from white to dark gray made the correlation very difficult; indeed one did not exist through all tones of coloring. Generally speaking the pure white specimens had lower strengths while the extremely dark specimens had higher strengths for identical specimens; however, there were directly conflicting cases in which a white specimen was quite strong and a dark specimens was quite weak with no apparent explanation such as a visible flaw.

Further analysis did reveal that the strength varied among the different tiles from which the specimens were machined. This is demonstrated in Figure 10 where strength has been plotted versus tile number with the tile number arranged in a proper sequence to illustrate the increase in strength of different tiles. From the figure it is apparent that there were several tiles which yielded significant extremes in tensile strengths. In order that the data would be more representative of a uniform material, specimens machined from the low strength tiles 746, 788, 858, 866, and 870 and high strength tile 806 were eliminated from consideration.

A total of five configurations (types) of alumina specimens were evaluated under this program. The types were numbered I through V and consisted of gage volumes of 1.33 in.^{3}, 0.62 in.^{3}, 0.25 in.^{3}, 0.031 in.^{3}, and 0.012 in.^{3}, respectively. The specimens were machined at Southern Research Institute from blanks supplied by AVCO. AVCO prepared the blanks, shown in Figure 11, by cutting them from the 12" x 12" x $1\frac{1}{8}$" tiles according to the cutting plans shown in Figures 12, 13, 14, and 15. The blanks supplied by AVCO were all within the tolerances specified with only a few exceptions. The specimens, which were final machined at Southern Research, had the configurations shown in Figures 16 through 20. The final machining was performed with diamond wheels and all tolerances were maintained except for the gage radius which varied with wear of the diamond wheel; however, this had no adverse effects since during the runs few breaks occurred in the gage radius after the other problems were eliminated. A 100 grit diamond wheel was used to "rough out" the specimen configurations and a 400 grit wheel was used to finish the specimen. This provided a consistent surface finish of 5 to 10 rms for all specimens.

A total of 295 specimens was prepared with the following distribution:

Type I - 1.33 in.^{3} - 20 specimens
Type II - 0.62 in.^{3} - 120 specimens
Type III - 0.25 in.^{3} - 20 specimens
Type IV - 0.031 in.^{3} - 120 specimens
Type V - 0.012 in.^{3} - 15 specimens

This distribution provided two volumes (Types II and IV) of large sample size from which the Weibull constants could be determined. The remaining specimens provided the wide range of volume over which a comparison with Weibull theory could be made.

APPLICATION OF WEIBULL'S VOLUME EFFECT THEORY TO THE ULTIMATE STRENGTH DATA

It is impossible to state an exact value for the ultimate strength of a material since some data scatter will result from repetition of the experimental measurement regardless of how close the procedure is duplicated. In some cases, the data scatter is considerable. Weibull (1, 2) recognized this fact and reasoned that it should be possible to use the elementary laws of probability to determine the probability of fracture occurring at a given stress. According to Weibull's theory, a random distribution of flaws exists in each material and the probability that a given stress will cause fracture depends on the volume of the body, the state of stress, and certain constants associated with the material.

Synopsis of Weibull's Theory

The distribution function for the probability of fracture, derived by Weibull, based on the "weakest link" theory of fracture is

$$S = 1 - e^{-B} \tag{1}$$

where S is the probability of fracture and B is defined as the risk of fracture. B is a function of the stress and for a uniform stress is proportional to the volume. For an arbitrary distribution of stress in an isotropic body, the risk of fracture is given by

$$B = \int_V n(\sigma)\, dv \tag{2}$$

where $\int_V$ denotes a volume integral and $n(\sigma)$ is the function which expresses the dependence of the risk of fracture on the stress, σ. The function $n(\sigma)$ is independent of position and the direction of the stress.

If the material is an anisotropic one, $n(\sigma)$ will be a function of the stress, the coordinates, and possibly of the direction of the stress. Weibull indicates that in many cases an apparent departure from isotropy may be due simply to a difference in the material properties on the surface and the interior of the material as a result of the method of manufacture of the material. In this case B could be represented by

$$B = \int_V n_1(\sigma)dv + \int_A n_2(\sigma)dA \tag{3}$$

where $n_1(\sigma)$ is the material function for the interior of the body, $n_2(\sigma)$ is the material function for the surface, and $\int_A$ an area integral.

If the stress is uniform throughout a volume then Equation 2 yields a risk of rupture

$$B = V\, n(\sigma) \tag{4}$$

The formula for $n(\sigma)$ most frequently used is

$$n(\sigma) = \left(\frac{\sigma - \sigma_u}{\sigma_o}\right)^m \tag{5}$$

According to Weibull the only merit of this formula for $n(\sigma)$ is to be found in the fact that it is the simplest mathematical expression of the appropriate form which satisfies certain necessary conditions (3). Also experience has shown that, in many cases, it fits the observations better than any other known functions.

Now B becomes, for a uniform stress distribution,

$$B = V\left(\frac{\sigma - \sigma_u}{\sigma_o}\right)^m \tag{6}$$

where

σ = actual fracture stress of specimen

σ_u = a stress below which fracture cannot occur

σ_o = a normalizing factor

m = constant representative of the flaw density of the material

Substitution of Equation 6 into Equation 1 yields:

$$S = 1 - \exp\left[-V\left(\frac{\sigma - \sigma_u}{\sigma_o}\right)\right]^m \tag{7}$$

for the probability of fracture of an isotropic material of volume V subjected to a uniform stress of magnitude σ. If the constants σ_u, σ_o, and m are known, Equation 7 can be used to predict the probability of fracture for a given value of σ. Conversely, if ample experimental data are available, Equation 7 can be used to determine the constants. For this purpose Equation 7 is usually rewritten as

$$\log \log \left(\frac{1}{1 - S}\right) = m \log (\sigma - \sigma_u) - m \log \sigma_o + \log V + \log \log e \qquad (8)$$

where logarithms are to be the base 10 and e is the Naperian base constant. The probability of fracture for each specimen can be determined from the equation:

$$S = \frac{n}{N + 1} \qquad (9)$$

where N is the total number of specimens tested, n is the specimen serial number corresponding to a listing of the fracture stresses in an increasing order from one to N. Thus, the n = 1 specimen will be the one with the lowest fracture stress for the N coupons.

Once the material constants are known, the theory can be used to predict the mean fracture stress for specimens of different volumes. According to Weibull, the ultimate strength of the material, which corresponds to the strength of the material as determined by the arithemetic mean strength of a series of test specimens, is the expected value of the probability density function given by:

$$\sigma_m = \int_{\infty}^{\infty} \sigma \frac{dS}{d\sigma} d\sigma = \int_{o}^{1} \sigma \, dS = \sigma_u + \int_{\sigma_u}^{\infty} e^{-B} d\sigma \qquad (10)$$

Substitution of Equation 6 into Equation 10 yields:

$$\sigma_m = \sigma_u + \sigma_o V^{-\frac{1}{m}} \Gamma\left(1 + \frac{1}{m}\right) \qquad (11)$$

where Γ represents the gamma function. Similarly the variance is given by:

$$a^2 = \int_{-\infty}^{\infty} (\sigma - \sigma_m)^2 \; S(\sigma) \, d\sigma = \int_{\sigma_u^2}^{\infty} e^{-B} \, (d\sigma^2) + \sigma_u^2 - \sigma_m^2 \qquad (12)$$

Substitution of Equation 6 into Equation 12 yields:

$$a^2 = \sigma_o^2 \, V^{-\frac{2}{m}} \left[\Gamma\left(1 + \frac{2}{m}\right) - \Gamma^2 \left(1 + \frac{1}{m}\right) \right] \qquad (13)$$

The standard deviation a is given by:

$$a = \sigma_o \, V^{-\frac{1}{m}} \sqrt{\Gamma\left(1 + \frac{2}{m}\right) - \Gamma^2 \left(1 + \frac{1}{m}\right)} \qquad (14)$$

Methods of Determining Weibull's Constants

The usual procedure for determining the material constants of the distribution function when data are available from one test volume is an iterative graphical procedure using Equations 8 and 9. This method utilizes a plot of log log $\left[\frac{1}{1-S}\right]$ versus log $(\sigma - \sigma_u)$. For the correct value of σ_u this plot will be a straight line with slope m and intercept log V - m log σ_o + log log. This method presupposes a knowledge of the constant σ_u which, as a rule, is not known. When σ_u is not known, the usual procedure is to plot log log$\left[\frac{1}{1-S}\right]$ versus log σ. If the plot follows a straight line, then σ_u is equal to zero. If the plot is a curve, then a tentative value of σ_u is assumed and the data replotted using log $(\sigma - \sigma_u)$ as the abscissa. If the selected value of σ_u is too high, the curve will be concave upwards and further tentative values for σ_u are tried until the data approximates a straight line. Once the correct value of σ_u is known, m is determined directly from the slope of the plot and σ_o is calculated from the value of the intercept, the volume of the test specimen, and m.

One other point should be made regarding the above procedure. It was noted in the previous paragraph that a concave upward curve indicated that the assumed value of σ_u was too high. If σ_u has been assumed equal to zero and the plot of log log$\left[\frac{1}{1-S}\right]$ versus log σ still yields a concave upward curve, then no single positive value of σ_u will produce a straight line. This follows from the fact that the lowest possible value of σ_u for a tensile specimen is zero. One explanation of this behavior is that the material yielding this type of result is anisotropic and will require more than one material function to characterize it. Methods of analyzing such materials are covered in Weibull's paper "The Phenomenon of Rupture in Solids."

When data are available from tensile test specimens of two different volumes, then Equation 6 may be used to determine m if $\sigma_u = o$ or σ_u is assumed known. If B_1 is the risk of fracture of a uniform tensile specimen of volume V_1 and B_2 is the risk of fracture of a uniform tensile specimen of volume V_2 then:

$$B_i = V_i \left(\frac{\sigma_i - \sigma_u}{\sigma_o} \right)^m \qquad i = 1, 2$$

If the two specimens have the same probability of fracture, then $B_1 = B_2$ from which the following equation may be obtained:

$$\left(\frac{\sigma_1 - \sigma_u}{\sigma_2 - \sigma_u} \right) = \left(\frac{V_2}{V_1} \right)^{\frac{1}{m}} \tag{15}$$

Then m may be obtained when $\sigma_u = o$, or is assumed known, and σ_1 and σ_2 are the average fracture strengths for test specimens with volumes V_1 and V_2 respectively.

Another method suggested by Weibull (4) for determining the material constants is to let

$$Z = \frac{\sigma - \sigma_m}{a}$$

Then Equation 7 may be written:

$$S = 1 - \exp \left\{ -\left[Z \sqrt{\Gamma\left(1 + \frac{2}{m}\right) - \Gamma^2\left(1 + \frac{1}{m}\right)} + \Gamma\left(1 + \frac{1}{m}\right) \right]^m \right\} \tag{16}$$

Now S versus Z may be plotted for different values of m. On this graph points (S, Z) can be plotted where S is taken from the data using Equation 9, and Z is calculated using the fracture strengths, the mean strength, and the standard deviation. From these points, an estimation of m may be obtained if the distribution is simple. If the distribution is complex, this also will be illustrated on the plot. Once m is determined, σ_u, and σ_o may be determined using the equations:

$$\sigma_o = \frac{a V^{\frac{1}{m}}}{\sqrt{\Gamma\left(1 + \frac{2}{m}\right) - \Gamma^2\left(1 + \frac{1}{m}\right)}} \tag{17}$$

and

$$\sigma_u = \sigma_m - \sigma_o V^{-\frac{1}{m}} \Gamma\left(1 + \frac{1}{m}\right) \tag{18}$$

The determination of the material constants m, σ_u, σ_o was carried out utilizing a computer program based on the iterative graphical procedure previously outlined (5).

The program used the method of least squares to calculate the best straight line and to converge on the most likely value of σ_u by minimizing the sum of the squares of the deviations of all the data points from the calculated straight line. From the best straight line, m and σ_u were determined, and σ_o was computed from the intercept and the volume. Once this was accomplished, m, σ_u, and σ_o were printed out along with the values of Log Log $\left[\frac{N+1}{N+1-n}\right]$ and Log $(\sigma - \sigma_u)$ for each breaking stress. Graphs such as Figure 31 were plotted with this information.

This program was modified so that assumed values for σ_u could be fed into the computer and values for m and σ_o calculated for this assumed σ_u. Also Log Log $\left[\frac{N+1}{N+1-n}\right]$ and Log $(\sigma - \sigma_u)$ were calculated for each breaking stress for the assumed σ_u. This permitted a closer look at the effect σ_u has on m and σ_o for a given set of data.

The computer program also was used to calculate the average breaking stress, the standard deviation, and the coefficient of variation for each set of data.

DATA AND RESULTS

Graphite

The results for the ATJ graphite are given in Tables 1 and 2 and Figures 21 through 24. The individual values of the tensile strengths are listed in Table 1 for all specimens; Table 2 lists the specimen gage diameter, length, surface area, surface finish, surface area to volume ratio and average tensile strength. Figures 21 through 24 exhibit graphs of tensile strength versus volume, surface area, surface area to volume ratio, gage length, and gage diameter for the graphite specimens of types I through XI. All data plotted are the average values of specimen groups.

Figure 21 illustrates the effect of volume and surface area on the ultimate strength. As can be seen from the figure, the strength remained fairly constant with a change in both volume and surface area except for the highest and lowest volume specimens which tended to follow the prediction of Weibull's theory by exhibiting the lower strengths at the largest volume and the higher strengths at the smallest volume. However, the values generally did not agree well with the strength theoretically predicted from material constants obtained from any one test volume. This suggests that graphite is not sufficiently brittle to be a representative Weibull material or that the numerous voids do not permit the normal and orderly propogation of a crack. Values for m for the different sets of data points were determined by assuming $\sigma_u = 0$ and using the graphical technique to find m. The range was from 9.83 to 13.25. It would be difficult to separate the effects of volume and surface area.

Examination of the effects of the other parameters of gage length, gage diameter, and surface area to volume ratio revealed no significant or correlative trends. These conclusions were confirmed by studies of the graphs in Figures 22, 23, and 24 which indicate that these parameters (not including volume) did not influence strength by much. Prior work here on ATJ graphite had indicated about a 15% reduction in strength as the surface finish became rougher proceeding from about 30 to about 300 rms. Since the pore sizes of graphites are relatively large and do extend to the surface finish, perhaps it is reasonable to assume that the actual surface finish of the protruding portion of the material, at least up to the pore diameter or grain size, often has a minimum effect and may not be measurable for some particular billets but slightly detectable for others.

Alumina

The results of all tensile runs on the alumina specimens are given in Table 4. There were 15 specimens using a gage volume of 0.012 in.^{3}, 20 each using gage volumes of 0.25 in.^{3}, and 1.33 in.^{3}, and 120 specimens each using gage volumes of 0.031 in.^{3}, and 0.62 in.^{3}. For various reasons, satisfactory breaks were not obtained on all specimens so that some culling was necessary.

Influence of Large Flaws - Large flaws, (internal and surface) not typical of "Griffith cracks" but related to inclusions were found in 26 fractured specimens. Table 5 lists the specimens which had visible flaws, the specimen type, the approximate flaw size, and the ultimate tensile strength for each of the specimens. The weakest one had a strength of 16,600 psi and the majority were somewhat weaker than the average for

their respective lot. Figures 25 and 26 are plots of the difference between the average strengths of specimens with flaws and specimens without flaws versus cross-sectional area and versus volume. As can be seen from the graphs, the difference between the average strengths decreased for both increasing cross-sectional area and increasing volume indicating that the presence of a macro flaw is less critical in a large specimen than in a small one. If these were "Griffith cracks," they would have the same influence on specimens of this size range.

Fractures Out of Gage Section - Another example of unsatisfactory breaks included those fractures that occurred outside the gage length. There were 33 such breaks recorded. One of these breaks was attributed to the unsatisfactory performance of the flat gas bearing and 20 were attributed to visible flaws. The visible flaws in these specimens generally were of two different types; internal voids or inclusions and surface flaws. Eighteen of the 20 radius breaks resulting from flaws were initiated at the surface, 2 of the 20 probably were caused by internal voids or inclusions. There was no apparent explanation for 12 of the radius breaks, but two of these twelve had small fracture planes perpendicular to the primary fracture surface. Some of the unexplained radius breaks might have been caused by insufficient control of the surface finish at this early stage in the program but this could not be confirmed. Some of the fracture planes had small, extremely flat zones; however, these (in this group) did not correlate with strength in general.

General Test Conditions - The surface finishes for the gage sections were held between 5 and 10 rms for all alumina specimens. The stress rate was maintained constant at 5000 psi/sec for all runs. This stress rate was selected as one about which there was little influence on strength as reported on Wesgo Al 995 in AFML-TR-65-129 and observed here and reported in ASD-TDR-63-245.

Grain Size Effect - Table 6 gives values of average ultimate tensile strengths for given average grain sizes. The grain sizes were the average values as reported for the alumina tiles. The average tensile strengths were computed using all the Type II specimens taken from tiles that had a given grain size. The number of points used to compute the averages is included in the table. There was no correlation between strength and average grain size in terms of these values. Probably, the correlation could not be developed because the grain sizes were obtained from a given tile rather than each specimen and because the ranges of grain sizes for the different tiles overlapped considerably. Recall that the presence of a few large grains or of unbonded "islands" of grains did reduce the strength. This was mentioned in a prior section and will be expanded upon later.

Density Effect - Figure 27 is a plot of strength versus density where the density value used for this plot was the average value reported for a specific parent tile as presented in Table 3. This graph indicates a trend of increasing strength with increasing density; however, the statistical correlation is extremely weak. This aspect is discussed further in the section on Fractology.

Average Properties - Neglecting variations from density and grain size and using all the values for specimens that broke in the gage length without a visible flaw, the average tensile strength for the alumina ranged from 29,700 psi for the Type I specimens (1.33 in.^{3}) to 41,800 psi for the Type V specimens (0.012 in.^{3}). The standard deviations ranged from 4730 psi for the Type II to 7720 psi for the Type V specimens, and the coefficients of variation varied from 0.148 for Type II to 0.185 for the Type V specimens.

Three Type II specimens were tested with stress and strain being recorded in order to obtain the modulus of elasticity for the alumina used in this program. The values obtained were: 51.9×10^6 psi, 56.5×10^6 psi, and 53.6×10^6 psi for an average of 54.0×10^6 psi. This static modulus compared favorably with an elastic modulus value of 59×10^6 psi determined by ultrasonic techniques on AVCO hot pressed alumina of similar density.

Since the primary concern of this part of the project was the clarification of Weibull's volume effect on brittle materials, specimen sizes and designs were chosen on this basis. Thus the data obtained for this phase of the project could not be used specifically to correlate strength with such parameters as: surface area to volume ratio, gage length, and gage diameter. In order to ascertain the effects of these parameters, the specimens would require gage volumes large enough so that the volume effect would not influence the results. That is, the volumes should be large enough so that a curve of strength versus volume would be essentially flat such as the right portion of the curves in Figure 28.

Volume Effect and Fracture Probability - Figure 28 is a plot of the average ultimate tensile strength versus volume for all specimen types. The standard deviations also are shown on the graph along with some theoretical curves that will be discussed later. It can be seen that, in agreement with Weibull's theory, tensile strengths decreased with increasing volume. Also the standard deviation decreased with increasing volume except for the last set of data for the largest volume, a deviation which might be partially due to the small number of Type V specimens tested.

Figures 29 and 30 are frequency plots for the Type II and IV specimens respectively. The smooth curve superimposed on each of the plots is Weibull's probability function using the best values for m, σ_u, and σ_o, discussed below, for the given specimen type as determined by the computer method. There was considerable disagreement between the frequency plot and the Weibull functions for both cases; however, this disagreement was more pronounced for the Type IV smaller specimens. The fact that the frequency plot for the Type IV specimens was bimodal might indicate that not enough data was available or that the sampling was not done from a single population; that is, the material from which the specimens were machined was not uniform. Still another explanation may be that inclusions not visually detected were more influential in the smaller specimens. Recall that this was true for the larger inclusions. An inspection of the data in Table 7 reveals that the specimens involved in the first mode were well distributed among the various tiles. Their color was random. A detailed check on machining practices used when these specimens were tested revealed no reasons for this anomaly. One striking observation is that if the strengths of the specimens included in the first mode were more properly distributed through the frequency graph or deleted from the analysis entirely, the measured average strength of the small specimens would have been much closer to the value predicted by the Weibull analysis when using the larger specimens as the base point. Conversely, the strengths of the larger specimens would be quite precisely predicted using the smaller specimens as the base point.

Recall that in order to use the fracture data obtained for one volume to predict the average tensile strength of a specimen with a different volume, the constants m, σ_u, and σ_o must be determined. First, consider basing the calculations on the larger Type II specimens of which there were a large number. Using the fracture data obtained from these specimens, the best values for the constants were found to be m = 5.25, σ_u = 9350 psi, and σ_o = 22,400 psi by the "computer method" discussed previously in the Data Analysis section of this report. Figure 31 shows the actual fracture data and the best straight line fit, as determined by the computer, for a plot of Log Log $\left[\frac{N+1}{N+1-n}\right]$ versus Log $(\sigma - \sigma_u)$. Using Equation 15, the values for m, σ_u, and σ_o given above, and the average breaking stress for the Type II specimens, the theoretical curve for average breaking stress versus volume is plotted along with the actual data in Figure 28. This graph shows that there is good agreement between the theoretical and the observed strength for the large volumes, but that for the smaller

volumes the differences were quite large, as much as 25% for the Type V specimen. That is, the predicted strength for the smaller specimens is higher than was experimentally determined.

As a result of this lack of agreement between the theoretical and observed average breaking stresses, σ_u was assumed to be zero and m and σ_o were recalculated from the larger Type II values using the computer program. The new values for m and σ_o were m = 7.68 and σ_o = 31,900. Figure 32 shows a plot of Log Log $\left[\frac{N+1}{N+1-n}\right]$ versus Log $(\sigma - \sigma_u)$ for the actual data with the new values of m, σ_u, and σ_o, and Figure 28 includes the new strength versus volume relation that was obtained. The two theoretical curves for strength versus volume practically coincide for the larger volumes and differ only slightly for the smaller volumes. Thus the two curves did not differ enough to warrant artificially choosing $\sigma_u = 0$ in place of σ_u = 9350.

Figures 33 and 34 show plots of Log Log $\left[\frac{N+1}{N+1-n}\right]$ versus Log $(\sigma - \sigma_u)$ for the data of the larger Type II specimens where σ_u = 20,000 psi and σ_u = 15,000 psi. A value of σ_u = 20,000 psi was chosen based on the observation that no specimens, of any type in the culled data, had a tensile strength less than 20,650 psi. (The smallest breaking strength observed for all data was 16,600 psi for a smaller Type IV specimen). The σ_u = 15,000 psi was an arbitrary choice used in order to gain some insight into the effect of varying of σ_u on the values obtained for m and σ_o when the computer method was used to compute the constants, and also the effect of changes in σ_u on the plot of Log Log $\left[\frac{N+1}{N+1-n}\right]$ versus Log $(\sigma - \sigma_u)$. Observe that the higher values of σ_u dropped m significantly from 3.69 to 1.88. Also, the higher values of σ_u introduced more nonlinearity at the lower end of the curve.

The original proposal was to use the data from the Type II, or larger, specimens to compute the constants m, σ_u, and σ_o and then to use the data from the Type IV, or smaller, specimens to confirm, or deny, these values. Now consider basing the results on the smaller Type IV specimens. Using the computer program to get the best straight line fit again, the values of the constants for the smaller Type IV specimens were calculated to be: m = 2.51, σ_u = 21,500 psi, and σ_o = 4540 psi. Figure 35 has a plot of Log Log $\left[\frac{N+1}{N+1-n}\right]$ versus Log $(\sigma - \sigma_u)$ for the actual data and also the best straight line fit. The relation between strength and volume was calculated using the values of m = 2.51 and σ_u = 21,500. This relation is plotted on Figure 28. The theoretical curve fits the data for volumes less than 0.031 in.^{3},

but departs quickly from the observed data for volumes greater than 0.031 in.^{3}, predicting lower strengths than actually measured for the larger volumes. Observe the strength versus volume curves for Types II and IV (larger and smaller respectively) and note that the two curves are essentially parallel, but that the smaller specimen type predicts a lower strength throughout. If σ_u was considered as a zero failure stress below which fracture cannot occur, then the value of 21,500 psi obtained from the smaller specimens for σ_u would be unrealistic as a material constant since nominal fracture stresses less than 21,500 psi were observed during the tests for some type of specimens (20,650 psi for all culled data and 16,600 psi for all data). However, no fracture stress for the smaller Type IV specimen was less than 21,500 psi.

Values for m and σ_o also were computed from the smaller Type IV specimen data for σ_u = 0 psi, 9350 psi, and 15,000 psi since these values were used for the larger specimens discussed previously. Figures 36, 37, and 38 include the values of m and σ_o for these values of σ_u and a plot of Log Log $\left[\frac{N+1}{N+1-n}\right]$ versus Log $(\sigma - \sigma_u)$. Increasing σ_u decreased m from 6.77 to 3.88. Each of these graphs shows a reasonably straight line except for a few points on the lower end. These artificial values of σ_u when used with the base point for the smaller specimens did not provide a better overall fit for the strength versus volume relation.

These extreme points that fall out of the linear zone of the curves have considerable influence on the determination of m and σ_u using the normal computer solution. When two specimen values of 29,680 psi and 31,810 psi (compared with an average strength of 37,510 psi) were removed from a collection of 68 values for the smaller Type IV specimens, the value of σ_u changed from 21,500 psi to 20,400 psi while the value for m changed from 2.51 to 2.80. When the two weakest specimen values were removed from the same set of data, σ_u changed from 21,500 psi to 22,700 psi; however, m only changed from 2.51 to 2.47. From these results, it is obvious then that one cannot cull data heedlessly nor introduce procedures in inspection, handling or otherwise that would eliminate a certain class of specimens such as the weaker ones. However, it also is obvious that with sufficiently large sample quantities, reasonable care, and precision data, the loss of a few specimens does not invalidate the results particularly from the design standpoint.

Since precise agreement could not be obtained between the material constants as determined for the Type II and IV specimens, another approach was explored to see if a common set of values might satisfy both conditions and provide reasonable numbers. Figure 39 is a plot of m versus σ_u for the two types of specimens using the computer analysis for the best straight line fit and assuming different values of σ_u, then solving for m. The two curves intersect at m = 4.24 and σ_u = 13,000 psi. Calculated values for σ_o at this point of intersection are 18,000 psi for the Type II specimens and 12,600 psi for the Type IV specimens indicating considerable disagreement; however, if departure is necessary it seems intuitively preferable to have it in σ_o. In Figure 40, σ_o is plotted versus m for assumed values of σ_u. When these points are approximated by straight lines, the lines intersect at m = 12.7 and σ_o = 51,000 psi. It is probably only fortuitous that the values of m, σ_u and σ_o as obtained by the intersections of the curves for the two sets of data give numbers that appear "right". That is, a value of zero failure strength of 13,000 psi seems reasonable, and a value of 51,000 psi for the strength of the "unflawed" structure agrees with the value for the strongest specimens. This approach deserves more study for consistency and could lead to a working design theory.

Figure 41 is a plot of probability of fracture versus tensile strength showing the actual data for the Types II and IV specimens. Viewed in conjunction with Figures 31 and 37 this figure gives some insight into the reasons for the different sets of Weibull constants obtained for the Types II and IV specimens. Notice that the data points in Figures 31 and 37 are essentially parallel except for a few points at the lower end. These are the points, as previously mentioned, which have a considerable influence on the value for σ_u. Observe in the probability plot in Figure 41 that the data for the smaller Type IV specimens at the lower end of the plot more or less approach the abscissa at a constant rate whereas the data points for the larger Type II specimens tail off toward lower strength as they approach the abscissa. On the basis of Weibull's theory, it would be expected that the data for the smaller Type IV specimens would tail off more than the larger Type II since both types should have the same σ_u and there should be more scatter in the smaller Type IV data. The indication is that either there were not enough data points to properly define the probability distribution curve, or the mode of fracture for the smaller specimens was different from that of the larger ones which results in a different set of constants. As inferred from the prior observations on the visible flaws, it appears possible that a given

crack (or inclusion) can behave differently in specimens of different size or volume. This observation might strike at the credulity of a single set of material constants. Additional observations have been made from the probability plot in Figure 41. Observe that for a 10% probability of failure, the predicted strength of the smaller specimen (predicted from the data on the larger ones) was 37,000 psi compared to a measured value of 28,000 psi. Thus, the safe design would be obtained by testing the smaller specimens and making a prediction of the volume effect for larger sections by Weibull. Also, there is the possibility that design with a 5% probability of failure and subsequent proof testing would provide a quite adequate design criteria. It should be emphasized that the tensile strengths obtained from the small test specimens should not be used as a basis for design without allowing for the volume effect.

When making minimum weight designs, one might test larger specimens to obtain design allowables at local spots in the structure (such as at joints) where the stress is concentrated and the analysis more uncertain. Since the large flaws and inclusions were less influential in the larger specimens, it seems entirely possible that large sections could accommodate to some degree the local high stress points. Thus, the so called "plastic hinge" employed in concrete design might operate in some fashion in ceramics. This aspect needs specific study.

Still another observation can be made from Figure 41. Extrapolating the straight line portion of the data curves for the large and small specimens provides an intersection at the abscissa where the probability of fracture is zero and the tensile stress is about 25,000 psi. This infers a common value of σ_u or "zero strength". A similar observation was made in ASD-TR-61-628 using flexural data for another alumina. Perhaps this is a coincidence or perhaps it is an indication of physical events in the material, but the thought warrants further study. It is possible that σ_u is a material constant but m is not.

Using the relationship of probability of fracture versus stress, an attempt was made to "work backwards" to obtain better values for a common set of constants of m, σ_u and σ_o. This method was outlined at the end of the section "Methods of Determining Weibull's Constants"; the data for the larger Type II specimens were utilized. The results of this effort are shown in Figure 42 where different constants have been used to obtain the relation of probability of fracture versus stress and the relations are overplotted on the experimental data to permit a visual study of the best apparent fit. As can be seen in the figure, the parametric curves for difference values of m fell too close together to permit a selection of m although it does appear that m must be greater than 5. Because of the nature of the curves, no further analysis was attempted using this particular method. That is, all of the curves fell too close together to use one for an arbitrary selection.

In order to obtain a comparison of the Weibull constants between two different sets of alumina data, fracture data was taken from our prior report ASD-TDR-63-245 and used to determine the Weibull material constants. The material was Wesgo, AL995 alumina supplied by Western Gold and Platinum Corporation. The specimens which were used to obtain this data had different geometrical configurations than those used in this program, hence a direct comparison of the data is not possible. Also the surface finish of the specimens reported in ASD-TDR-63-245 was 20 rms whereas the surface finish for this program was 5-10 rms, and the data in ASD-TDR-63-245 was for specimens tested at two different cross-head speeds. However, there was little difference in the strength values found for these two different speeds. The values obtained for m and σ_u for the Wesgo alumina were $m = 5.55$, $\sigma_u = 0$ for Volume 1; $m = 1.09$, $\sigma_u = 17,800$ for Volume 2. It was not feasible to calculate Volume 1 and Volume 2 for these data because of the nature of the specimen configurations. Since the calculations of σ_o depends on the volume, these were also omitted. These values for m and σ_u were the best values as determined by the computer method. Again there were wide variations between the material constants for the different volumes; however, these values were of the same magnitude and range as the ones obtained in this program. It should be noted that there were only eleven fracture strengths available for these calculations, a number which was probably insufficient for an accurate determination of the material constants.

From the total analysis, it was evident that a volume effect did exist and was "almost" predicted by Weibull theory; however, one set of constants did not satisfy completely both sets of data; hence, for the material used in this program m, σ_u, and σ_o could not be defined rigidly as material constants that could be related to some physical characteristics of the material, or to some mode of fracture. They might be considered parameters whose arrangement was such that they permitted a relatively good fit for a given set of data. However, it must be restated that material variability might have confounded these results and that better correlations would be possible. The evidence suggested that the gas-bearing does provide a uniform tensile field and that the method of testing was quite adequate to detect the relationship that existed.

Minimum Samples for Various Properties - Using the same data for the Type II specimens as just presented in the Weibull analysis, a study of the number of specimens needed for an accurate determination of the material characteristics was conducted. This study had to be somewhat limited in scope because of the number of specimens that were culled.

The method of the study was to select random subsets of the fracture strengths of size N. That is, there were "N" number of coupons in each subset. The strengths from each of these subsets were then used to calculate the average breaking stress, the standard deviation, the coefficient of variation, and the Weibull material constants. The values of N used were 10, 15, 20, 40, 60, and five subsets of each size were selected. The method of selection of the random breaking strengths was accomplished by assigning to each breaking strength a number from 0 to 71. The pseudo-random numbers were selected from 0 to 71 using a random number generator computer program. The numbers were pseudo-random in the sense that each number from 0 to 71 could be chosen only once for a given subset.

The results of this investigation are presented in Table 8 and in Figures 43, 44, and 45. Table 8 gives the values of average breaking stress, the standard deviation, the coefficient of variation, m, σ_u, and σ_o for each of the subsets. Figures 43, 44, 45 are plots of standard deviation versus N, m versus N, and σ_u versus N respectively.

The values calculated for the average breaking stress for each subset revealed that the maximum difference between the average breaking stress for all of the data and from any one subset was 2090 psi, or 6.5%, and this difference was for a subset that contained only 10 values. Hence, the average breaking stress could be calculated reasonably accurately with as few as 10 test specimens.

Figure 43 shows that the standard deviation varied quite significantly for the subsets containing 10 and 15 breaking strengths. For the subsets having 40 breaking strengths the variation was much less and the spread was about the same as that of the subsets having 60 values.

Figures 44 and 45 show that there were wide variations for the values of m and σ_u (as determined by the modified graphical technique) for the subsets with 10, 15, 20, and 40 breaking strengths. This indicates that more than 40 coupons would be required to obtain an accurate determination of these parameters. Perhaps 60 coupons would be adequate for a good indication.

FRACTOGRAPHY STUDY OF THE ALUMINA TENSILE SPECIMENS

A post mortem fractography analysis of the high density, polycrystalline alumina tensile specimens was conducted by the Metals and Ceramics Division, Air Force Materials Laboratory. This analysis was in direct support of Southern Research Institute's program to experimentally determine the volume effect on the tensile strength of brittle materials and follows:

The results of the program demonstrated that the tensile strengths of the alumina specimens decreased with increasing gage volume; however, unexpected strength variations occurred from tile to tile for a specific gage volume. Since the density and grain size variations reported by AVCO for all tiles were small (97.9-99.5% theoretical density and 1-3 microns average grain size), these strength differences between some tiles required additional investigation. Therefore, fractured samples from the tile that exhibited the high tile 806) and low (tile 858) strength extremes were selected for fractography examination. A specimen from the average strength tile 826 and a two-tone (gray-white) specimen from tile 830 were also chosen for fracture surface observation. The physical properties and gage volumes of the tensile specimens are given in Table 9. Density and average grain size measurements were not made on the individual specimens so that the values represented the average for the 12 in. x 12 in. x $1\frac{1}{8}$ in. tiles.

Experimental Procedures

Fracture Surface Replicas - The fracture surface of one-half of the broken specimen was replicated by the normal two stage plastic-carbon technique. The surface was first cleaned by two plastic replications which were discarded. A third replication was shadowed first with Pt-Pd at 45° and then with carbon normal to the surface. The plastic was dissolved in acetone and the carbon replica was placed on copper grids completing the same preparation phase. Fractography replicas were prepared for all samples listed in Table 9.

Polished Surface Replicas - Transverse and longitudinal cross sections of the 0.031 in.^{3} gage volume specimens were prepared for general microstructure examination adjacent to the fracture surface. The areas examined are indicated on Figure 46. Although there was no apparent microstructural differences between the longitudinal and transverse cuts, electron micrographs of only the transverse polished sections are presented in this report. Polishing was done on a Syntron vibratory polisher using 3μ diamond and $0.1\ \mu\gamma$ Al_2O_3. The specimens were etched with boiling H_3PO_4. After metallographically polishing and etching, the polished sections were replicated as outlined above for examination in the electron microscope. Cross sections of the larger (0.62 in.^{3}) specimens were not polished for microstructural observations.

Results and Discussion of Results

When viewed with the unaided eye, the low strength specimens from tile 858 exhibited flat, smooth fracture surfaces while the intermediate and higher strength samples featured ragged, rough fracture contours. The macroscopic smooth fracture breaks consistently yielded the lowest strength values, regardless of tile number.

The three low strength test specimens selected for the fractography study (858 AA, 858 A and 858 L) exhibited an unusual microstructure which is considered undesirable in high density-high strength pure oxide ceramics. Figure 47 is a low magnification view of this structure showing oriented exaggerated grain growth. This photomicrograph was made from a polished section area immediately adjacent to a fracture surface.

Although the major portion of the microstructure of these specimens consisted of equiaxed grains of uniform size, the detailed examination revealed three microstructural variations. Figure 48 which is an electron micrograph of a replicated polished surface from specimen 858 AA shows the three structures; normal grain structure at the top, exaggerated grain growth in the center, and a structure of doubtful integrity at the bottom. An electron micrograph of a fracture surface, (858 AA), Figure 49, also shows this three component structure. In this case the normal structure is at the base of the photograph. The most prominent anomalous feature of this structure was the occurrence of regions of small, rounded, "dimpled" grains shown at the bottom of Figure 48 and again at higher magnification in Figure 50. These "dimpled" grain regions were associated with normal grain structure as well as being adjacent to grains of exaggerated growth; see Figures 51 and 52. The exaggerated grains varied from 30 - 50 microns across a face as opposed to 1 - 5 microns for equiaxed grains, and 0.5 - 2 microns for the "dimpled" grains.

The fracture surfaces of the 858 tensile specimens were of low relief as was illustrated in Figure 49. The fracture path was predominantly intergranular in the equiaxed and "dimpled" grain regions for 858 specimens (Figure 52 and 53). The large, elongated grains appeared as flat, featureless areas on the fracture surface replicas (Figures 49 and 54); however, barely distinguishable grain boundaries in these regions indicated that the fracture path was primarily intergranular along these low angle boundary, oriented grains. Under applied stress, significant boundary stresses probably developed between these exaggerated grains and adjacent, equiaxed grains, particularly at three grain junctions. Thus, if a microcrack existed

or had been initiated along the boundary of one of these large, discontinuous grains, a moving crack could generate exceedingly high velocity and kinetic energy under stress. The dynamic nature of a moving crack along the boundaries of the exaggerated grain regions was emphasized by the predominance of transgranular fracture in contiguous, equiaxed grains.

The "dimpled" grain regions probably represented the weakest "link" in the low strength specimens. The rounded shape geometry of these grains was indicative of incomplete densification and bonding as found in early stage sintering of powdered compacts (7). Equilibrum between interfacial tensions of particles in contact requires that all boundaries meet at angles, producing sharp-edged grains forming 120° angles at the edges (8). Although real polycrystalline solids are composed of widely varying shaped grains, compliance with this interfacial boundary angle requirement (120°) is usually satisfied. The load carrying capability in these dimpled regions was, undoubtedly, much lower than in well bonded, equiaxed grain regions. Lower transverse bend strengths in hot pressed, submicron grained alumina (Linde A) were attributed to insufficient bonding between grains in a strength-microstructure study conducted by Spriggs et al (9). The critical stress for microcrack initiation or propagation might also be considerably reduced in these "dimpled" regions, since porosity was present which might behave as flaws. Regardless of the source of the microcracks in 858 tensile specimens, the microstructure resistance to propagation was sufficiently low to permit a catastrophic failure at a lower average stress level.

The polished and fracture surfaces of the intermediate strength specimen, 826-44A, are shown in Figures 55 and 56. This specimen was characterized by a mixed grain size and intergranular fracture. No exaggerated grain growth or "dimpled" grain regions were observed in this sample. However, the presence of micropores near grain boundaries as seen in Figures 56 and 57 must account for its lower strength (43,500 psi) in comparison to the tensile strength of a higher strength specimen, 806-QA (53,000 psi). This porosity or density difference between the intermediate, 826-44A, and high strength, 806-QA, tensile specimen was also reflected in the average densities reported for the bulk tiles from which they were machined (97.9% and 99.2% theoretical, respectively).

High strength specimen 806-QA was typified by a uniform sized, equiaxed grain microstructure (Figure 58). The mode of failure was 70 - 75 percent intergranular fracture (Figure 59) with the remainder consisting of cleavage and transgranular fracture across appropriately oriented grains (Figures 60 and 61). The marked increase in percentage of transgranular fracture was indicative of the absences of microporosity in the grain boundaries and the uniform size of grains. Because of the equiaxed-uniform grain size, one would expect fewer microcracks as a result of geometric mismatch.

Representative areas of the repressed two-tone (gray-white) tensile specimen are shown in the electron micrographs of Figures 62 and 63. Although the fracture path was consistently intergranular throughout the specimen cross-section, the average grain size in the white area was approximately twice that of the gray region. This result was not unexpected since the presence of colloidal graphite in the gray region should inhibit grain growth during the repressing operation (10). Although several grain intersections and faces on various replicas suggested evidence of colloidal graphite and/or microporosity (Figure 63), positive identification could not be made.

Fracture Mechanisms

Although the source of fracture initiation was not defined in this fractography examination, several theories have been proposed for alumina. The flaw concept has received the most attention, particularly with transverse bend test studies where surface flaws and imperfections become extremely critical. For example, investigators such as Passmore, Spriggs and Vasilos, proposed that the critical length of the microcrack or flaw was related to average grain size of the alumina specimen under test(11); hence, the inverse strength-grain size dependence observed experimentally. Atomistically, the fundamental fracture initiation and propagation mechanism, however, has not been resolved by this explanation. The fact that internal barriers such as grain boundaries, subgrain boundaries, pores, and other structural discontinuities cause dislocation and slip-band pile-up producing severe stress concentrations and crack initiation in single and polycrystalline MgO, has been largely ignored in alunina deformation studies due to immobility of dislocations at room temperature (12). Deformation studies by Conrad on sapphire indicated that plastic yielding occurred above 900°C by dislocation glide on the (0001) basal plane in the (1120) direction (13, 14). Conrad observed that twinning usually occurred in compression at lower temperatures and higher strain rates. Recent work on alumina in the prefracture and microstrain region at room temperature has shown that internal microcracks develop within grains from intersecting twin boundaries (15). The presence of etch pits adjacent to these intragranular microcracks suggested that some localized dislocation activity might also assist in crack nucleation. Petch's work on fracture surface energy experiments using elliptical predrilled cracks in thin alumina plates provided microscopic evidence that dislocation movement was involved in fracture initiation (16). Palmour and Kriegel conducted etch pit studies in the vicinity of room temperature microhardness indentations in alumina which revealed dislocation motion (17). With the accumulation of improved electron transmission and better etch pit data, the theory of a pre-existing flaw being necessary for the initiation of fracture in alumina might be challenged.

The current trend of thought for strengthening of alumina is towards finer grain size and solid solution alloying which could (1) prevent the occurrence of significant boundary stresses which result from crystal anisotropy, (2) dilute the concentration of impurities at boundaries, (3) increase resistance to dislocation motion, and (4) increase the cohesive energy of grain boundaries.

Conclusions

The large strength differences in various hot pressed tiles appeared more related to grain size variations and microstructure anomalies than to slight changes in density and grain size. The high strength samples (50,000 psi) consisted of equiaxed grains of uniform size; the intermediate strength (30-40,000 psi) specimens were composed of equiaxed grains of mixed size, and microporosity clustered near grain boundaries; the low strength test specimens (20,000 psi) were comprised of regions of large oriented grains with contiguous small rounded (dimpled) grains dispersed throughout an equiaxed grain matrix.

The "dimpled", nonequiaxed grain areas provided weak "links" resulting from poor intergranular bonds while the large, exaggerated grains enchanced boundary stress concentrations. Both features contributed to catastrophic failure at lower stress levels in the low strength tensile specimens.

A more detailed microscopy study of specimens with uniform sized, equiaxed grain structures is required to ascertain the effects of slight changes in porosity and density on the tensile strength of high density, polycrystalline alumina.

CONCLUSIONS

Most of the specific conclusions were included in the discussion of data and results; however, there were several conclusions which should be summarized and emphasized.

Perhaps the most important outcome of this program was the decisive evidence to show the dependence of strength on volume over a wide range of volumes (from 0.012 in.^{3} to 1.33 in.^{3} for a volume ratio of about 110) for the alumina. This volume effect was of the type predicted by the Weibull theory; yet, a single set of Weibull material constants could not be determined from the data that adequately described the total effect.

Another important conclusion was that the Weibull materials constants, m, σ_u, and σ_o, appeared not a constants of the material, but rather curve fitting parameters for a given set of data. There are possibly other forms of the material function $n(\sigma)$ which should be tried in hopes that the parameters involved could be given physical interpetations.

A volume effect on the strength of graphite was also illustrated, but this effect was not as clear-cut as that of the alumina. It also was shown that, for graphite, volume was the only variable of those investigated which did have a significant effect for the ranges of the variables considered.

The tensile strengths of alumina obtained on this study for the smaller specimens were of similar magnitude to the transverse bend strengths of AVCO hot pressed alumina of similar density and volume.

Fractography examinations revealed that the low strength tiles consisted of large, discontinuous grains and islands of unbounded grains in a fine grain matrix.

REFERENCES

1. Weibull, W. "A Statistical Theory of the Strength of Materials." Ing. Ventenskaps Akard Handl. No. 151. Stockholm (1939).

2. Weibull, W. "The Phenomenon of Rupture in Solids." Ing. Ventenskaps Akard Handl. No. 153. Stockholm (1939).

3. Weibull, W. "A Statistical Distribution Function of Wide Applicability." J. Appl. Mech. 18. pp. 293-297. 1951.

4. Weibull, W. Discussion of Weibull's paper, see reference 3. J. Appl. Mech. 19. pp. 233. 1952.

5. Jacobson, L. A. "The Weibull Statistical Distribution as Applied to Brittle Fracture." Technical Report AFML-TR-65-176. August 1965.

6. Anderson, O. and Saga, N., "Elastic Constants of Small Ceramic Specimens." AFML-TR-65-202. September 1965.

7. Coble, R. L. "Sintering Crystalline Solids." I. "Intermediate and Final State Diffusion Models." J. Appl. Phys. 32 (5) 787-792 (1961).

8. McLean, D. "Energies of Grain Boundaries and Microstructure." pp. 81-115. Grain Boundaries in Metals. Oxford at the Clarendon Press, London. 1957. pp. 346.

9. Spriggs, R. M. and Brissette, L. A. and Passmore, E. M. and Vasilos, T. "Microstructure Studies of Polycrystalline Oxides." Quarterly Progress Report Nr 2. Contract NOw 64-0217-d. August 1964.

10. Langrod, K., "Graphite as Grain Growth Inhibitor in Hot-Pressed Beryllium Oxide." J. Am. Ceramic Society 48 (2) 110 (1965).

11. Passmore, E. M. and Spriggs, R. M. and Vasilos, T. "Strength-Grain Size-Porosity Relations in Alumina." J. Am. Ceram. Soc. 48 (1) 1-7 (1965).

REFERENCES (continued)

12. Day, R. B. and Stokes, R. J. "The Mechanical Properties of Magnesium Oxide as a Function of Temperature." AFML-TR-65-93. May 1965. Air Force Materials Laboratory, Wright-Patterson AFB, Ohio. p. 86.

13. Conrad, H. "Mechanical Behavior of Sapphire." Report Nr ATN-64 (9236)-14. Aerospace Corporation. March 1964. p. 33.

14. Stofel, E. and Conrad, H. Trans. AIME 227. 1053 (1963).

15. Parikh, N. M. "Section III. Technical Background." pp. 17-74. Studies of the Brittle Behavior of Ceramic Materials. ASD-TR-61-628, Part III. June 1964. Air Force Materials Laboratory, Wright-Patterson AFB, Ohio, p. 409.

16. Petch, N. J. and Congleton, J. and Hardie, D. and Parkins, R. N. "Task 6: Effect of Surface Energy." pp. 133-174. Studies of the Brittle Behavior of Ceramic Materials. ASD-TR-61-628, Part III. June 1964. Air Force Materials Laboratory, Wright-Patterson AFB, Ohio. p. 409.

17. Palmour, III, Hayne and Kriegel, W. W. Engineering Study Report. "Brittleness in Ceramics I-Dislocations in Single Crystal Sapphire Revealed by Thermal Etching." Engineering Study Report. Contract Nr DA-36-034-ORD-2645. North Carolina State College. January 1961.

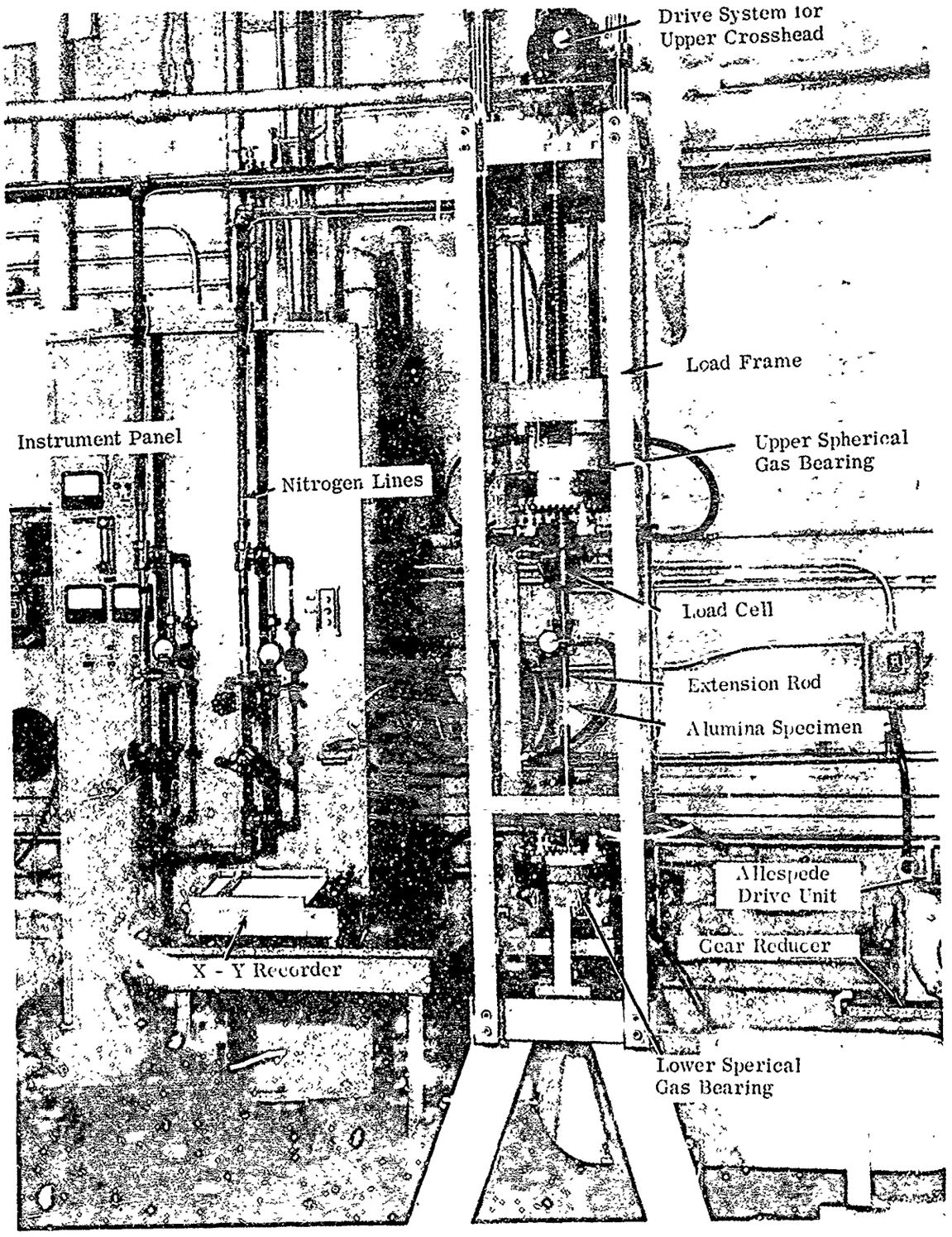

Figure 1. Gas-Bearing Tensile Facility

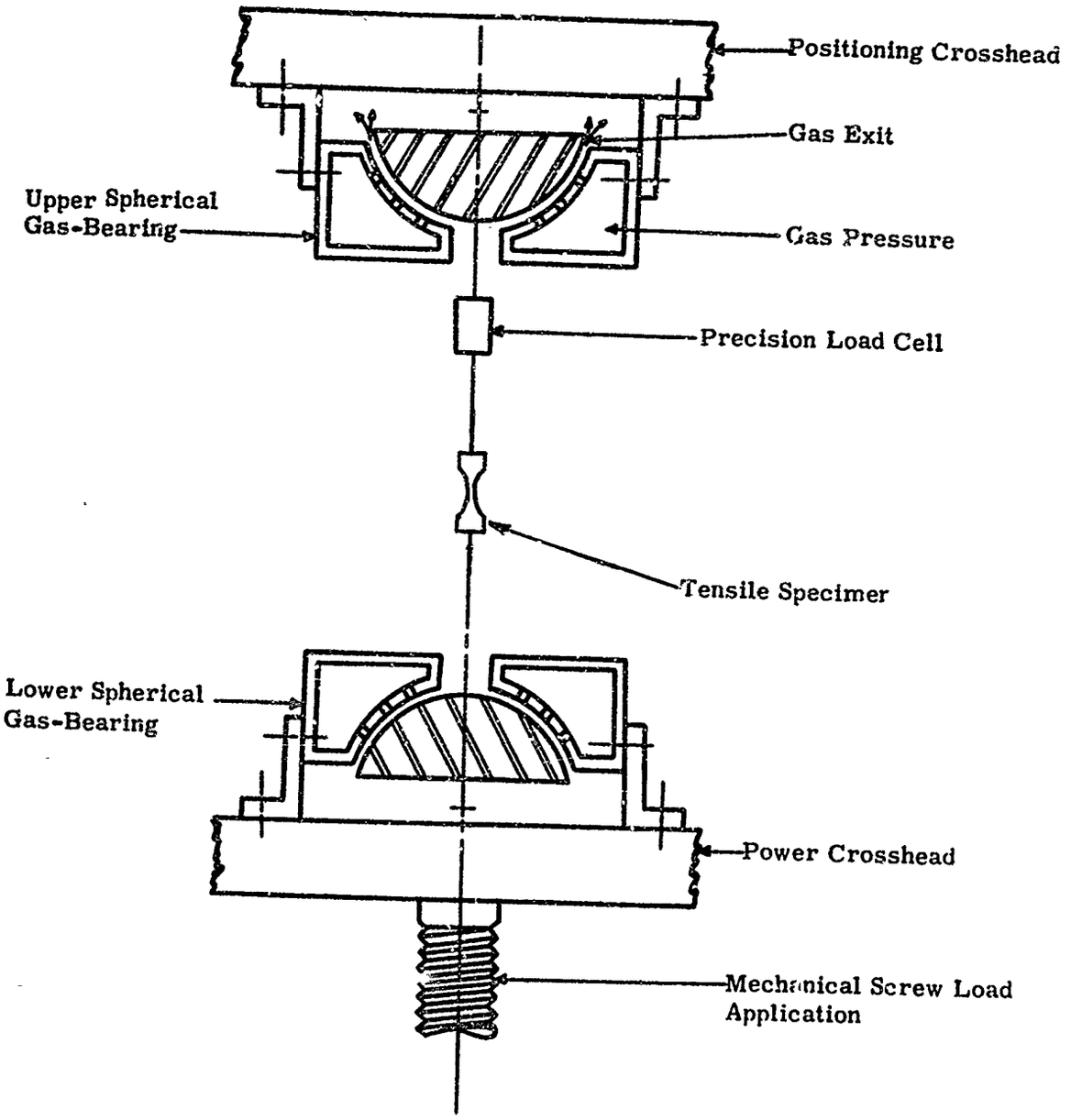

Figure 2. Schematic Arrangement of Gas-Bearing Universals, Specimen, and Load Train

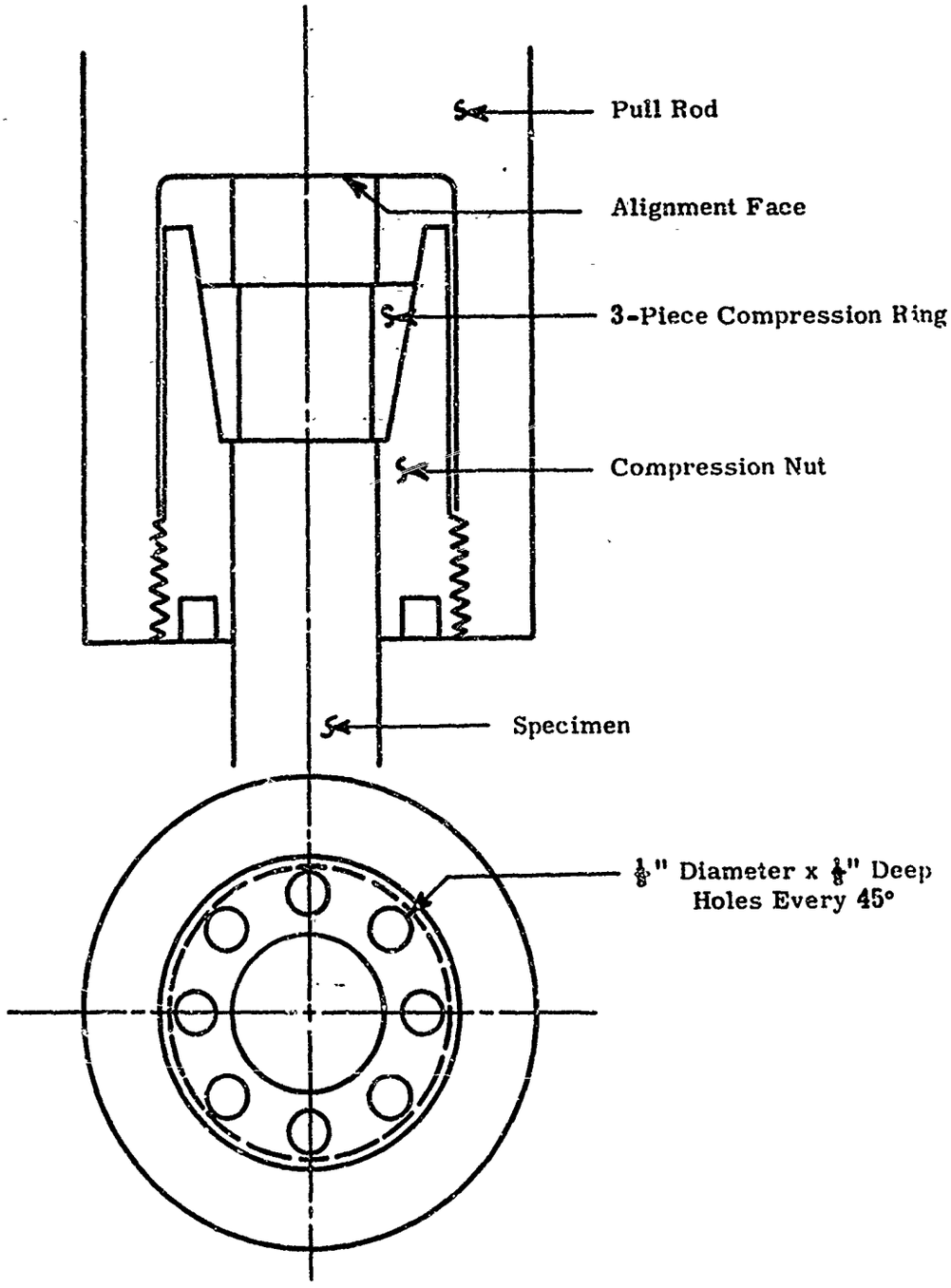

Figure 3. Schematic of Collet-Type Specimen Grip

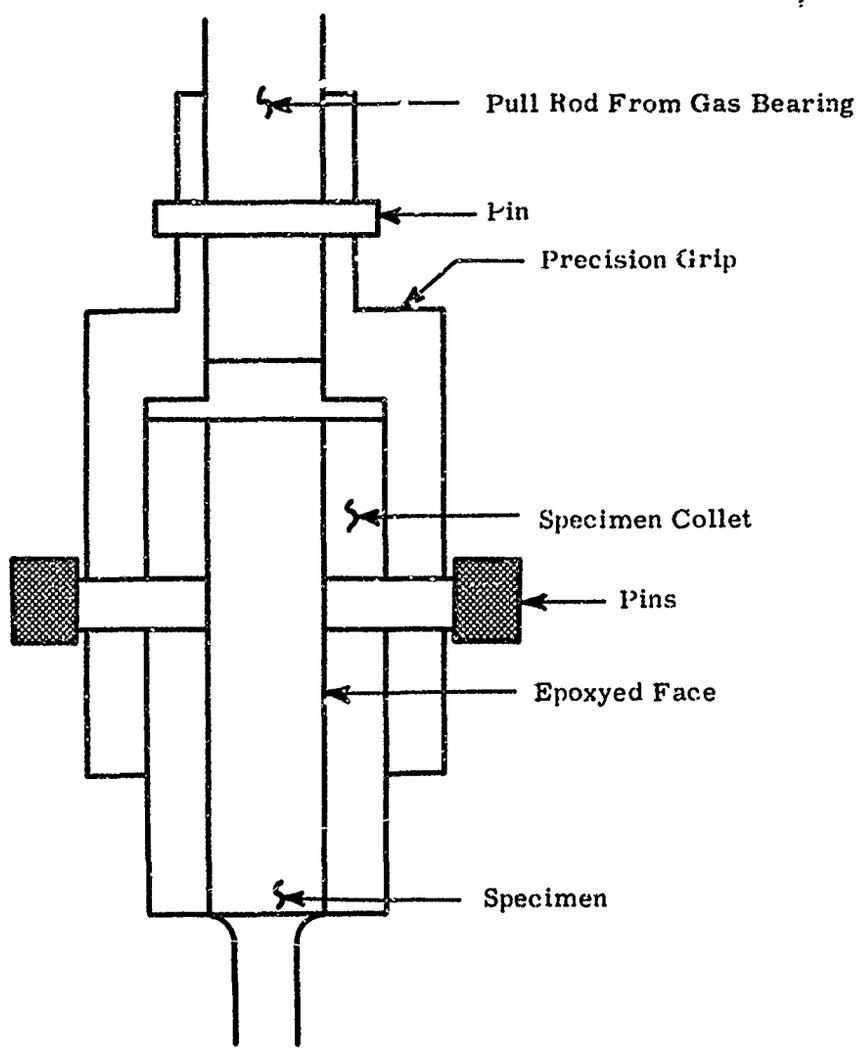

Figure 4. Schematic of Precision Sleeve-Type Grips

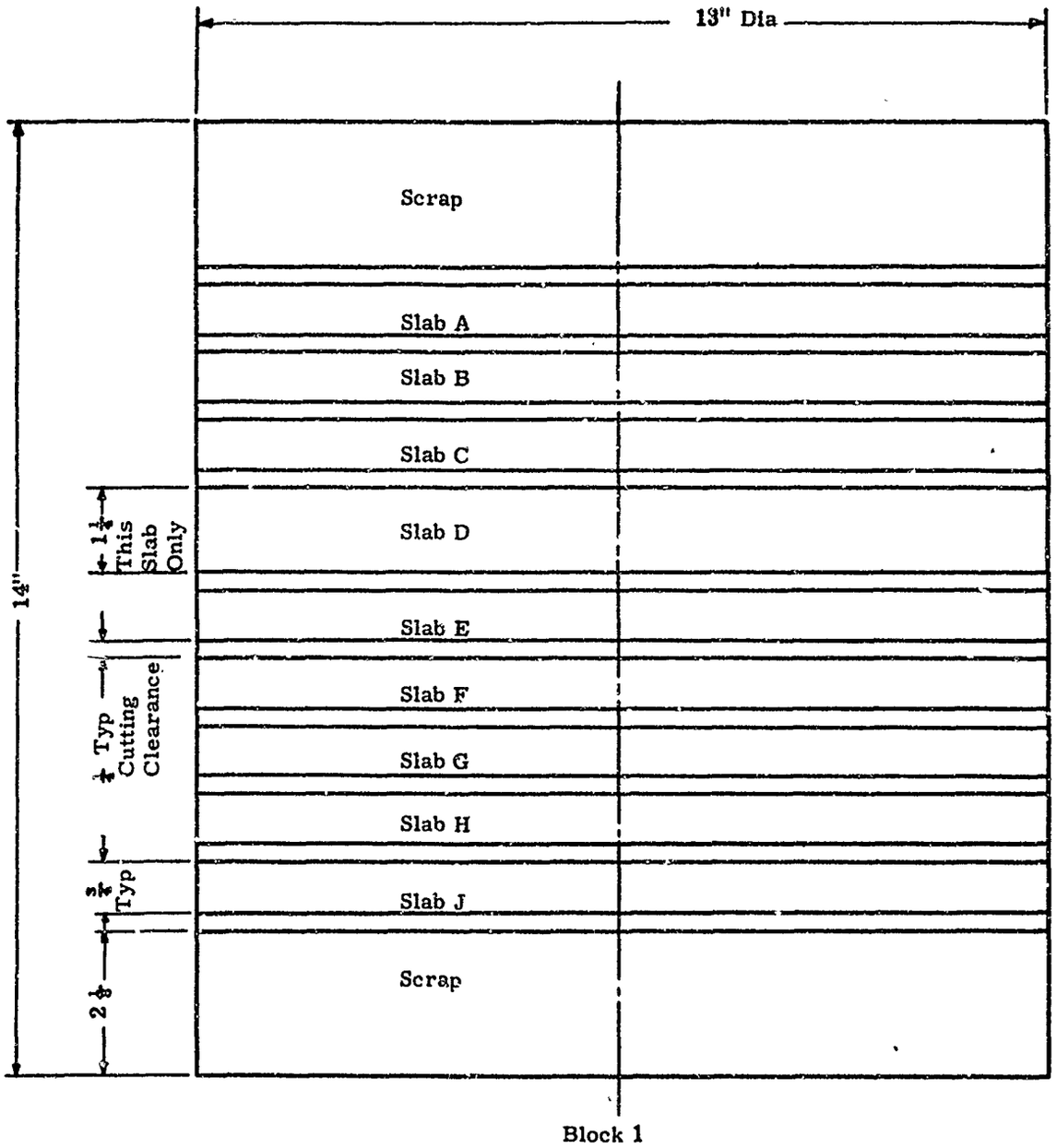

Figure 5. Cutting Plan for Block 1 of the ATJ Graphite

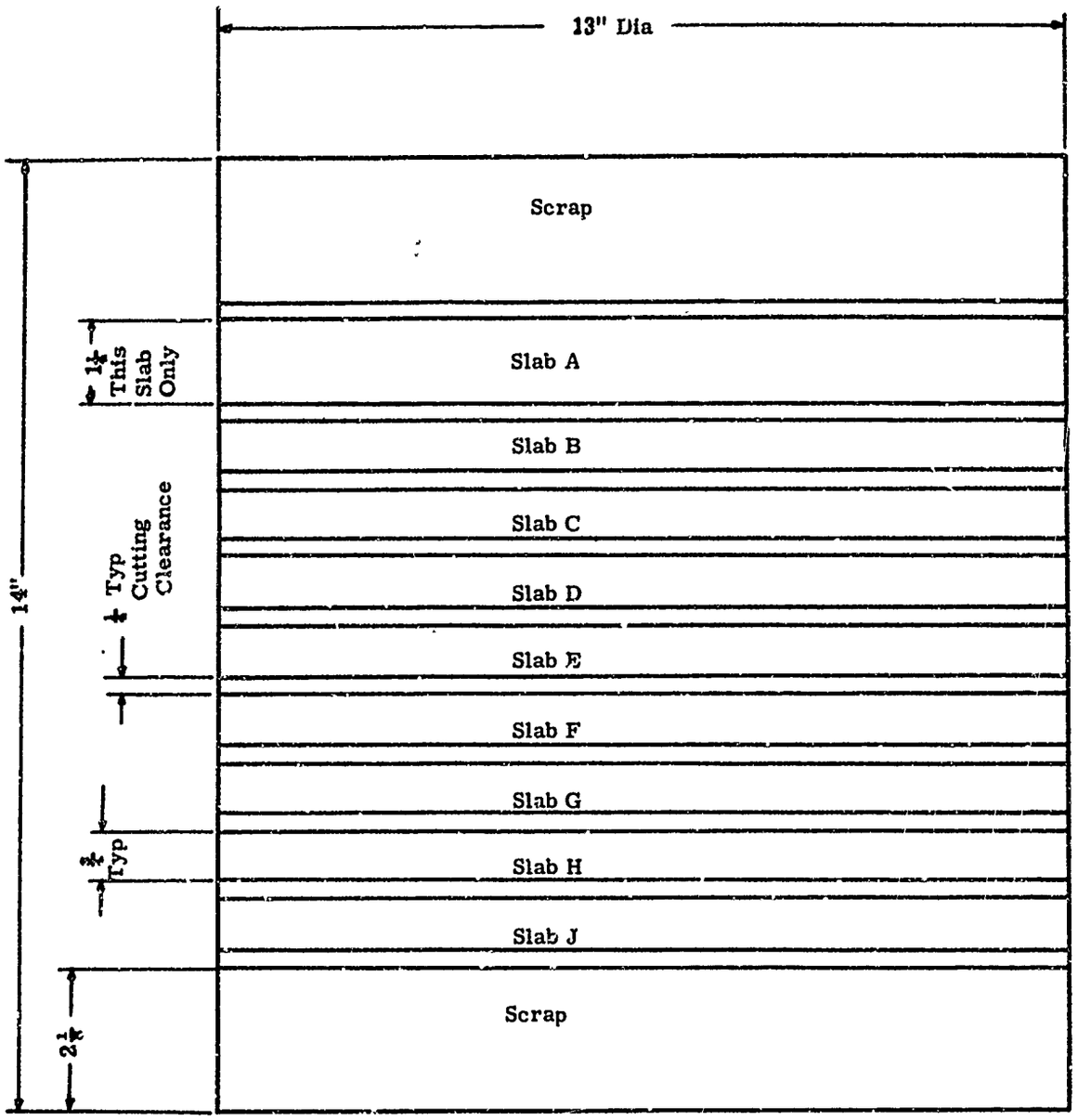

Block 2

Figure 6. Cutting Plan for Block 2 of the ATJ Graphite

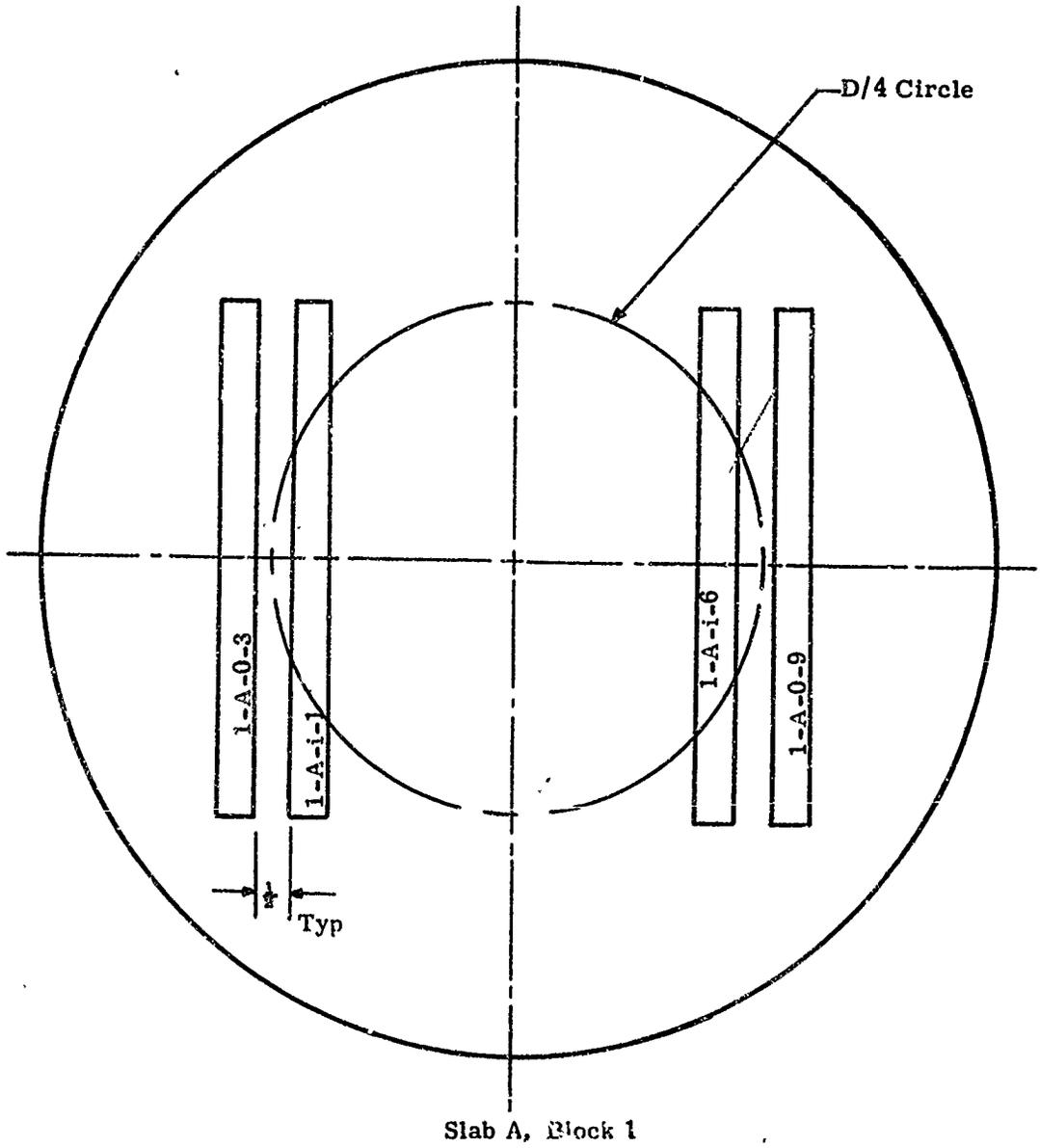

Slab A, Block 1

Figure 7. Typical Graphite Specimen Locations within the Slabs

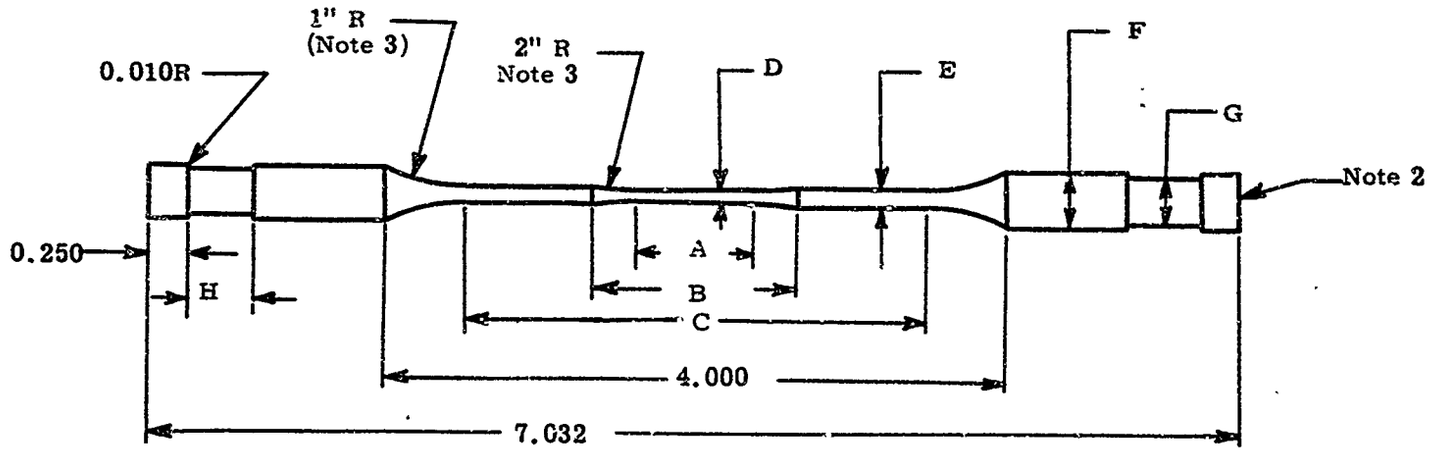

Specimen Type	A Length ± 0.002	B Length ± 0.002	C Length ± 0.002	D Diameter ± 0.002	E Diameter ± 0.002	F Diameter ± 0.002	G Diameter ± 0.002	H Length ± 0.002
I.	0.500	0.910	3.070	0.250	0.271	0.500	0.453	0.516
II	1.000	1.410	3.070	0.250	0.271	0.500	0.453	0.516
III	0.894	1.252	2.952	0.187	0.203	0.500	0.453	0.516
IV	2.000	2.296	3.052	0.125	0.136	0.375	0.347	0.438
V	1.000	1.296	3.052	0.125	0.136	0.375	0.347	0.438
VI	1.000	1.296	3.052	0.125	0.136	0.375	0.347	0.438
VII	1.400	1.722	3.104	0.150	0.163	0.375	0.347	0.438
VIII	1.334	1.588	2.992	0.094	0.102	0.375	0.347	0.438
IX	1.000	1.410	3.070	0.250	0.271	0.500	0.453	0.516
XI	0.188	0.440	2.992	0.094	0.102	0.375	0.347	0.438

Notes:

1. All diameters true and concentric to 0.0005".
2. Both ends flat and $\perp$ ℄ to 0.0005".
3. Do not undercut radii.
4. All dimensions are in inches.

Figure 8. Dimensions of the Graphite Specimens Types I through IX And Type XI for the Phase I Study

Notes:

1. All diameters true and concentric to 0.0005
2. Finish gage surfaces to 10 RMS
3. Both ends flat and ⊥ ℄ to 0.0005
4. Do not undercut radii
5. All dimensions are in inches

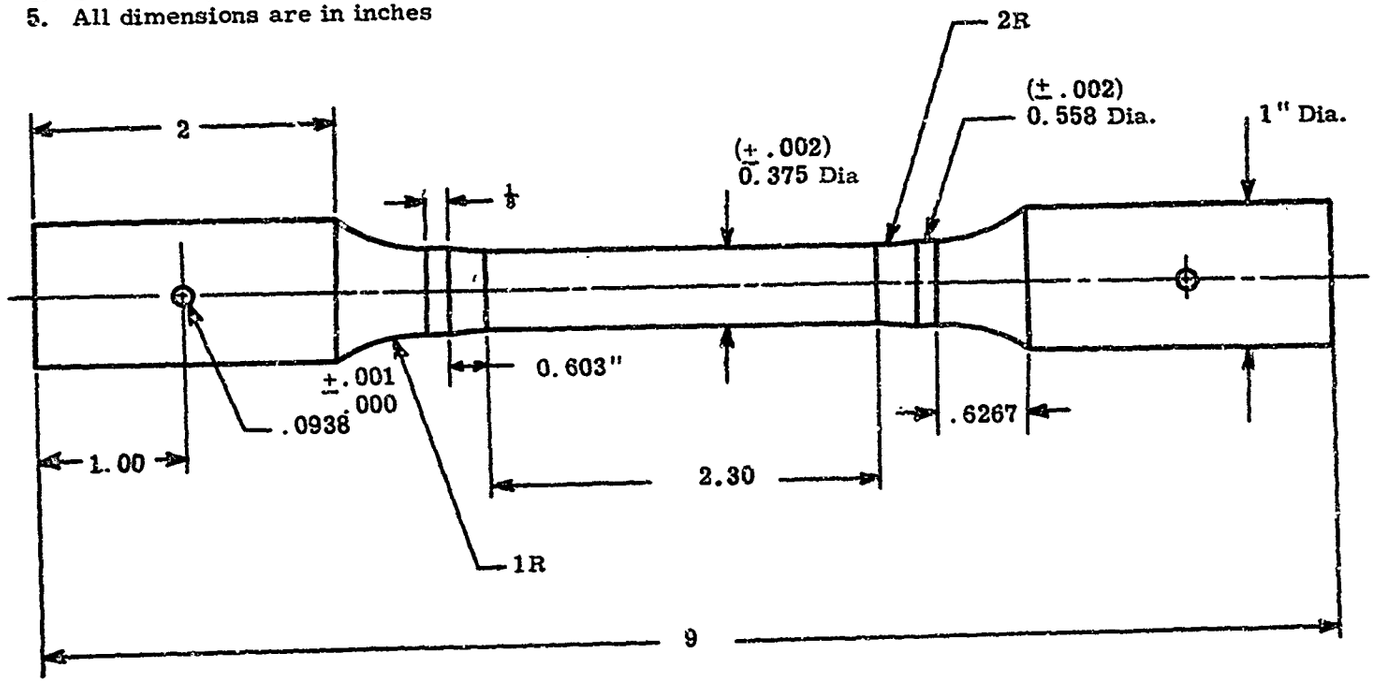

Figure 9. Configuration of the Type X Graphite Specimens for the Phase I Study

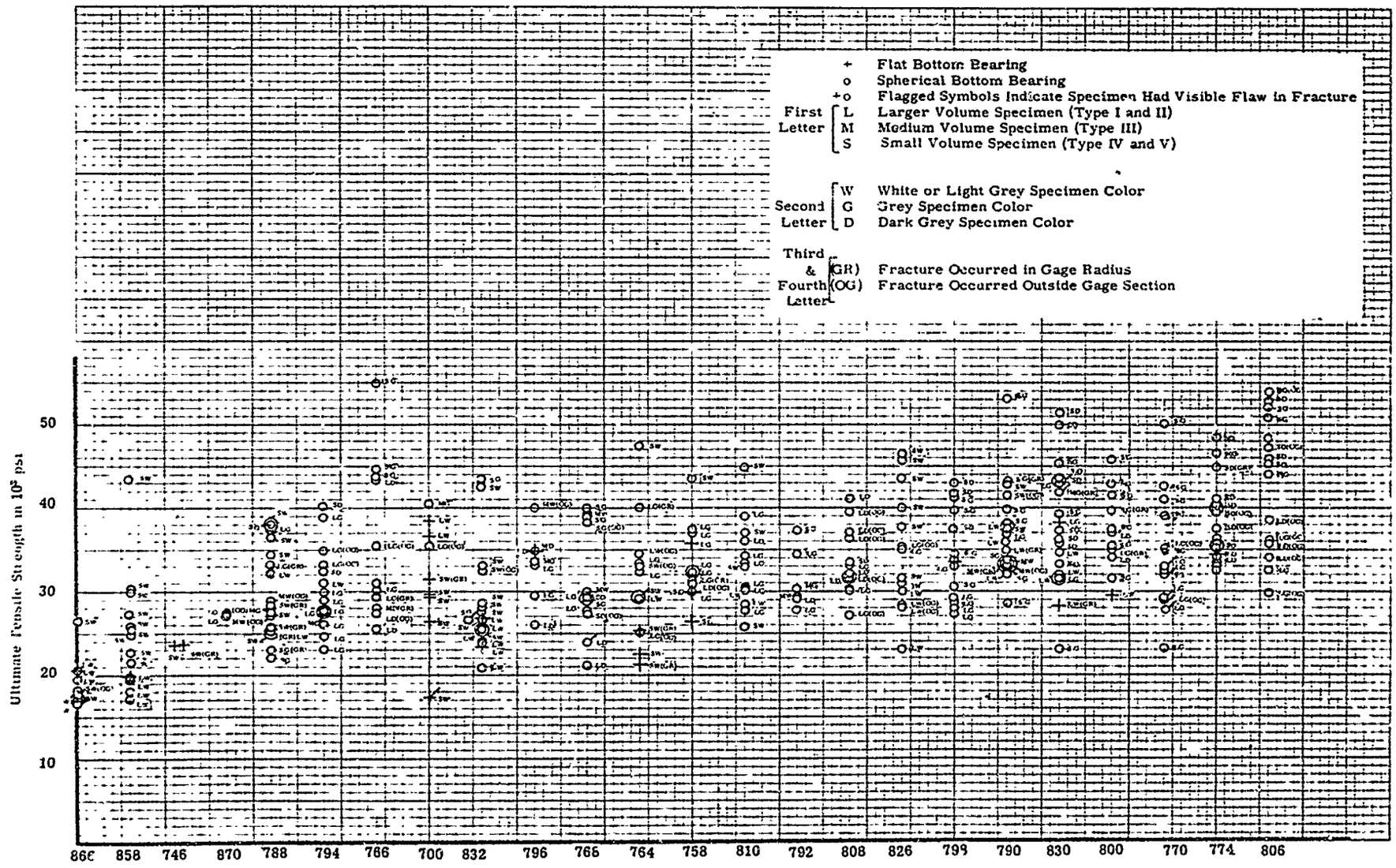

Figure 10. Ultimate Strength versus Tile Number Indicating Variation of Strength Between Tiles

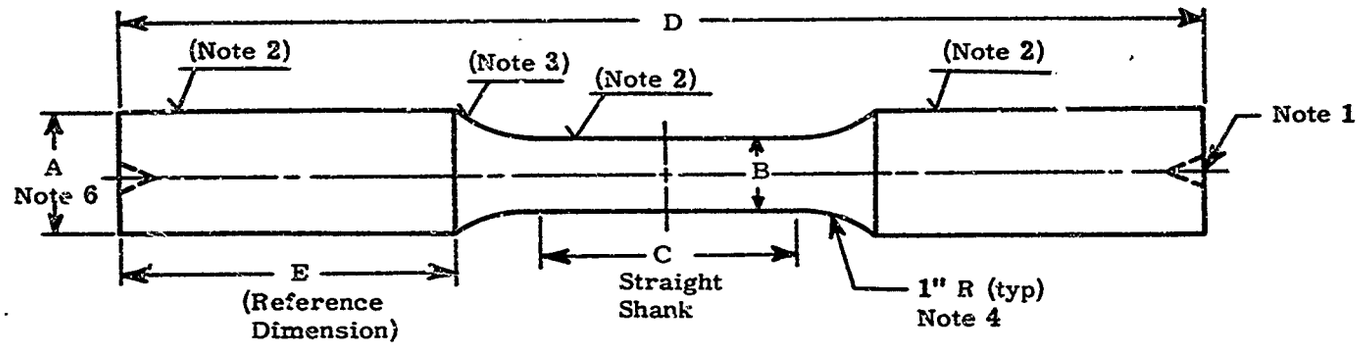

Specimen No.	No. of Specimen Required	A Diameter ±0.005	B Diameter ±0.002	C Length $\pm\frac{1}{32}$	D Length $\pm\frac{1}{16}$	E Length
I	22	1.000	0.815	4	11	3
II	120	1.000	0.611	$3\frac{3}{8}$	11	3
III	20	1.000	0.611	$1\frac{7}{8}$	$9\frac{1}{8}$	3
IV	120	0.500	0.136	$3\frac{1}{16}$	$7\frac{1}{4}$	$1\frac{1}{2}$
V	20	0.500	0.136	$1\frac{9}{16}$	$5\frac{3}{4}$	$1\frac{1}{2}$

Notes:

1. Small center holes desired.
2. This surface to be ground with 100 grit diamond wheel to surface finish of approximately 120 rms.
3. This surface (full radius plus $\frac{1}{8}$" extending into straight shank) to be ground with 400 grit diamond wheel to surface finish of approximately 20 rms or better.
4. Do not undercut.
5. All diameters true and concentric to centerline within 0.002.
6. All diameters to within ±0.001" from specimen to specimen.
7. Tolerances: Diameters as indicated
   Lengths $\pm\frac{1}{64}$
8. Specimen symetrical about centerlines.

Figure 11. Configuration of Alumina Sample Blanks Supplied by Avco

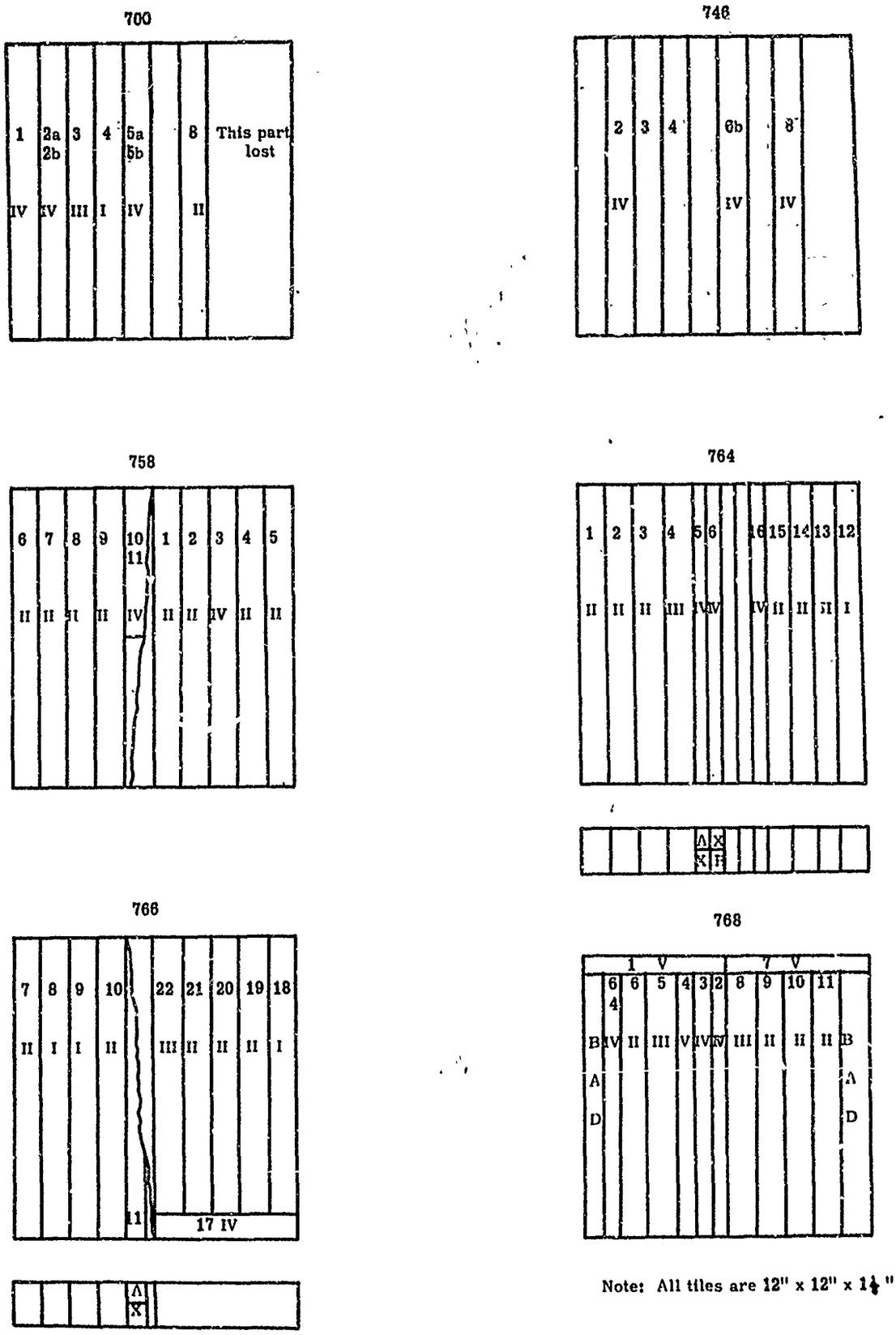

Note: All tiles are 12" x 12" x 1¼"

Figure 12. Cutting Plans for Alumina Tiles 700, 746, 758, 764, 766, and 768

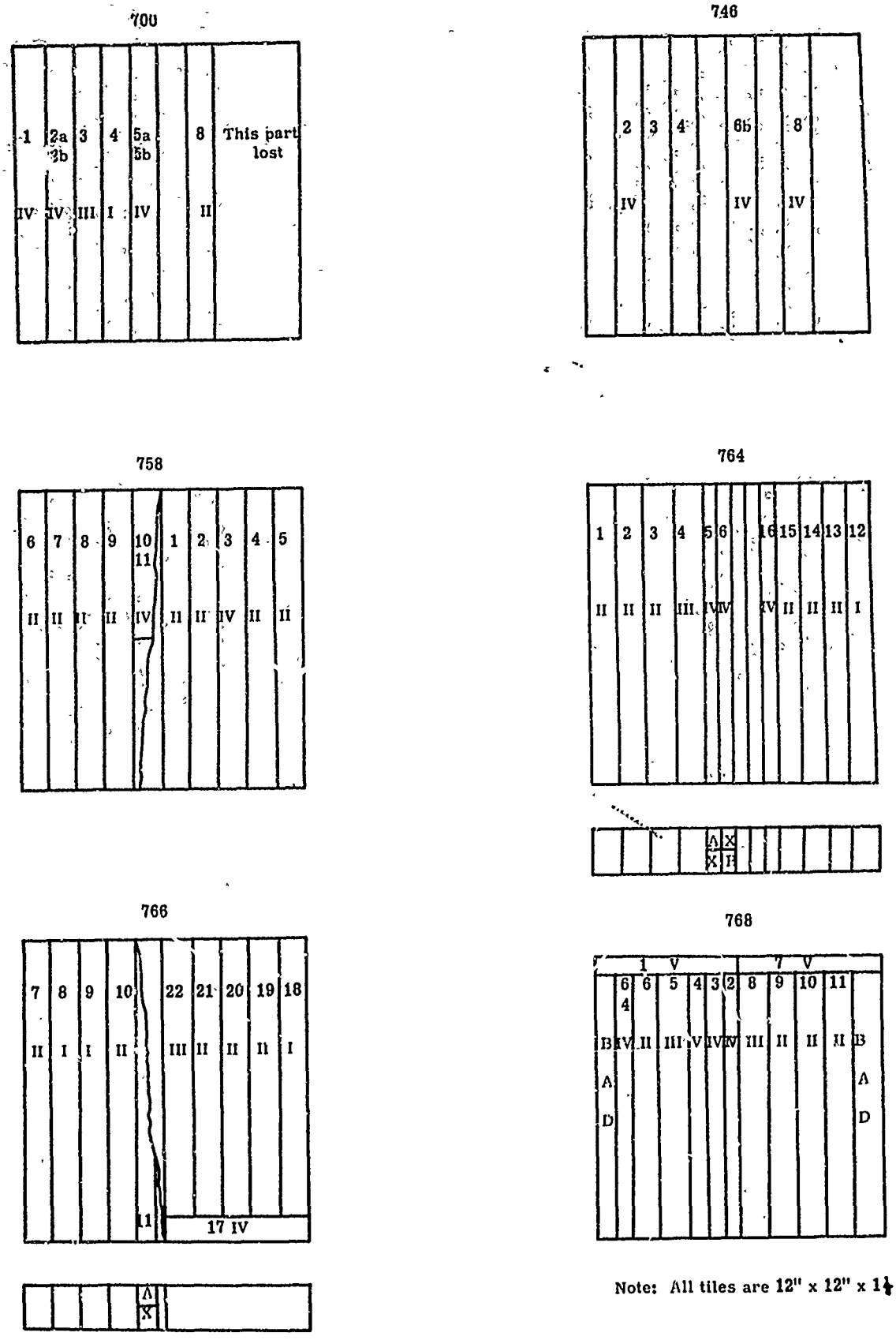

Note: All tiles are 12" x 12" x 1¼"

Figure 12. Cutting Plans for Alumina Tiles 700, 746, 758, 764, 766, and 768

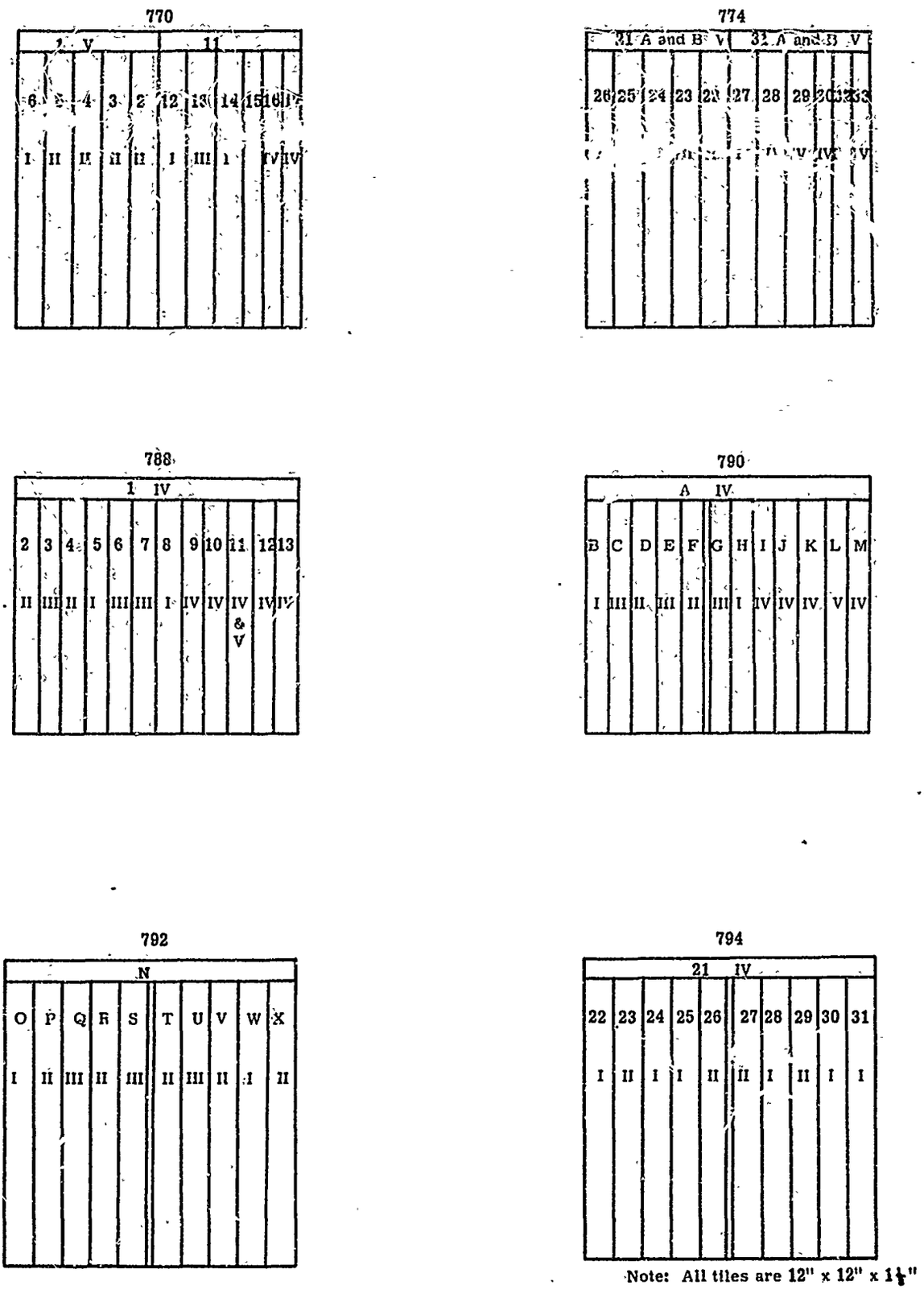

Note: All tiles are 12" x 12" x 1½"

Figure 13. Cutting Plans for Alumina Tiles 770, 774, 788, 790, 792, and 794

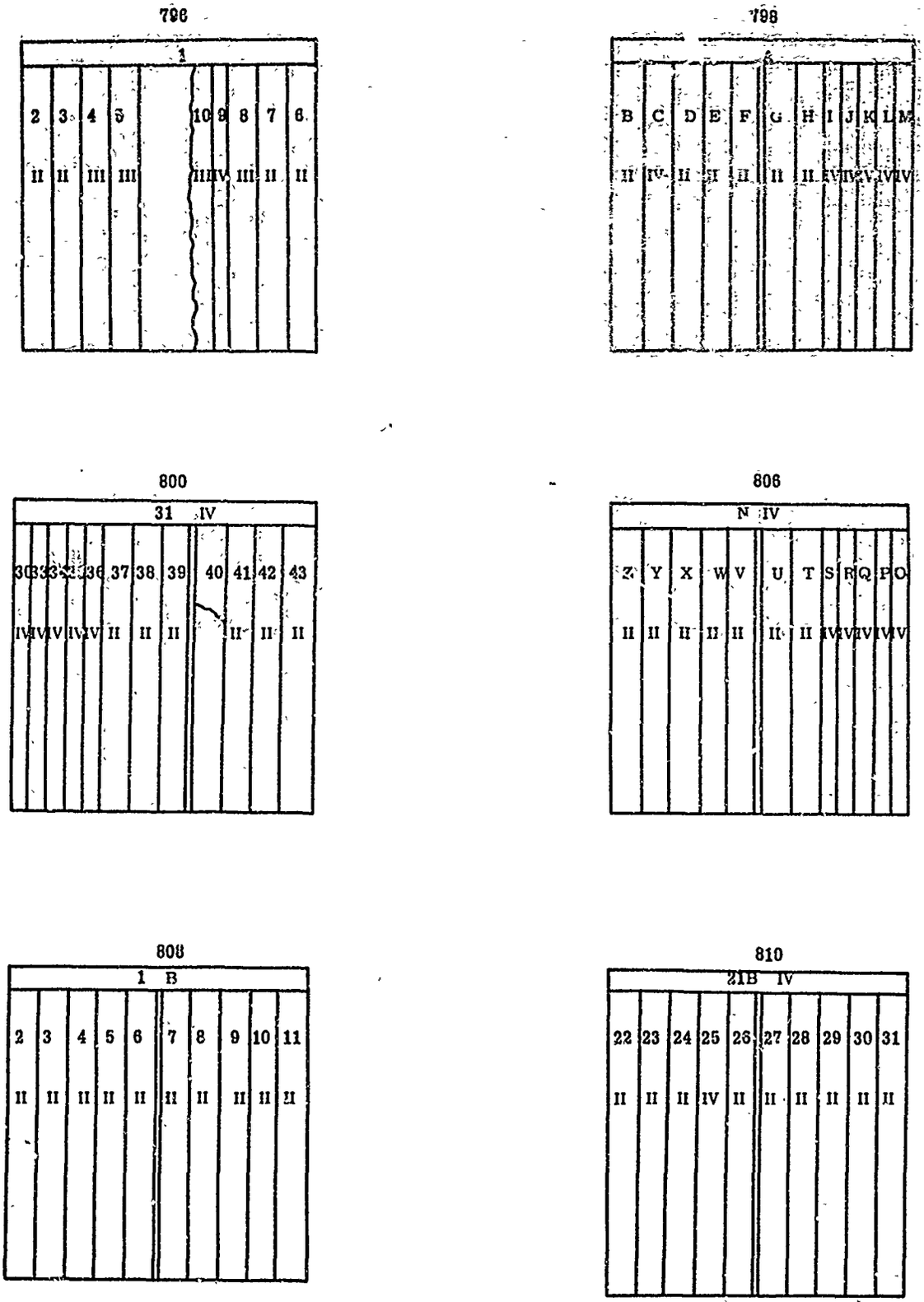

Note: All tiles are 12" x 12" x 1¼"

Figure 14. Cutting Plans for Alumina Tiles 796, 798, 800, 806, 808, and 810

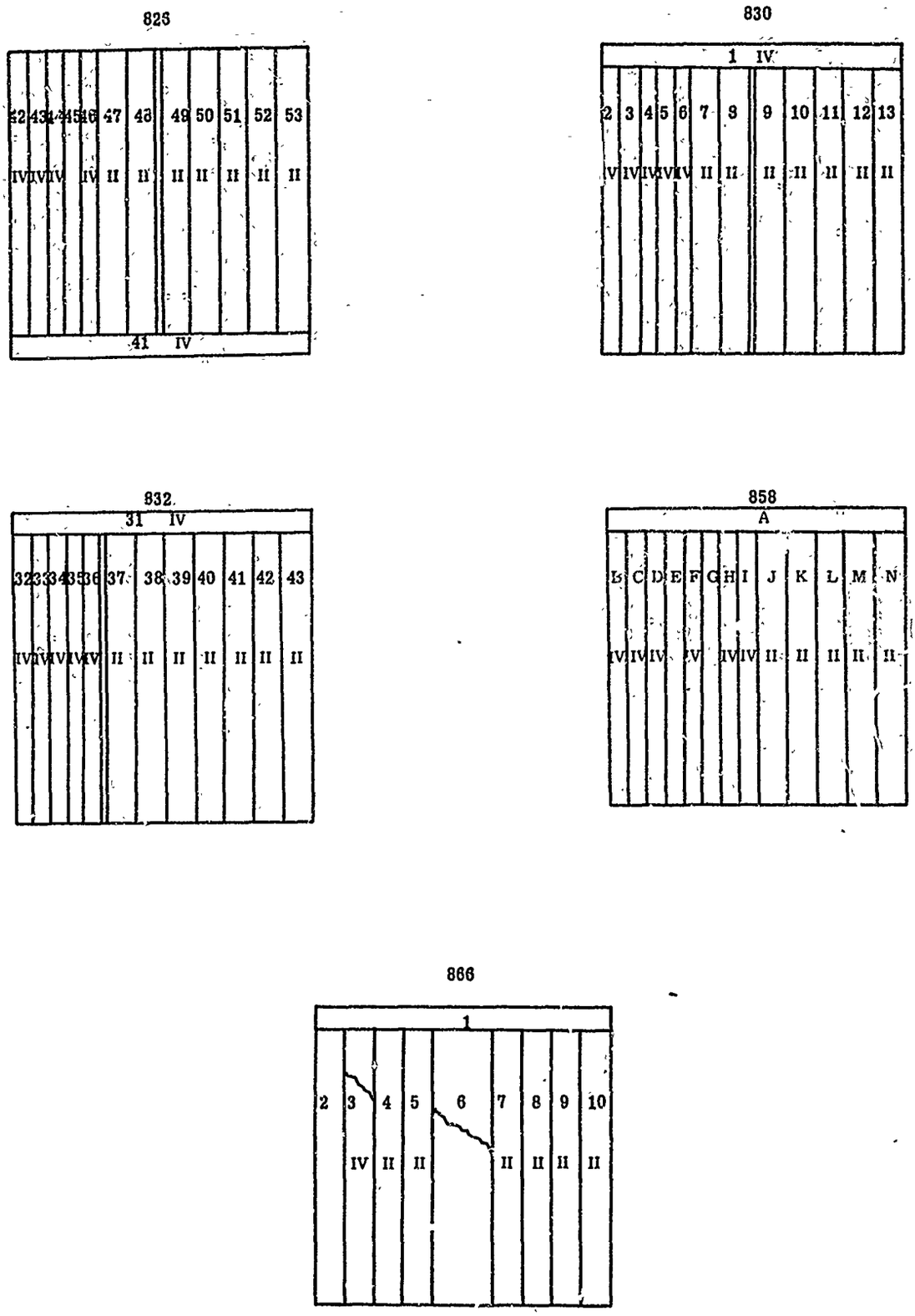

Note: All tiles are 12" x 12" x $1\frac{1}{8}$"

Figure 15. Cutting Plans for Alumina Tiles 828, 830, 832, 858, and 866

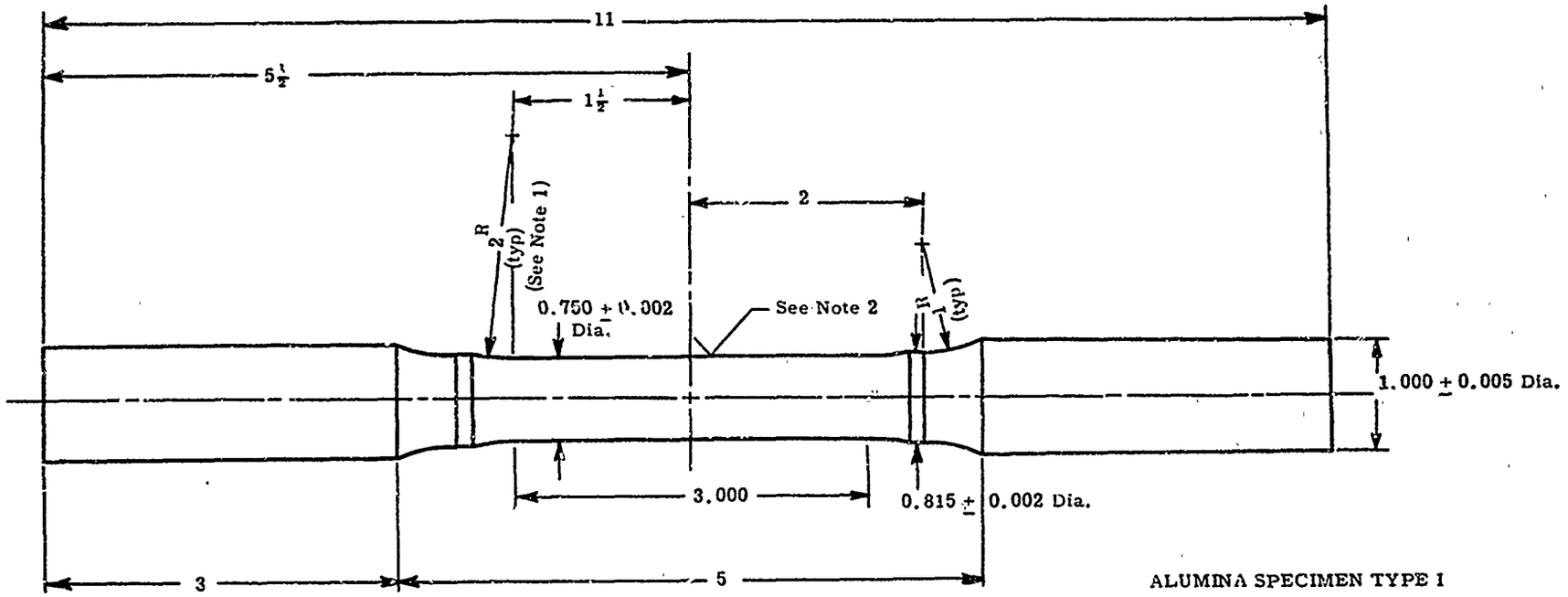

ALUMINA SPECIMEN TYPE I

Note:
1) Do Not Undercut Radii
2) Surface Finish to be Established on 1st Specimen (Approx. 10 RMS) and Held Within 5 RMS or Less on all Others
3) Do Not Handle Gage Portion of Specimen
4) All Diameters True and Concentric to Within 0.0005

Figure 16. Configuration of the Type I Alumina Specimen

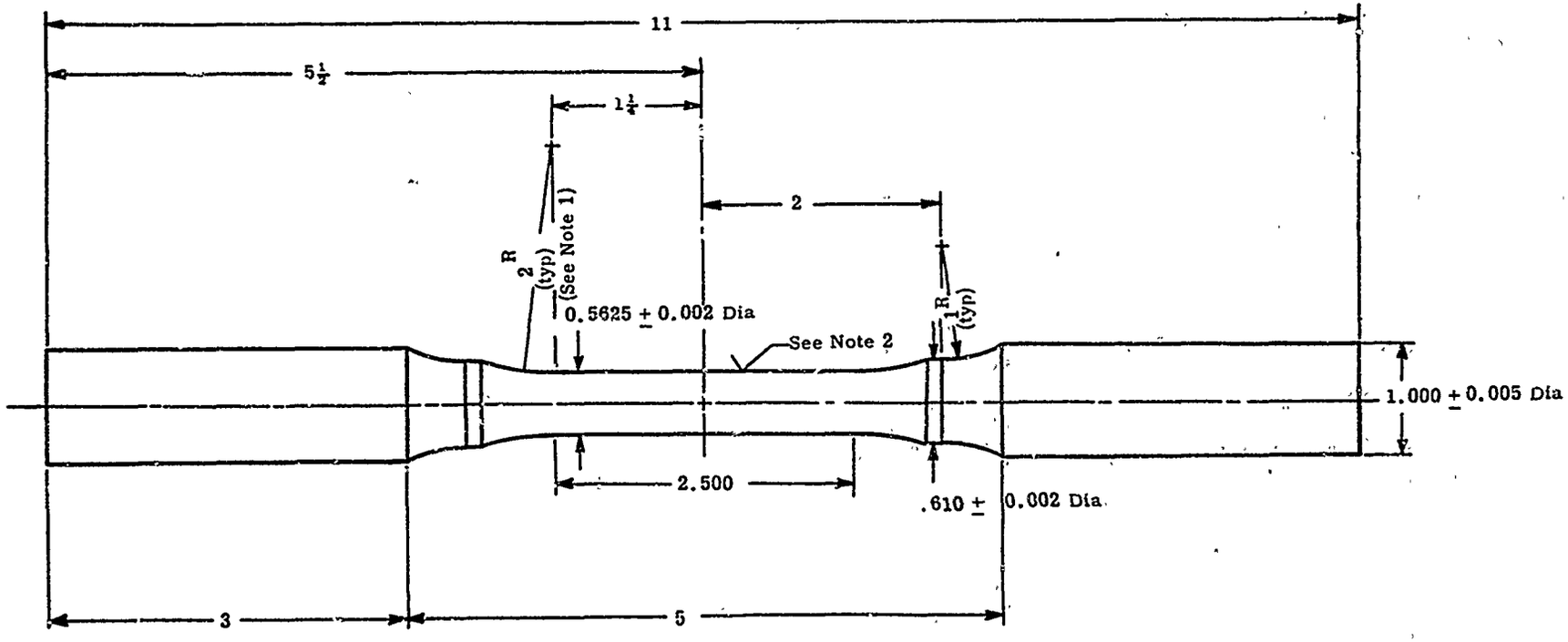

ALUMINA SPECIMEN TYPE II

Note:
1) Do Not Undercut Radii
2) Surface Finish to be Established on 1st Specimen (Approx. 10 RMS) and Held Within 5 RMS or Less on All Others
3) Do Not Handle Gage Portion of Specimen
4) All Diameters True and Concentric to Within 0.0005

Figure 17. Configuration of Type II Alumina Specimen

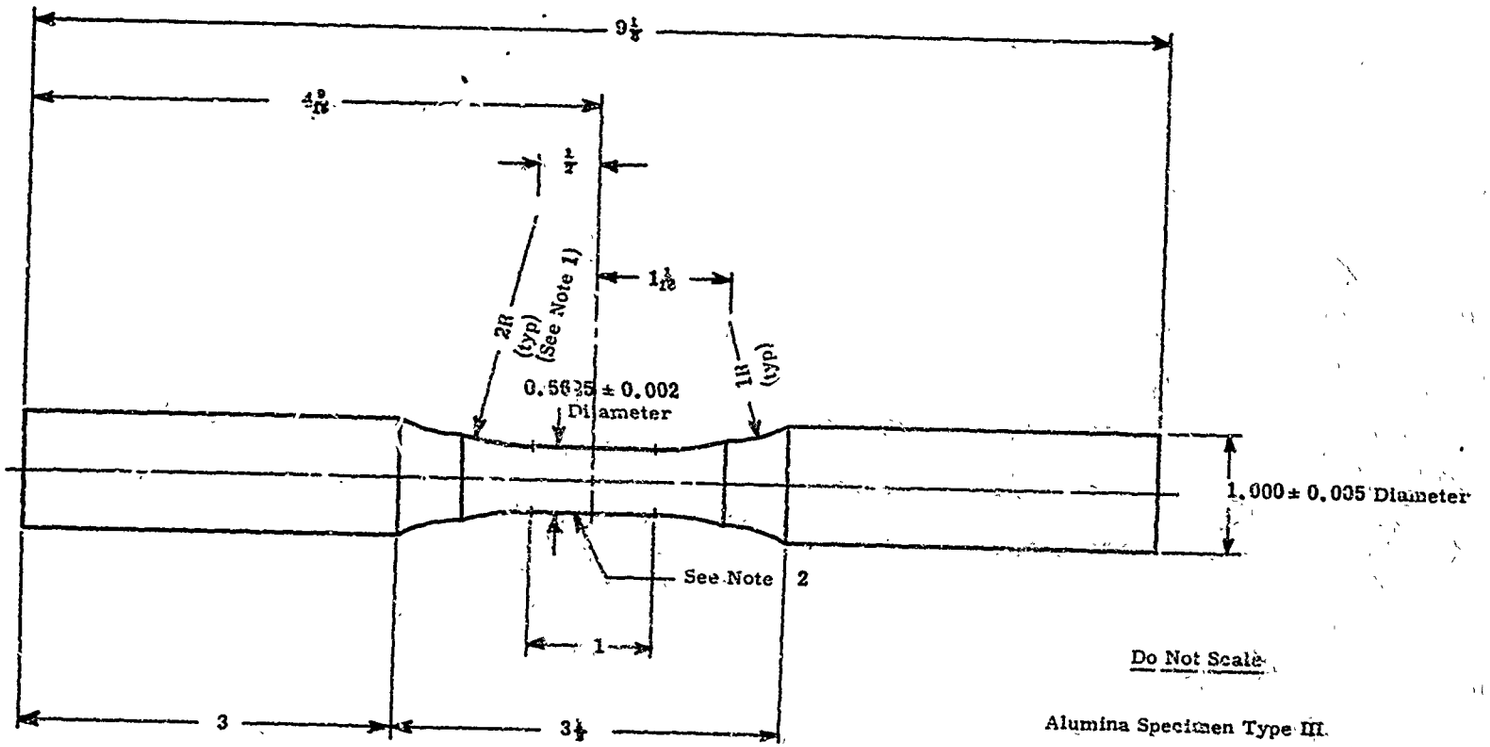

Do Not Scale

Alumina Specimen Type III

Note:

1. Do not undercut radii.
2. Surface finish to be established on 1st specimen (approximately 10 rms) and held within 5 rms or less on all others.
3. Do not handle gage portion of specimen.
4. All diameters true and concentric to within 0.0005.

Figure 18. Configuration of the Type III Alumina Specimen

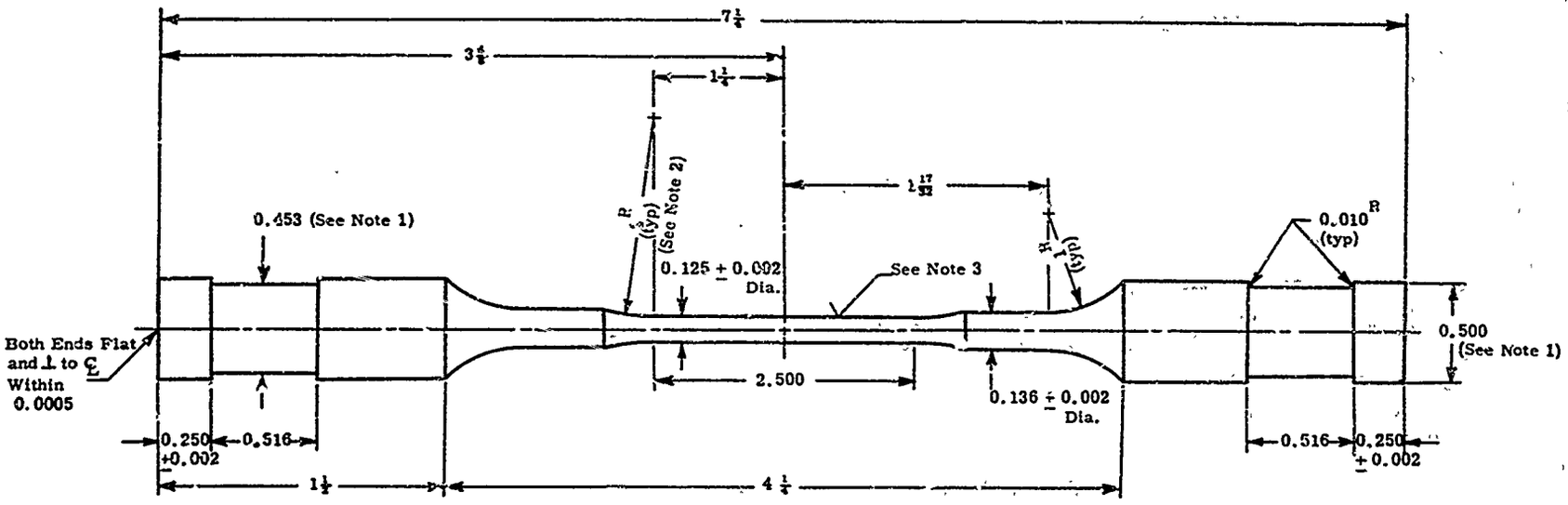

ALUMINA SPECIMEN TYPE IV

Note:
1) Fit to Furnished Compression Ring and And Nut Within 0.0005
2) Do Not Undercut in Radii
3) Surface Finish to be Established on 1st Specimen (Approx. 10 RMS) and Held Within 5 RMS or Less on All Others
4) Do Not Handle Gage Portion of Specimen
5) All Diameters True and Concentric to Within 0.0005

Figure 19. Configuration of the Type IV Alumina Specimen

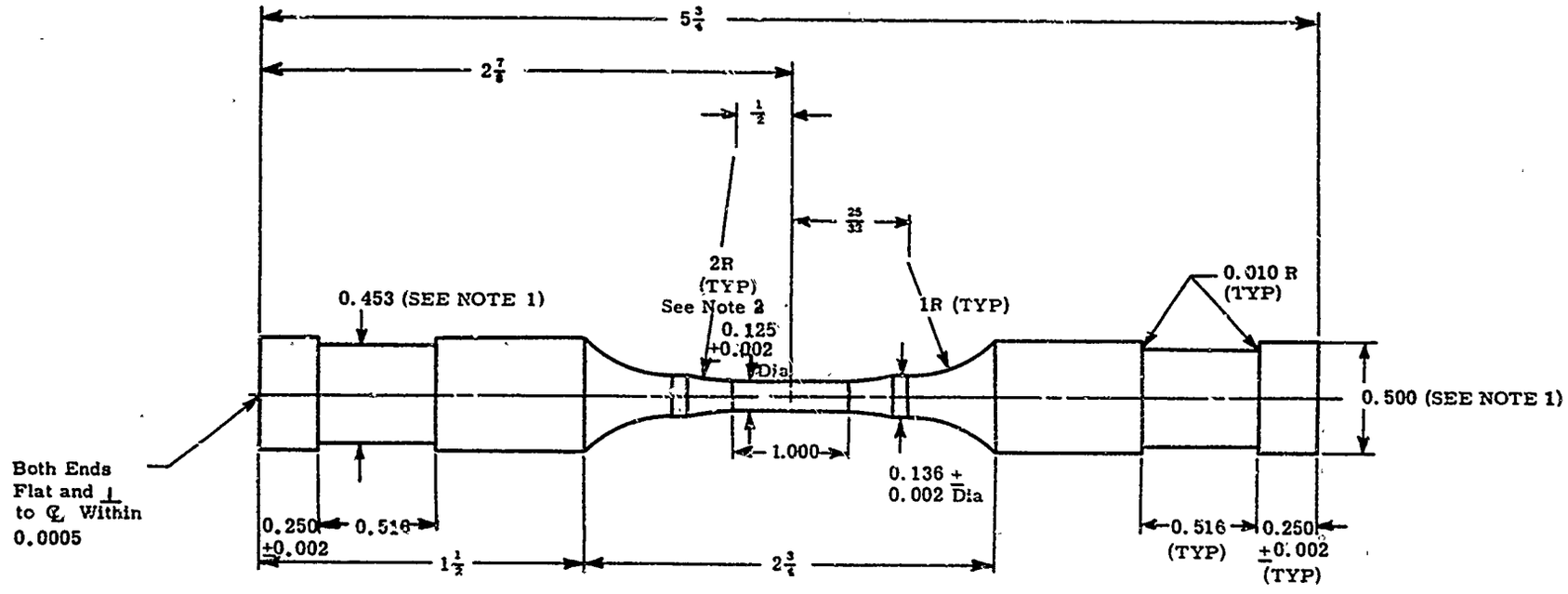

ALUMINA SPECIMEN TYPE V

Note:

1) Fit to Furnished Compression Ring and Nut within 0.0005
2) Do Not Undercut Radii
3) Surface Finish to be Established on 1st Specimen (Approximately 10 RMS) and Held within 5 RMS or Less on All Others
4) Do Not Handle Gage Portion of Specimen
5) All Diameters True and Concentric to within 0.0005

Figure 20. Configuration of the Type V Alumina Specimen

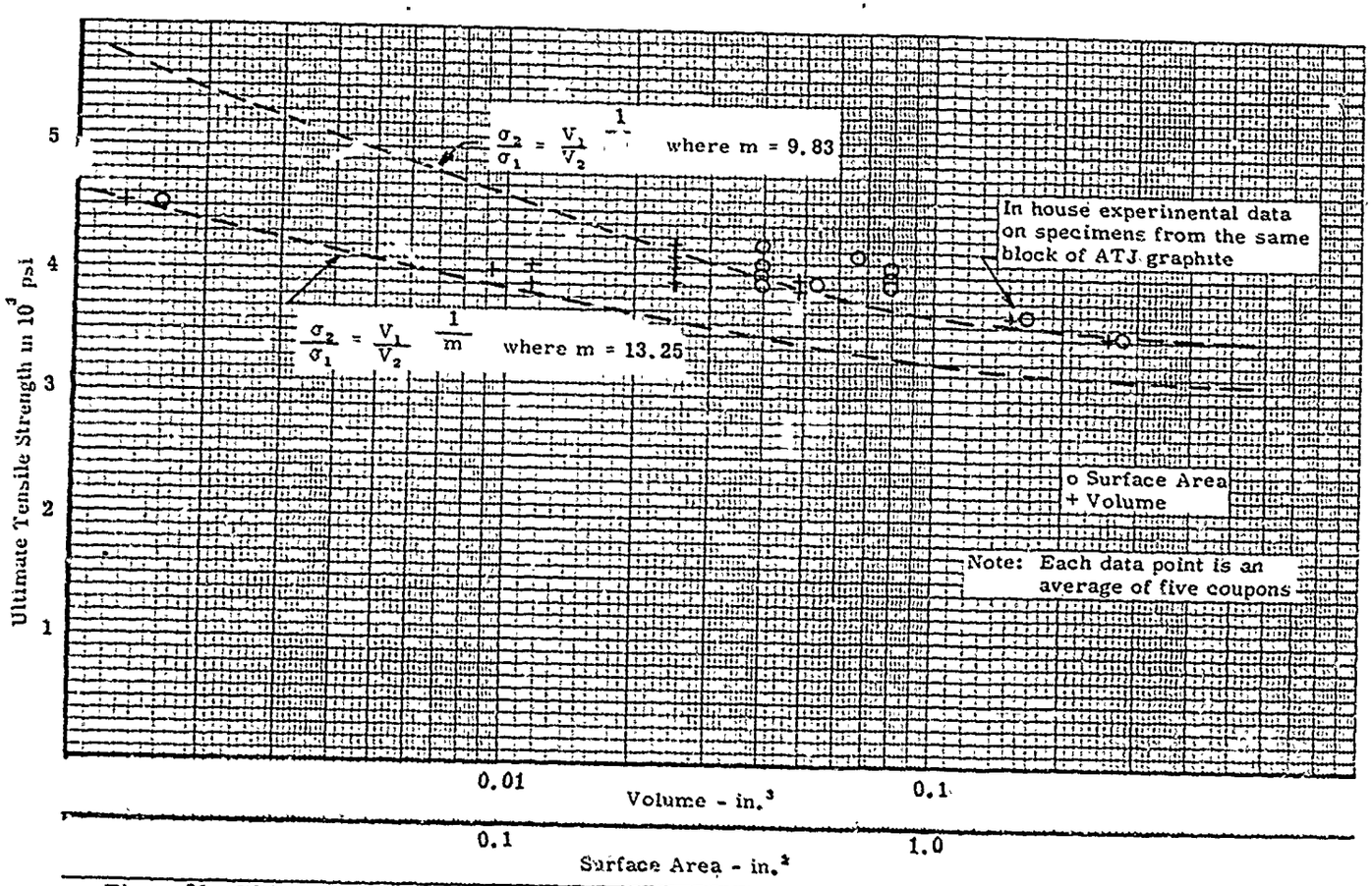

Figure 21. Ultimate Tensile Strength versus Gage Volume and Gage Surface Area for with Grain ATJ Graphite

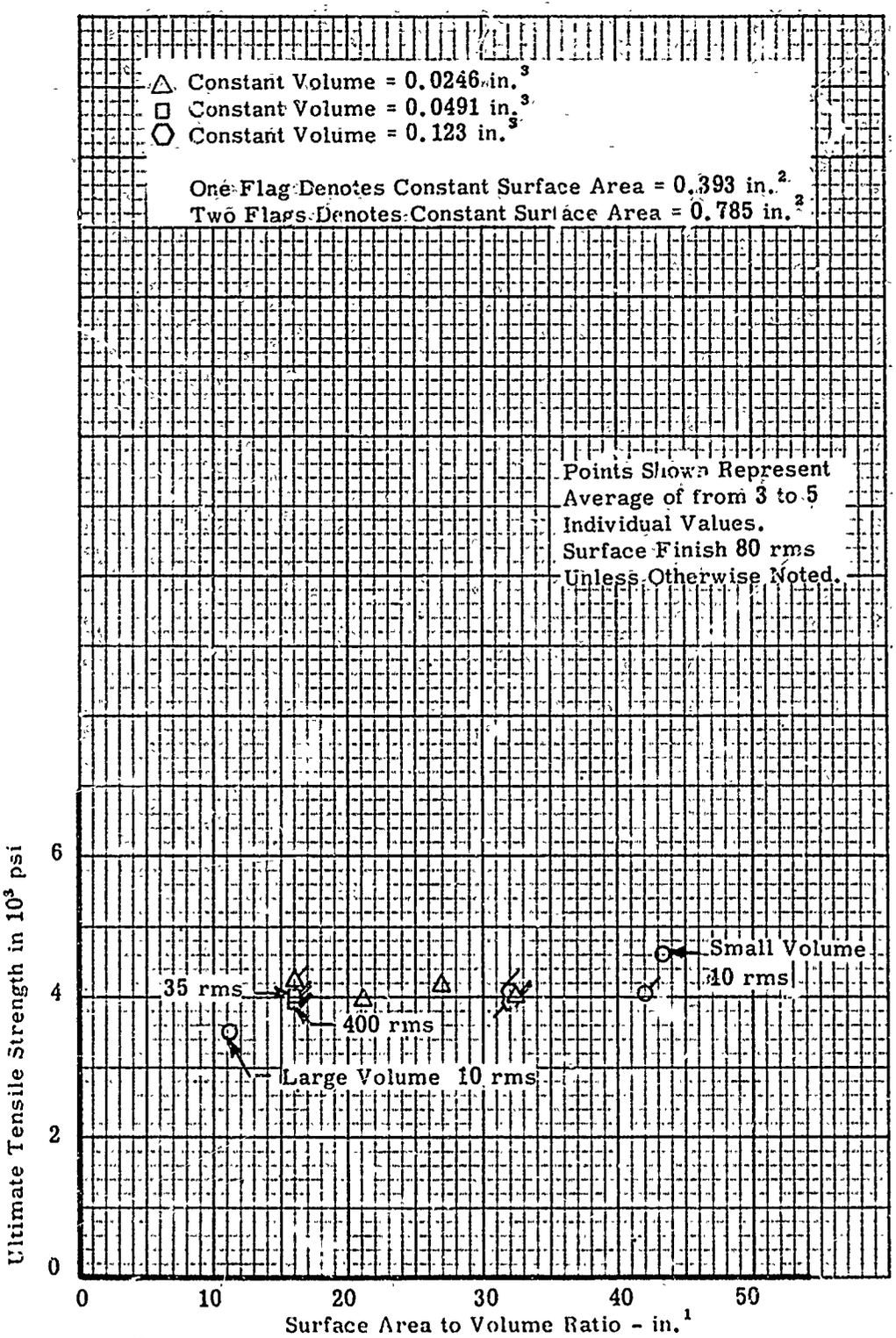

Figure 22. Ultimate Tensile Strength versus Gage Surface Area to Volume Ratio for With Grain ATJ Graphite

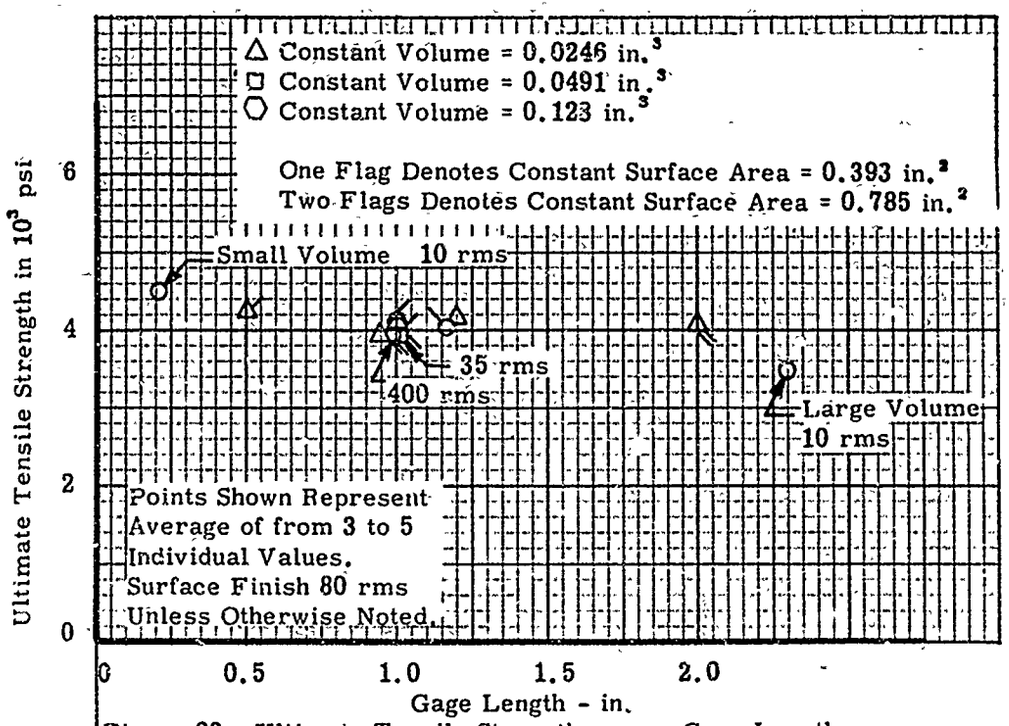

Figure 23. Ultimate Tensile Strength versus Gage Length for With Grain ATJ Graphite

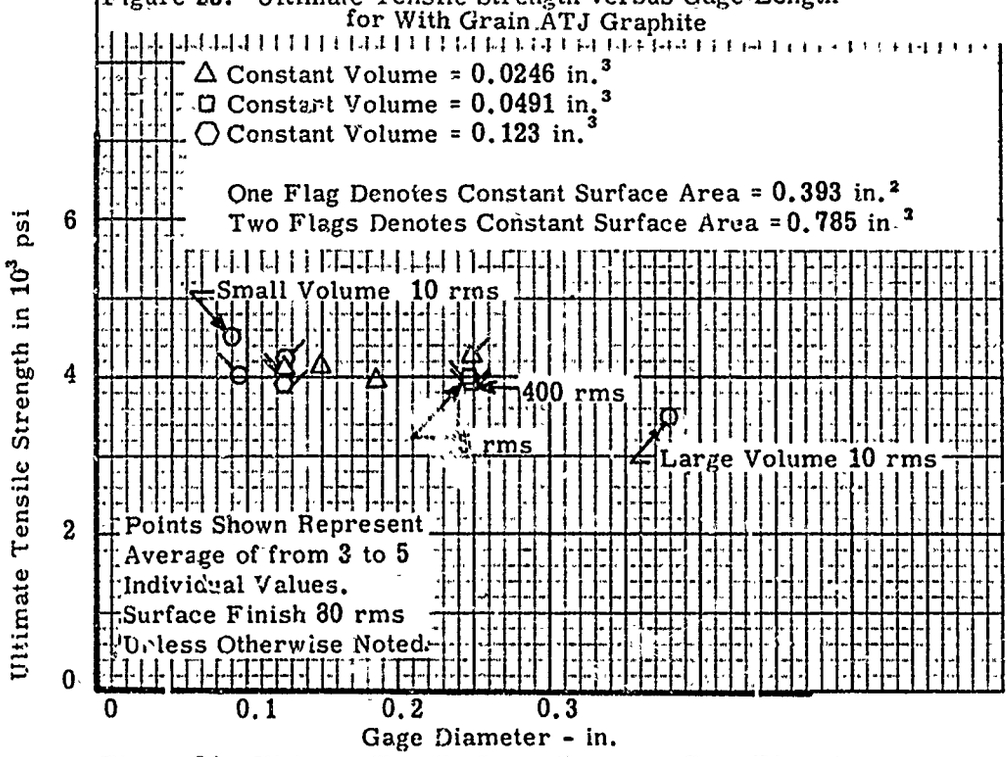

Figure 24. Ultimate Tensile Strength versus Gage Diameter for With Grain ATJ Graphite

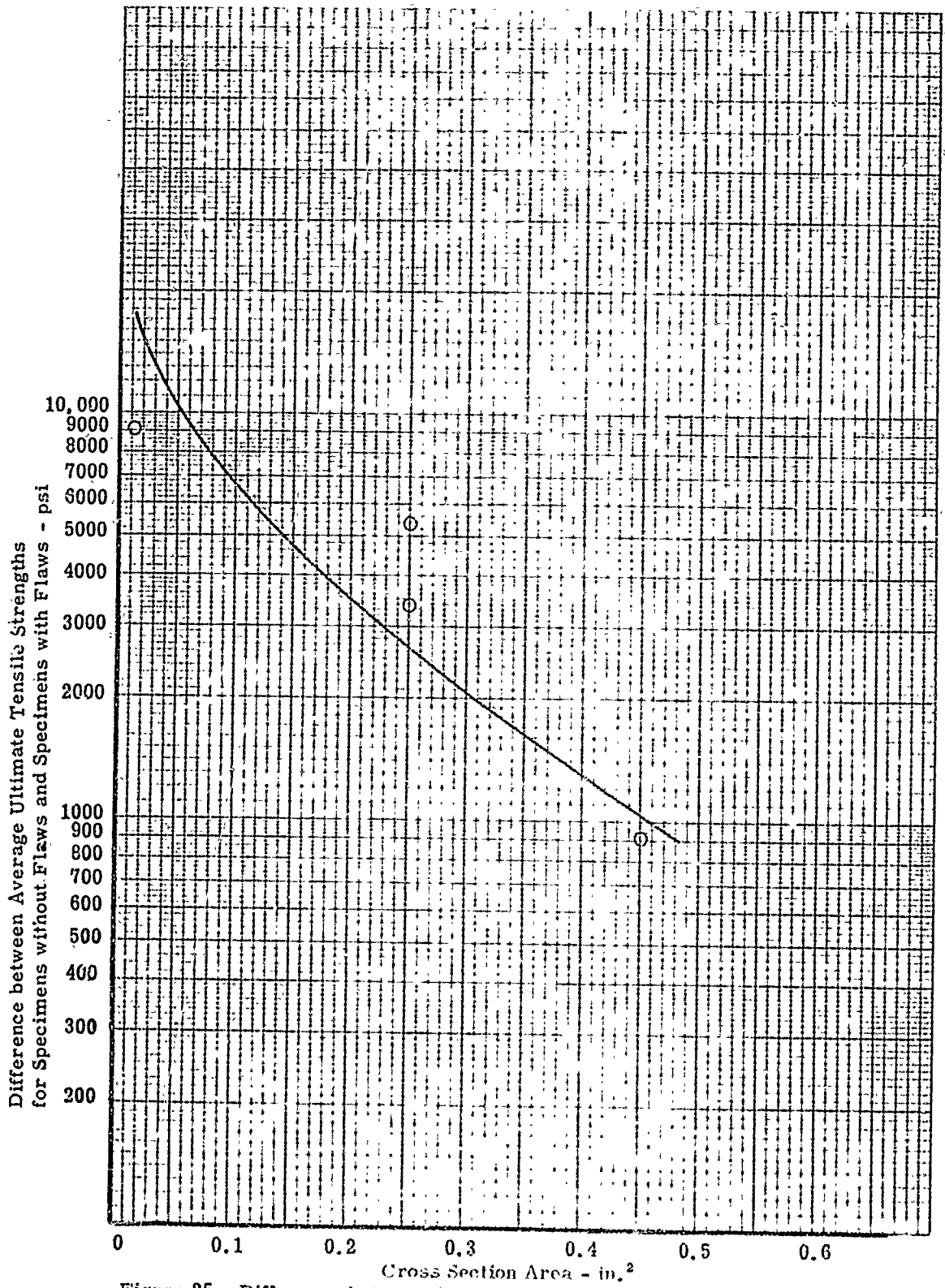

Figure 25. Difference between Average Ultimate Tensile Strength for Specimens without Flaws and Specimens with Flaws versus Cross-Sectional Area for Alumina Specimens

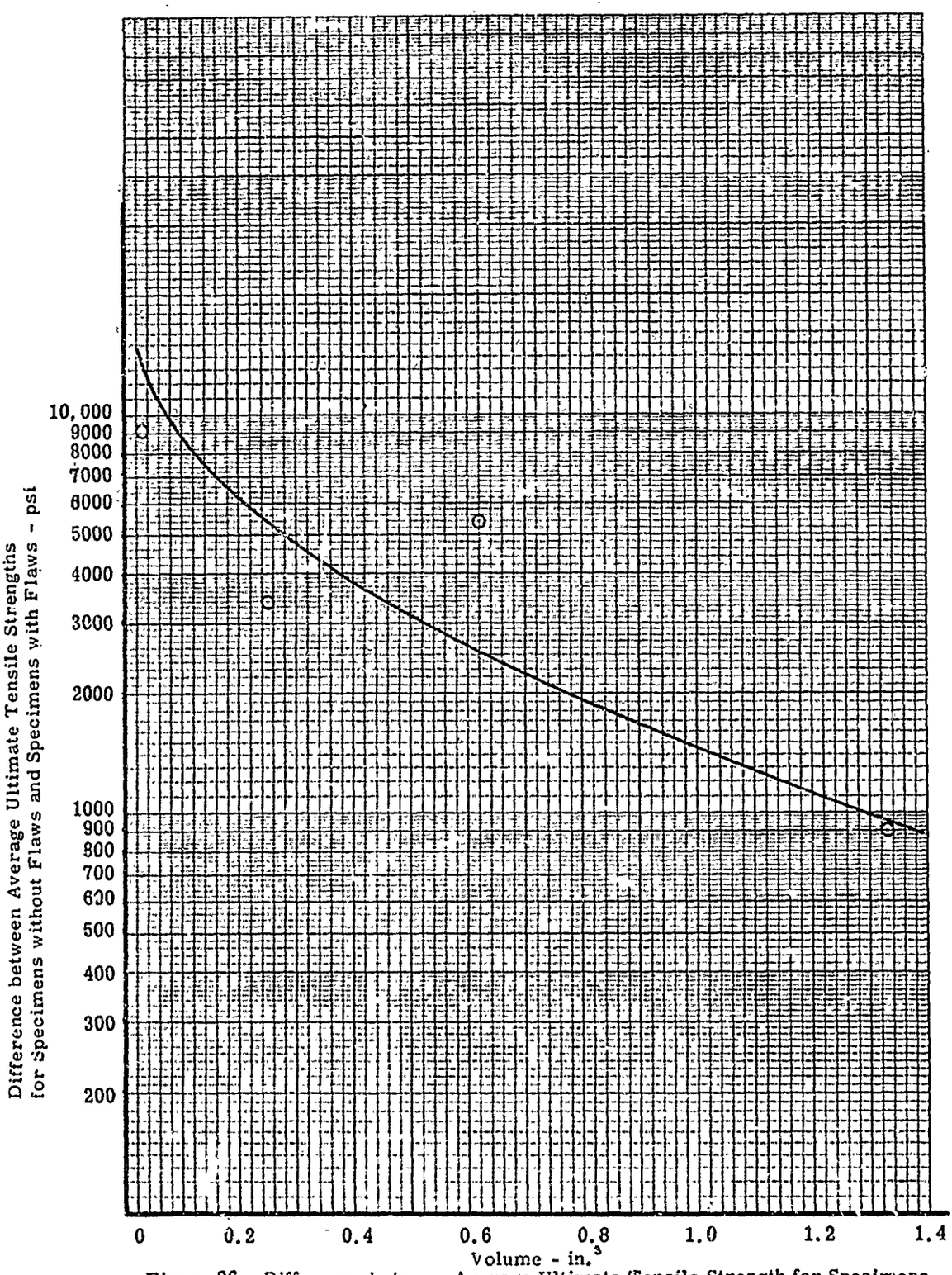

Figure 26. Difference between Average Ultimate Tensile Strength for Specimens without Flaws and Specimens with Flaws versus Volume for Alumina Specimens

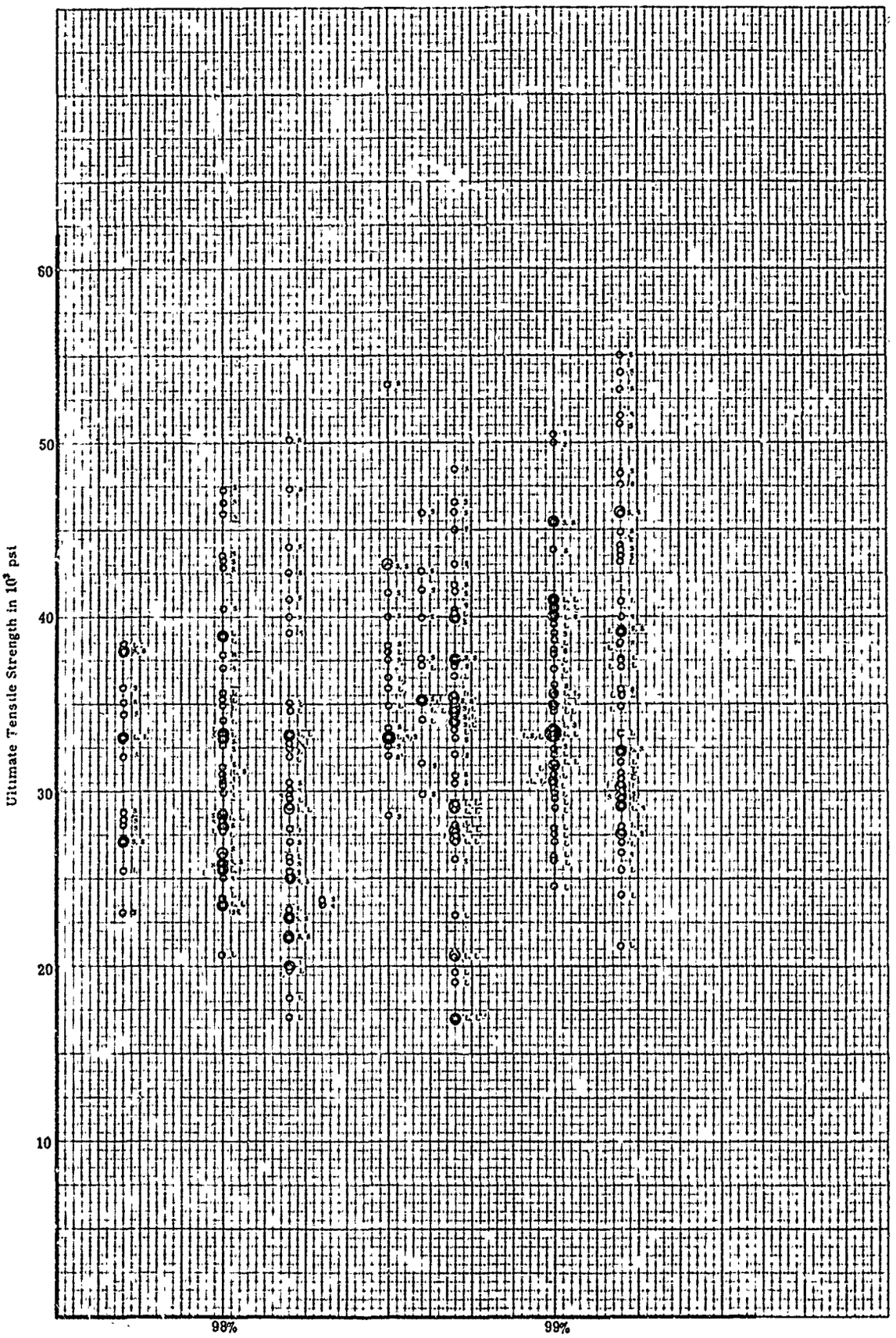

Figure 27. Ultimate Tensile Strength versus Percent Theoretical Density for All Alumina Data

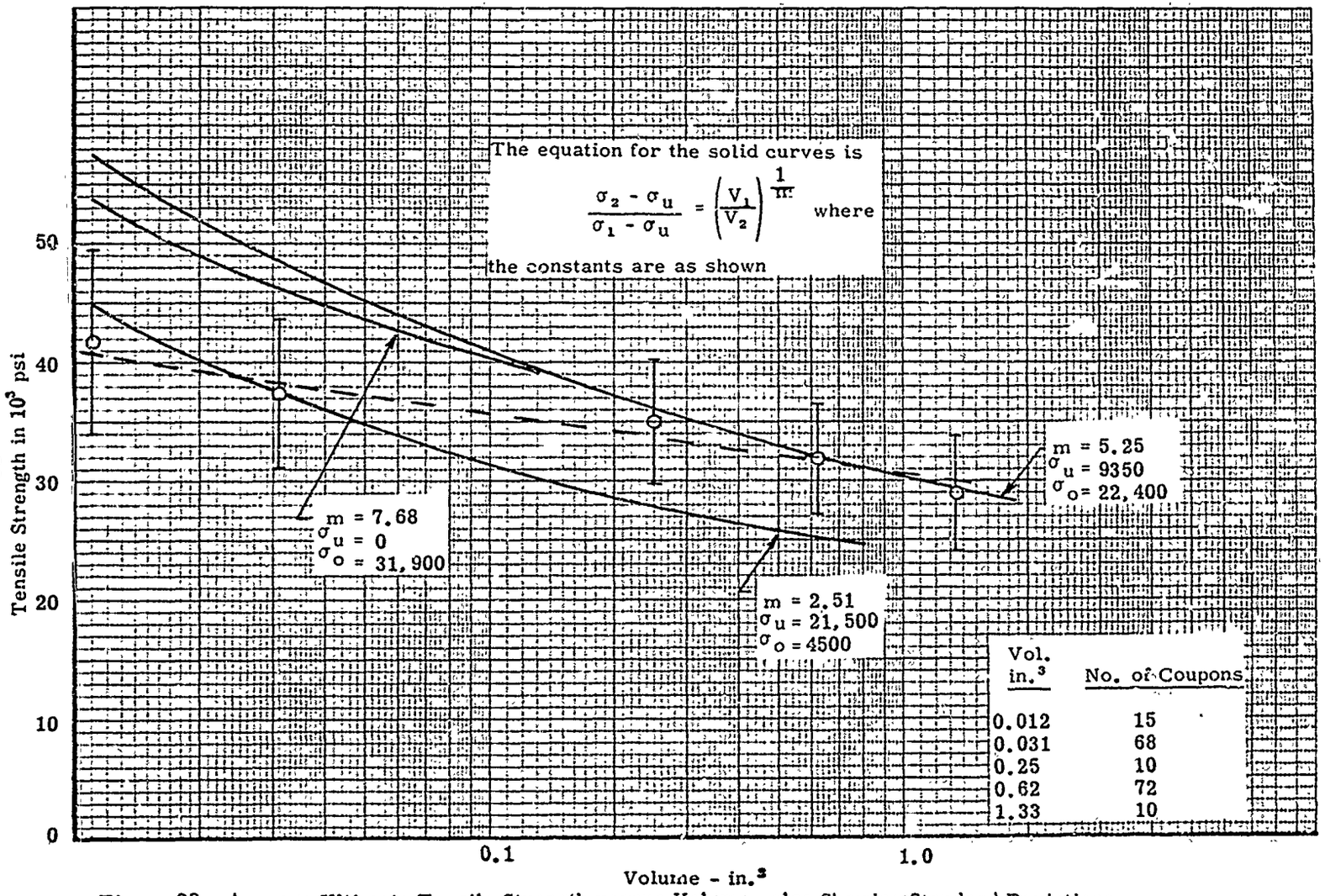

Figure 28. Average Ultimate Tensile Strength versus Volume, also Showing Standard Deviations, for the Culled Alumina Data

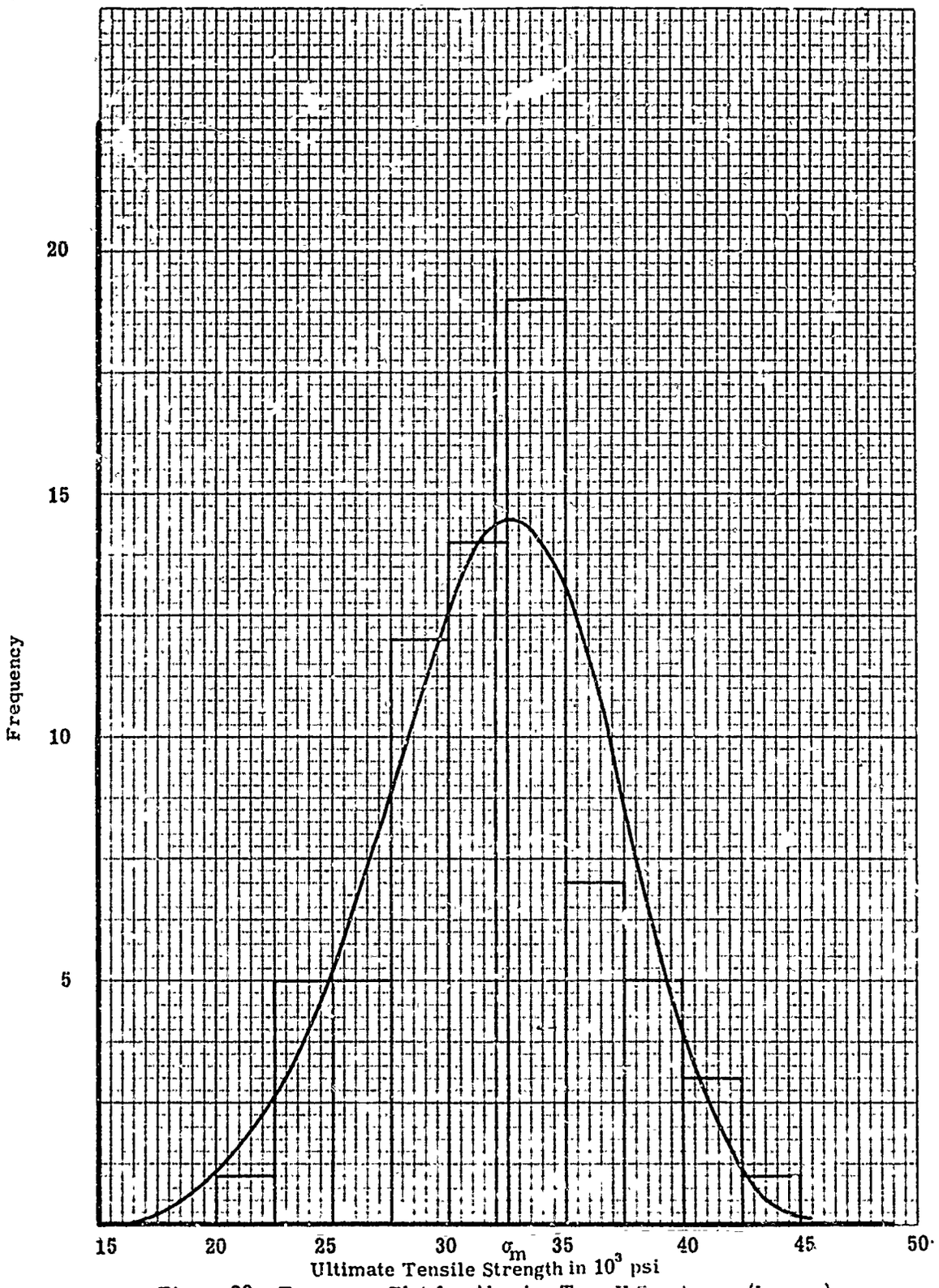

Figure 29. Frequency Plot for Alumina Type II Specimens (Larger)

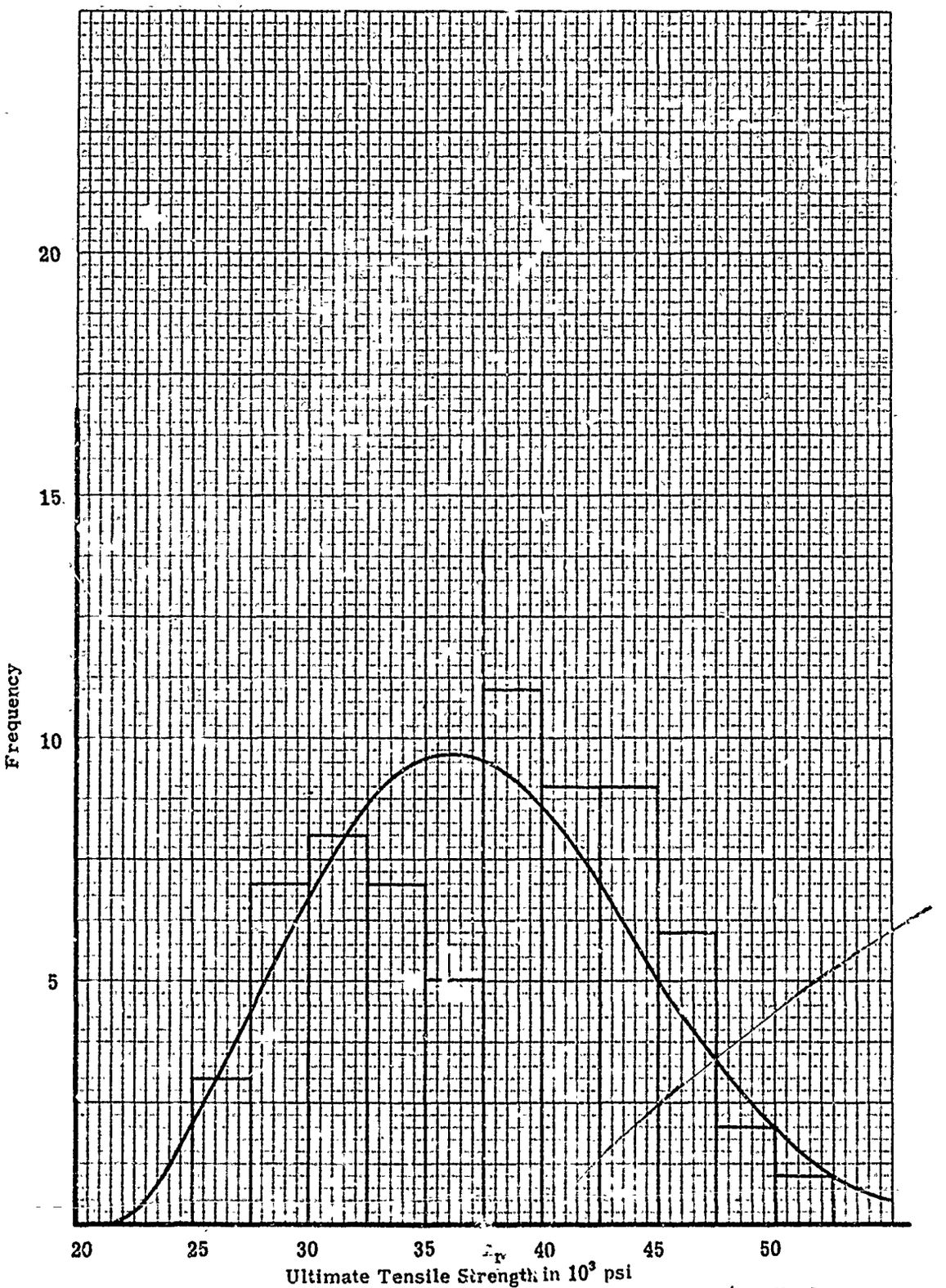

Figure 30. Frequency Plot for Alumina Type IV Specimens (Smaller)

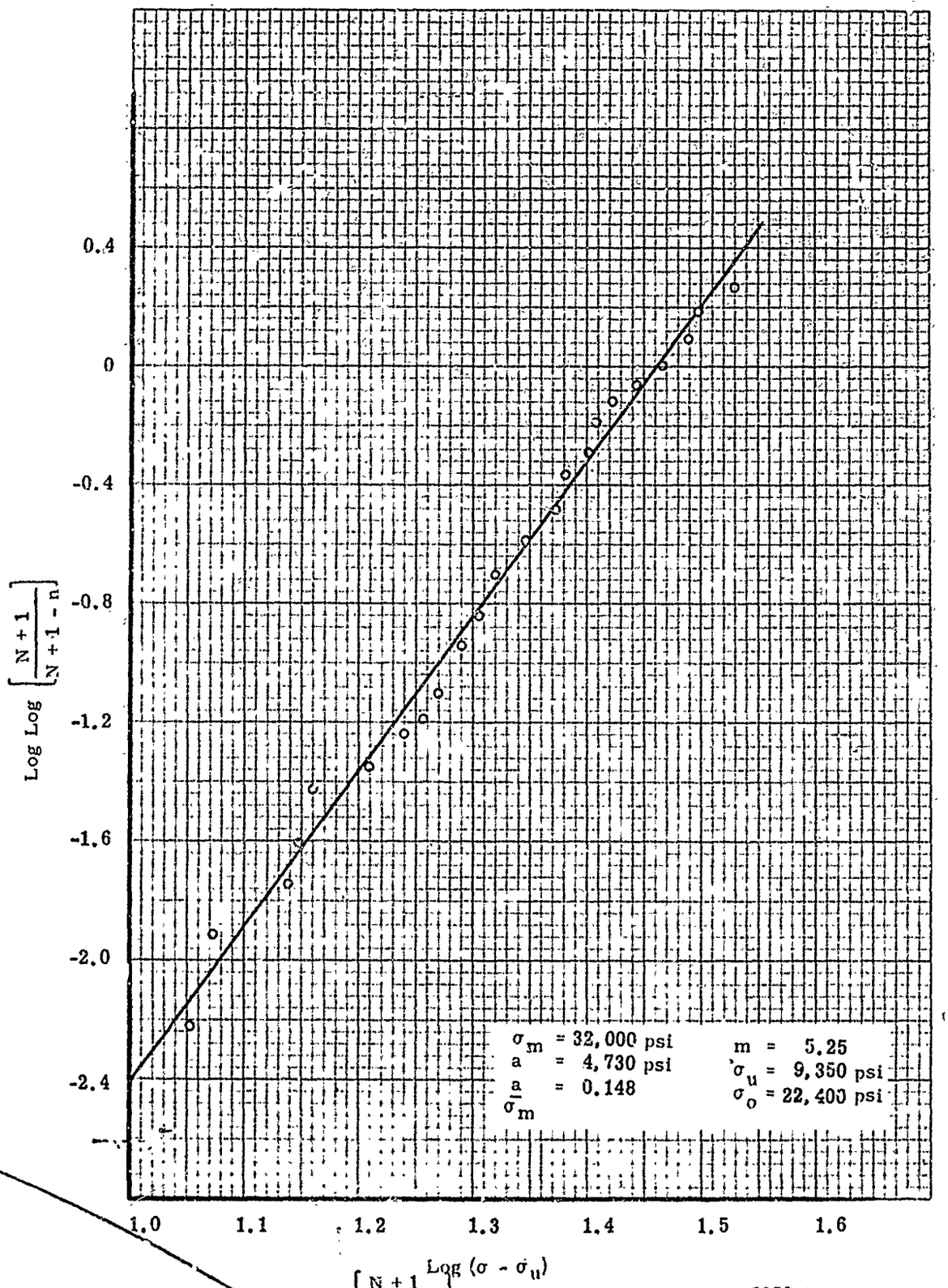

Figure 31. Log Log $\left[\frac{N+1}{N+1-n}\right]$ versus Log $(\sigma - \sigma_u)$ with σ_u = 9350 for Type II Alumina Specimens

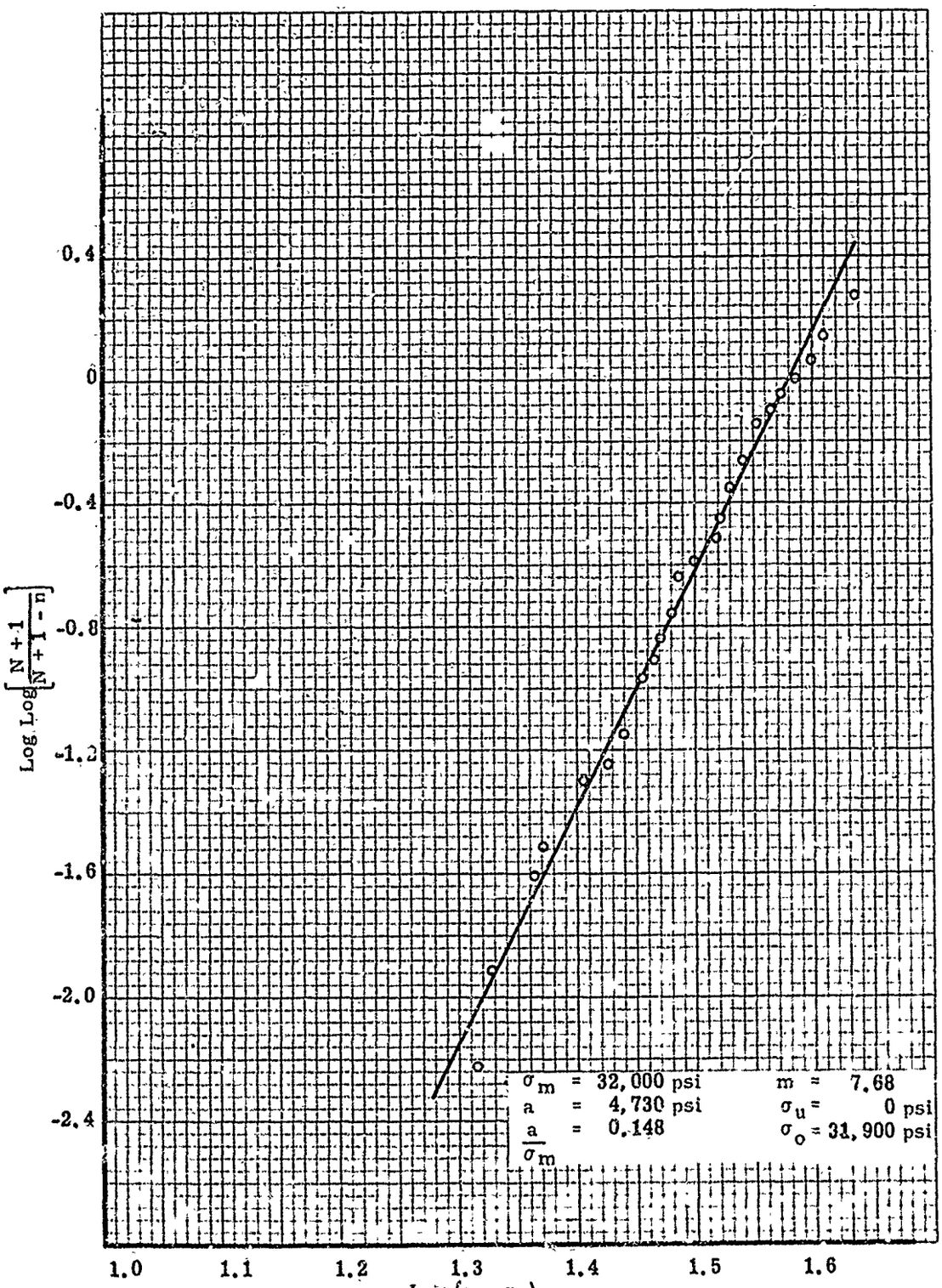

Figure 32. Log Log $\left[\frac{N+1}{N+1-n}\right]$ versus Log $(\sigma - \sigma_u)$ with σ_u = C for Type II Alumina Specimens

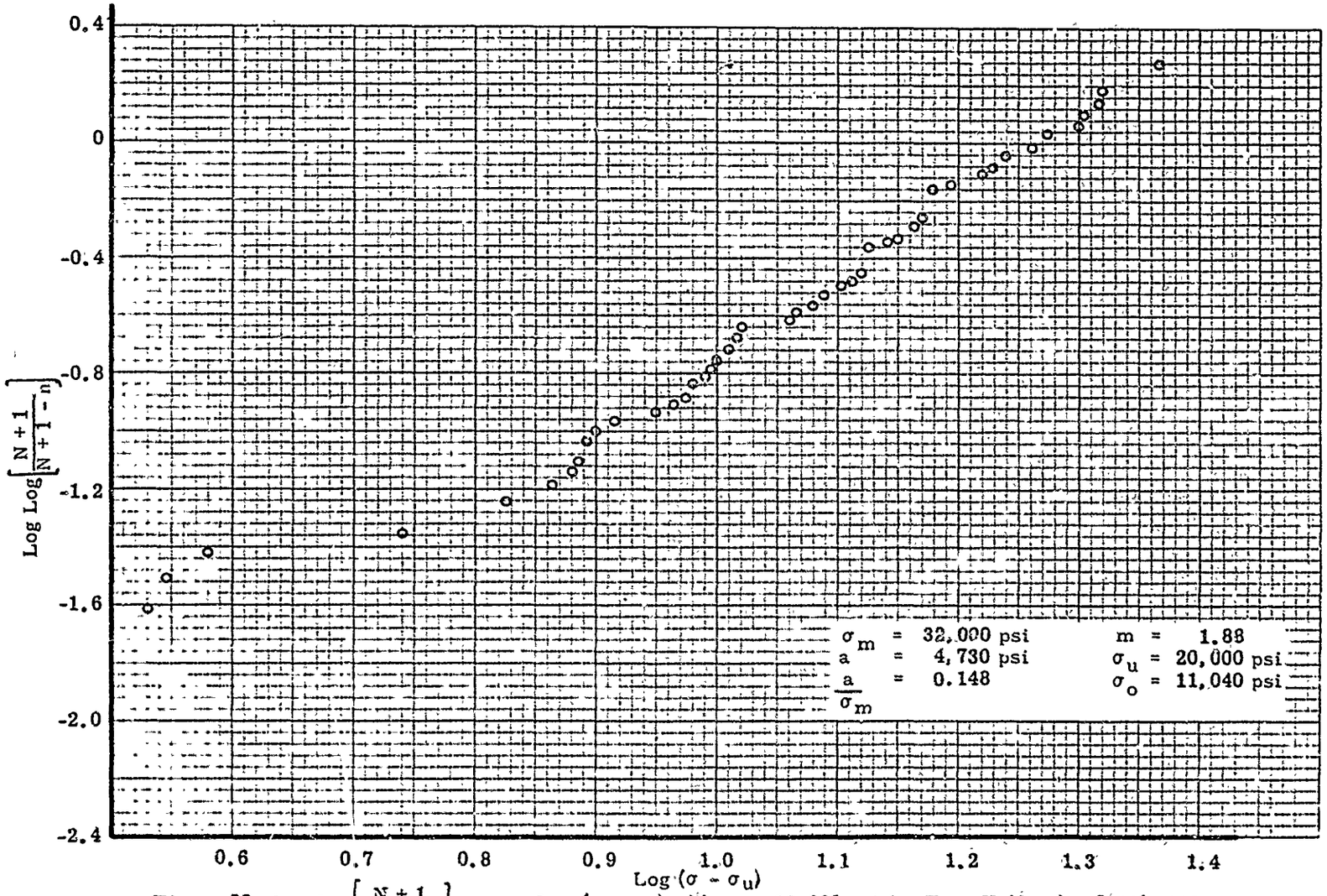

Figure 33. Log Log $\left[\frac{N+1}{N+1-n}\right]$ versus Log $(\sigma - \sigma_u)$ with σ_u = 20,000 psi for Type II Alumina Specimens

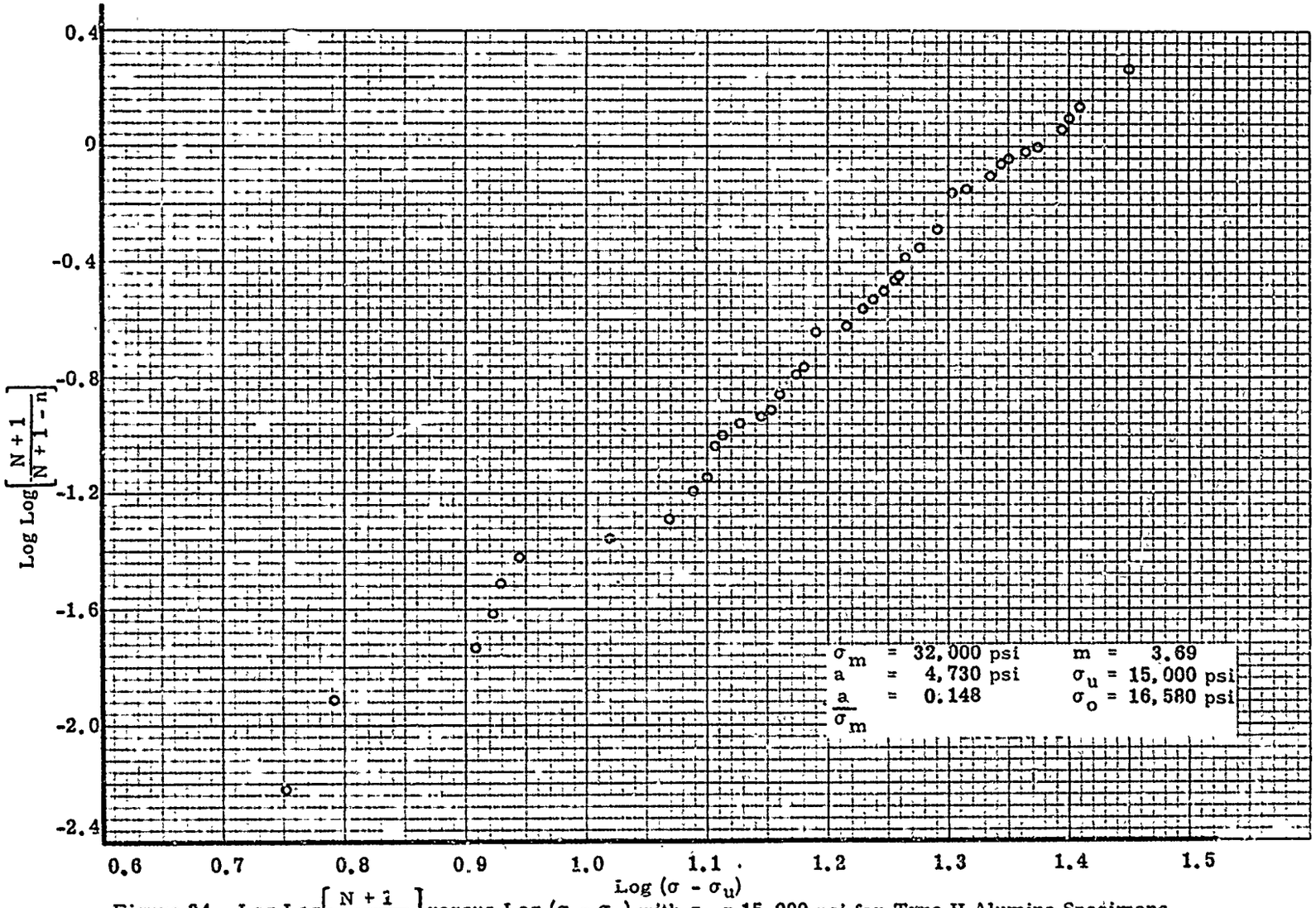

Figure 34. Log Log $\left[\frac{N+1}{N+1-n}\right]$ versus Log $(\sigma - \sigma_u)$ with σ_u = 15,000 psi for Type II Alumina Specimens

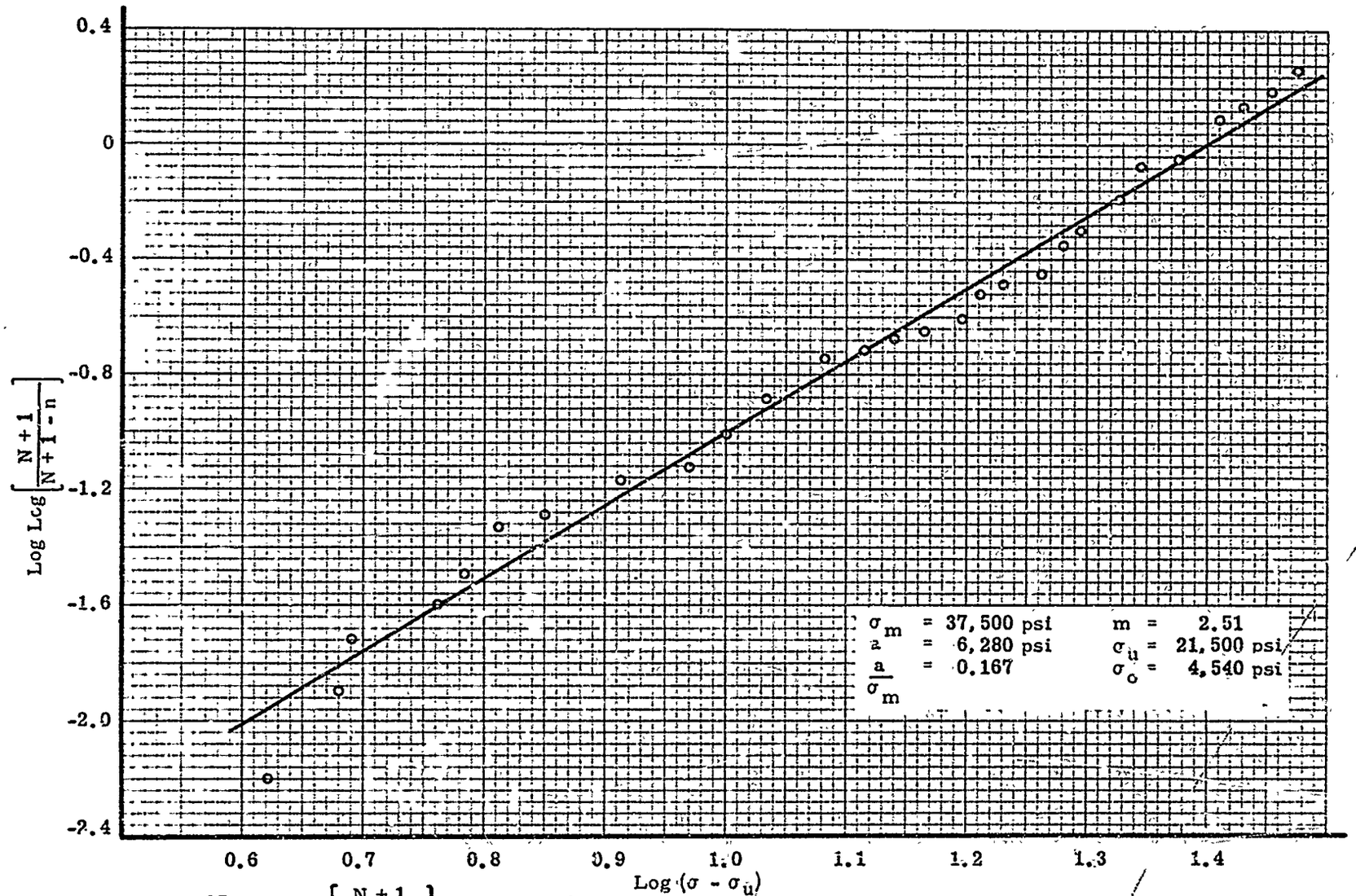

Figure 35. Log Log$\left[\frac{N+1}{N+1-n}\right]$ versus Log $(\sigma - \sigma_u)$ with σ_u = 21,500 for Type IV Alumina Specimens

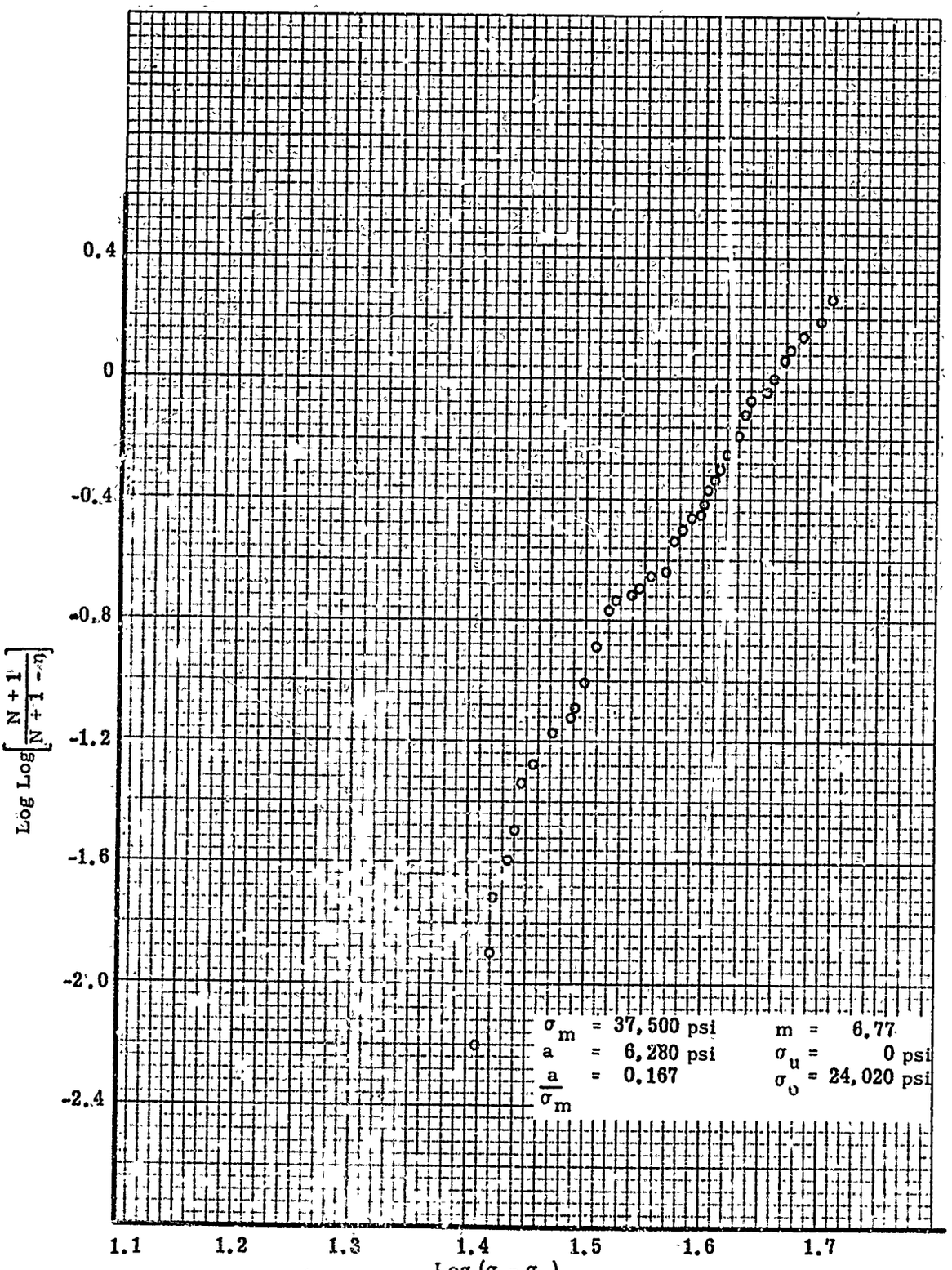

Figure 36. Log Log $\left\{\frac{N+1}{N+1-n}\right\}$ versus Log $(\sigma - \sigma_u)$ with $\sigma_u = 0$ for Type IV Alumina Specimens

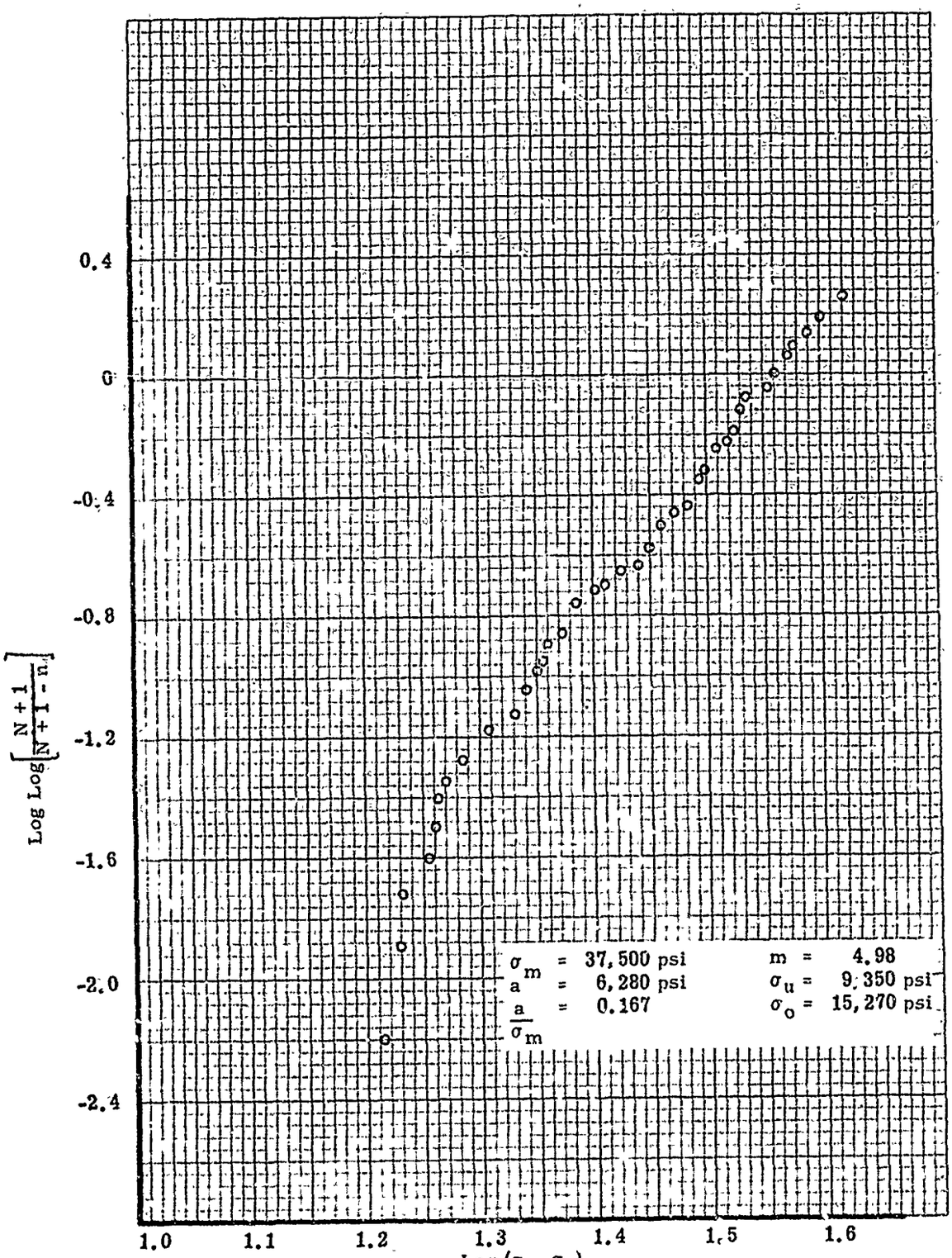

Figure 37. Log Log $\left[\frac{N+1}{N+1-n}\right]$ versus Log $(\sigma - \sigma_u)$ with σ_u = 9350 psi for Type IV Alumina Specimens

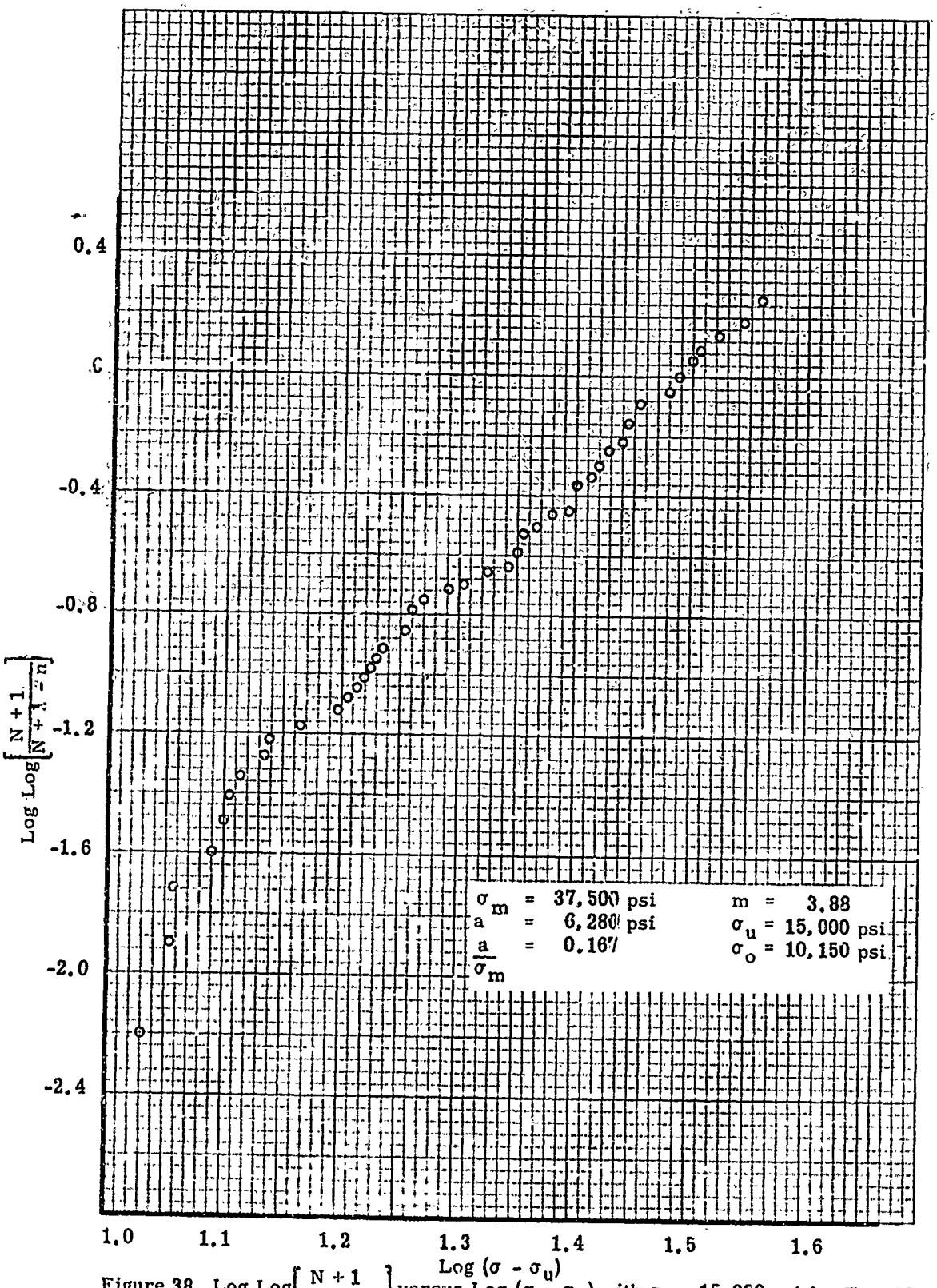

Figure 38. Log Log $\left[\frac{N+1}{N+1-n}\right]$ versus Log $(\sigma - \sigma_u)$ with σ_u = 15,000 psi for Type IV Alumina Specimens

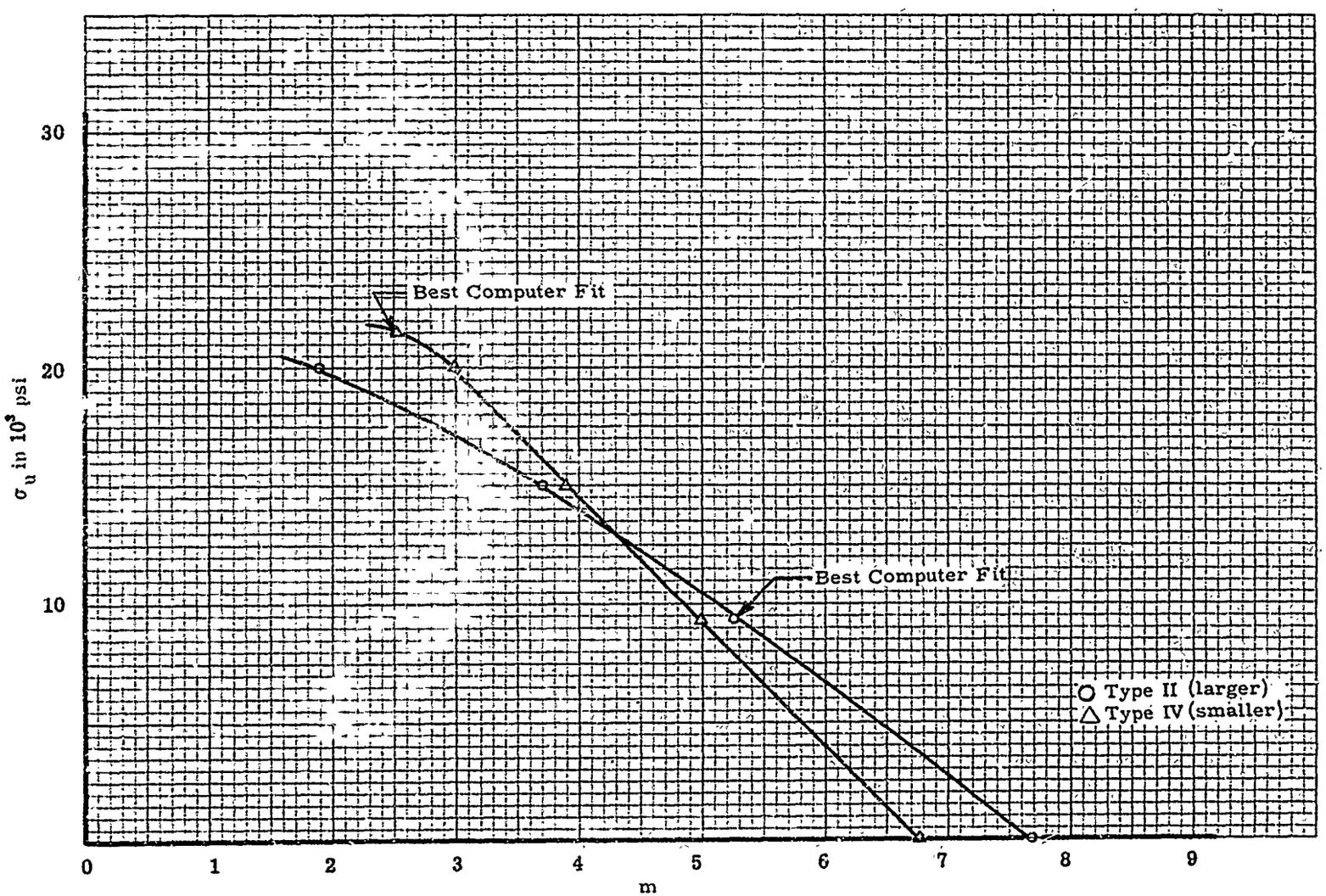

Figure 39. σ_u versus m for Type II and Type IV Alumina Specimens

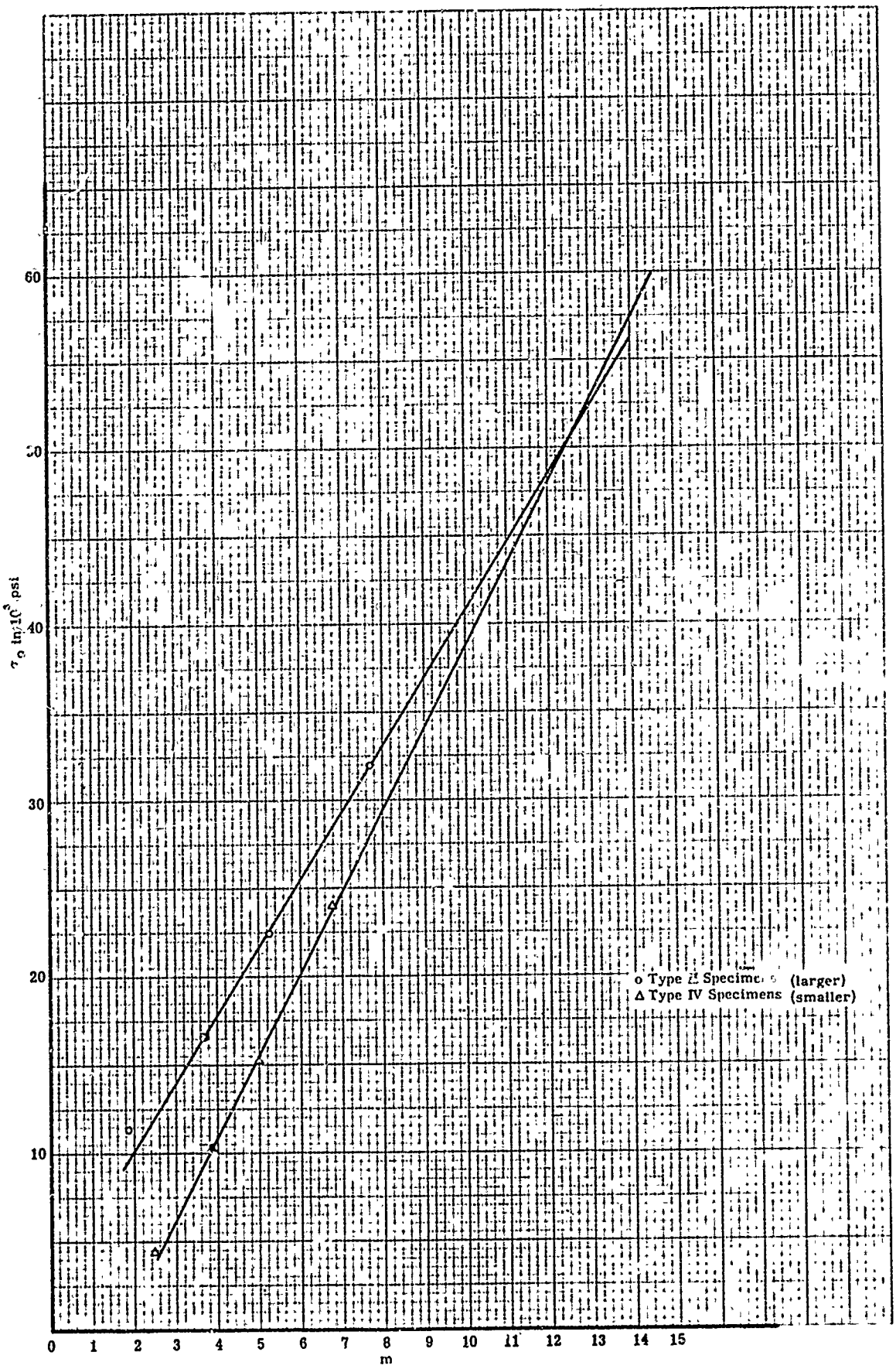

Figure 40. σ_o versus m for Type II and Type IV Alumina Specimens

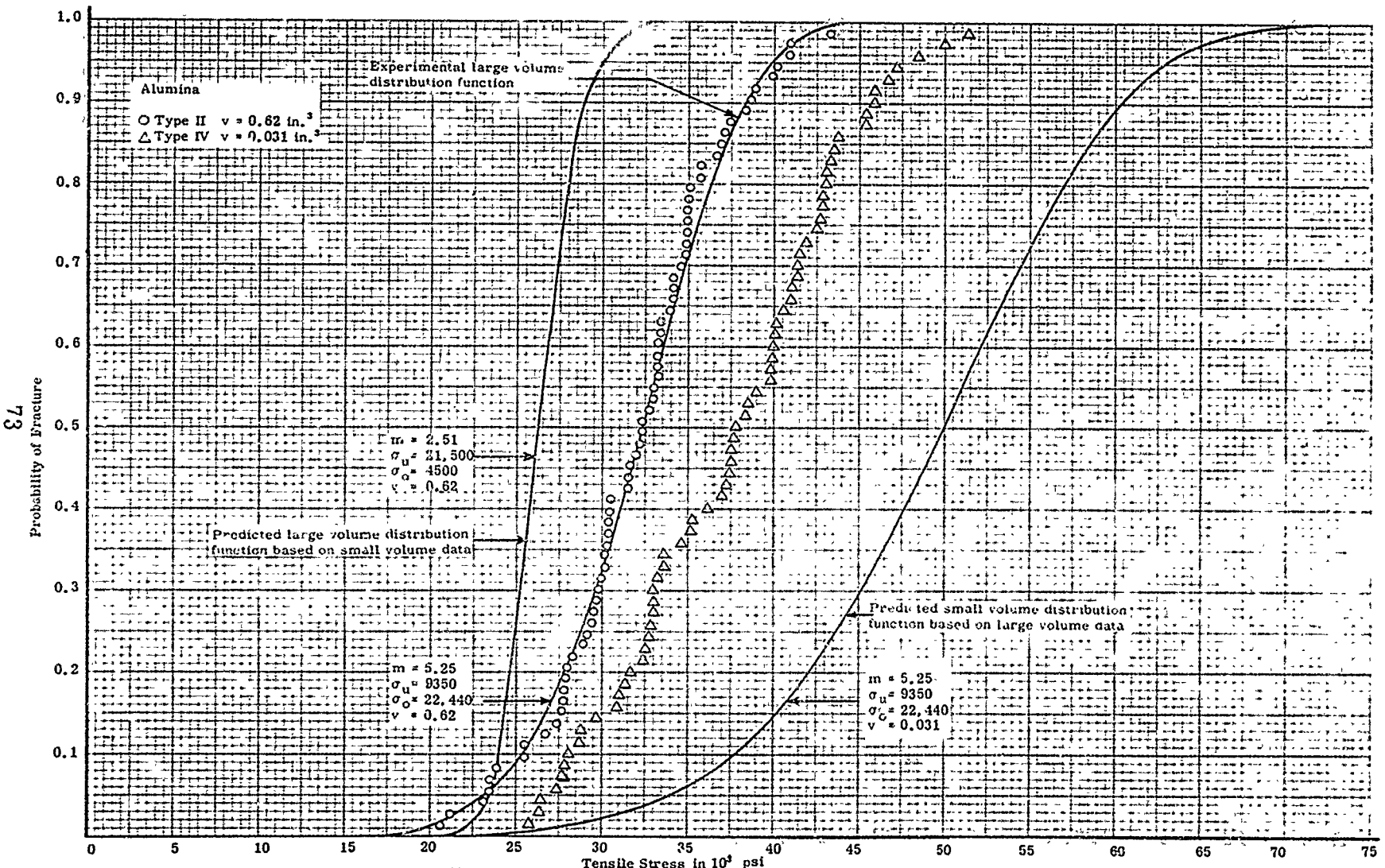

Figure 41. Tensile Stress versus the Probability of Fracture

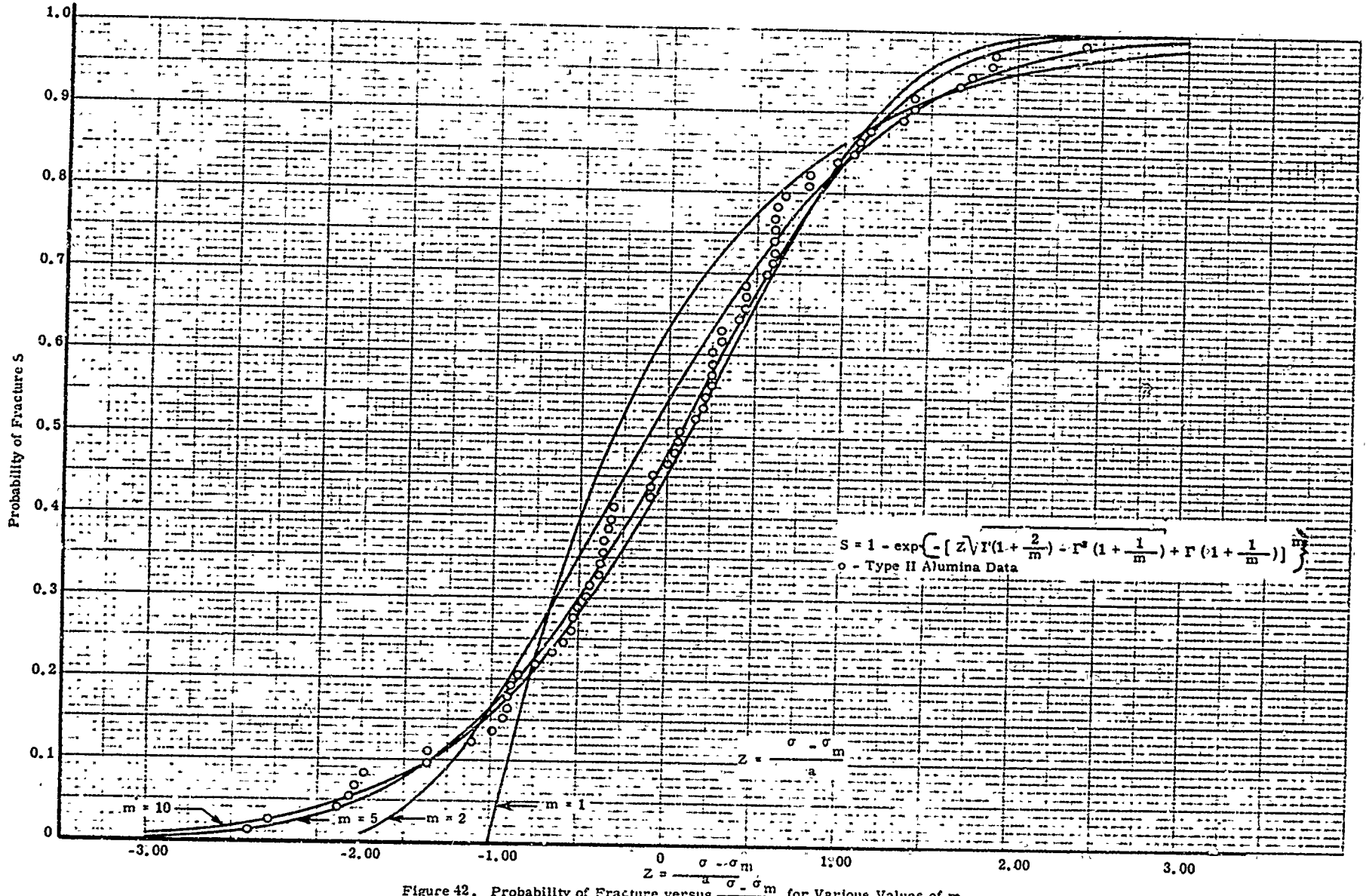

Figure 42. Probability of Fracture versus $\frac{\sigma - \sigma_m}{a}$ for Various Values of m

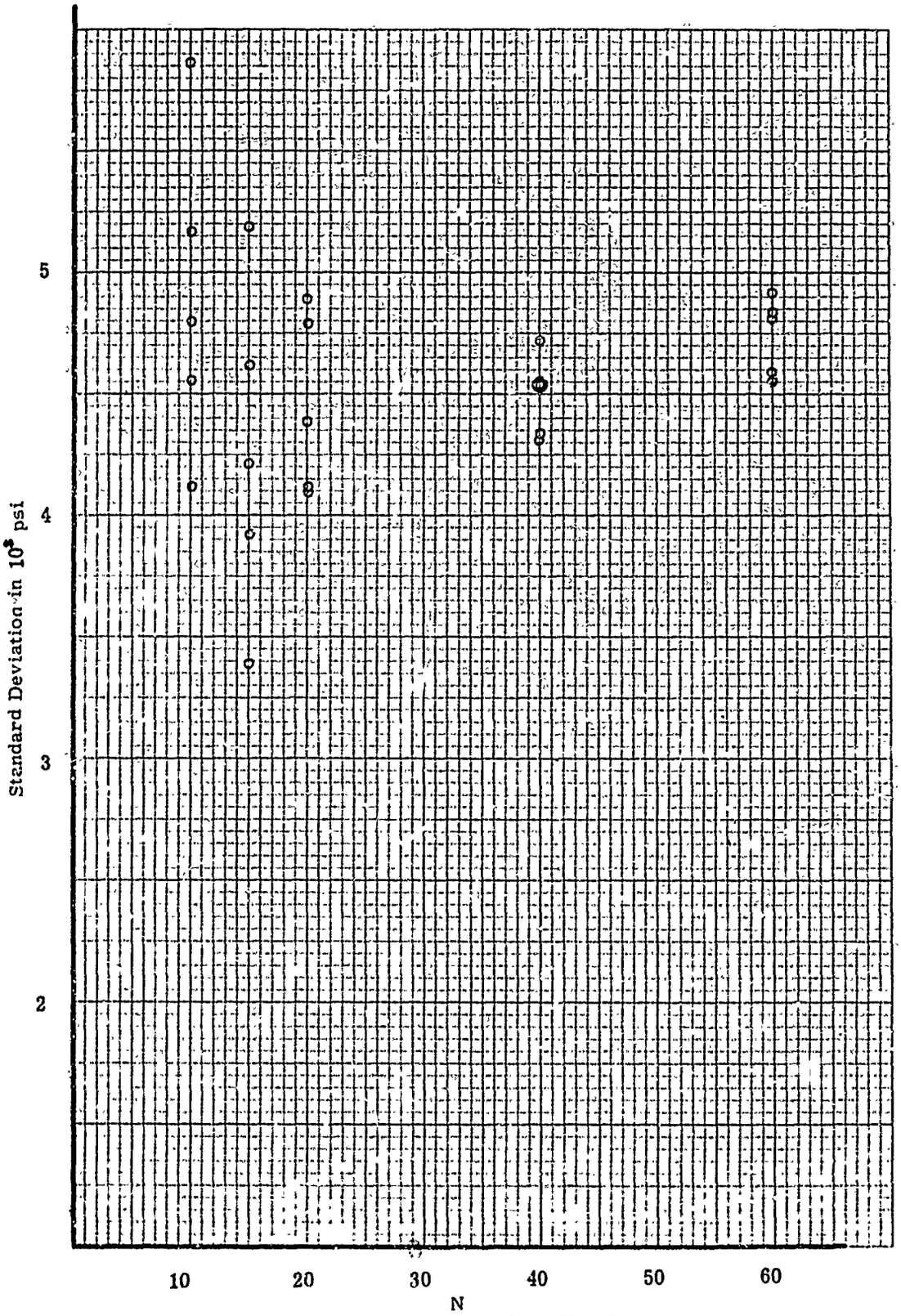

Figure 43. Standard Deviation versus Subset Size N

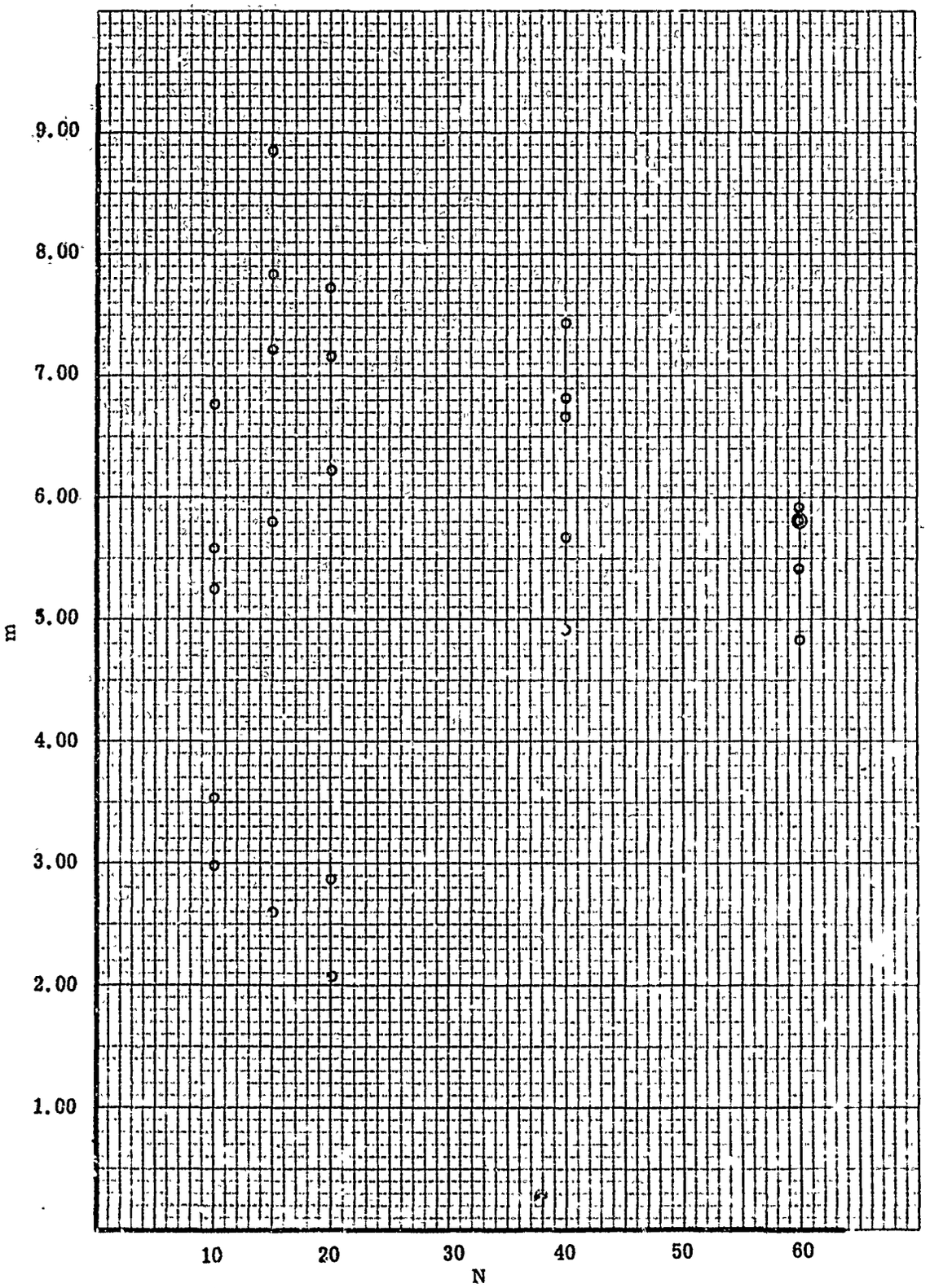

Figure 44. m versus Subset Size N

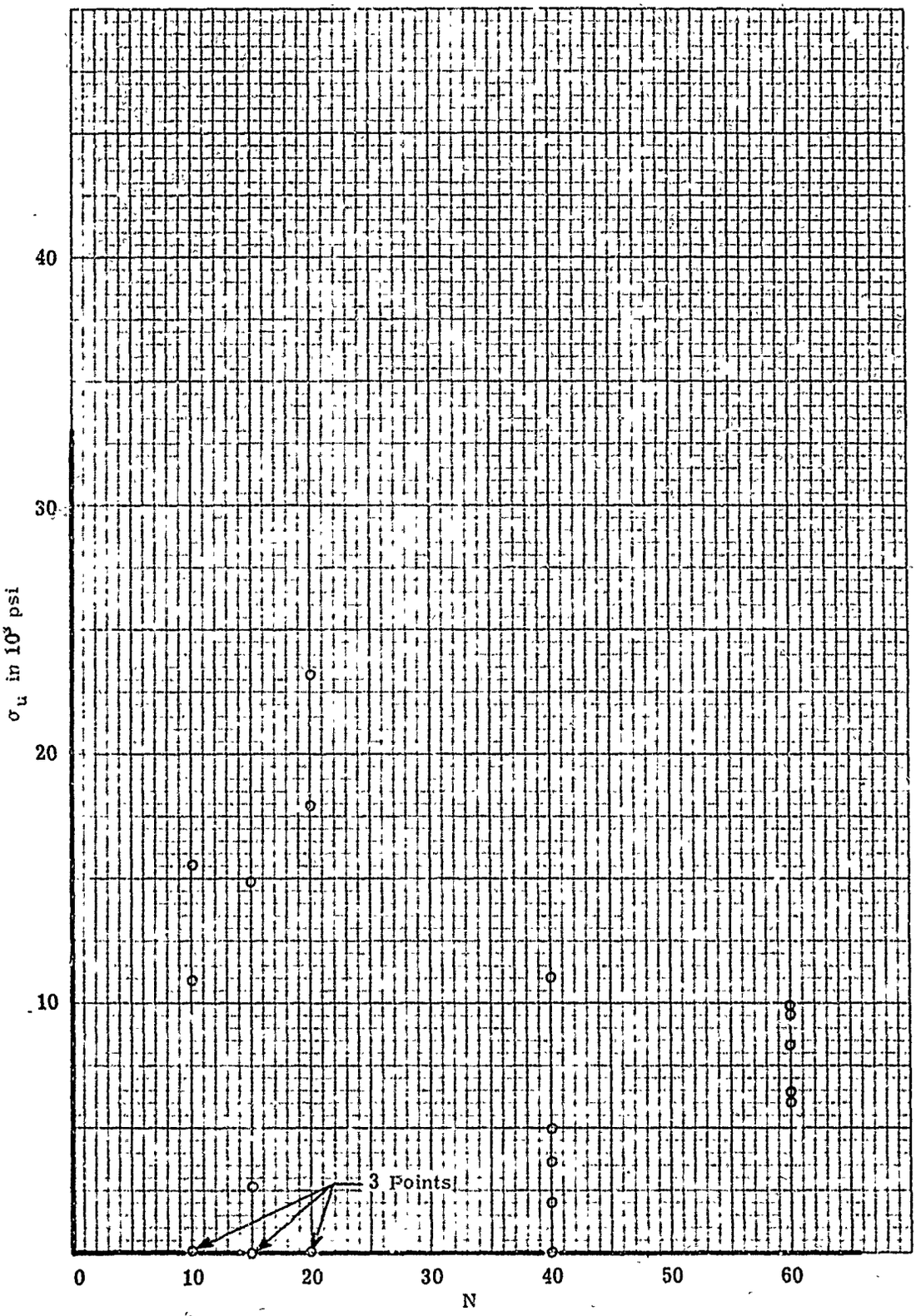

Figure 45. σ_u versus Subset Size N

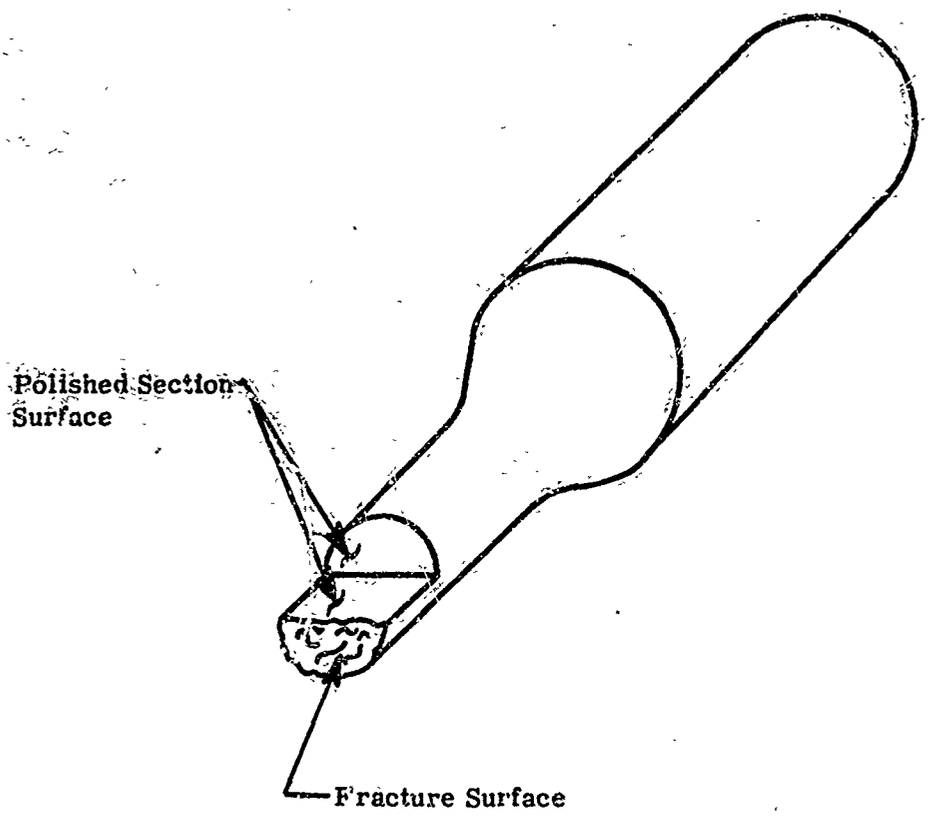

Figure 46. Schematic of Tensile Specimen Showing Areas Examined

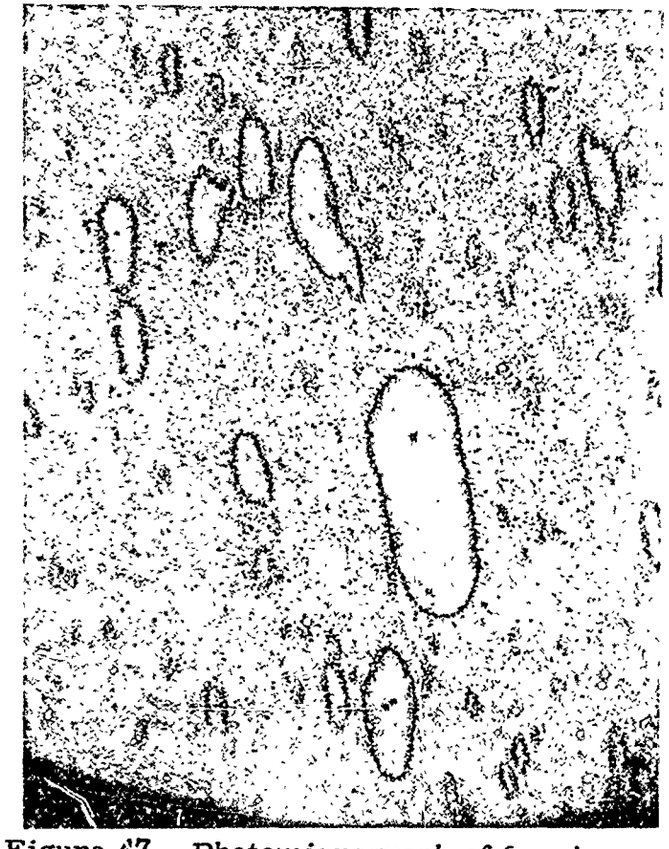

Figure 47. Photomicrograph of Specimen 858-A Showing Inhomogeneous Microstructure (70X)

Figure 48. Electron Micrograph of a Replicated Polished Surface of Specimen 858-AA Showing the Three Microstructural Variations

Figure 49. Electron Micrograph of a Replicated Fracture Surface of Specimen 858-AA Showing the Three Microstructural Variations

Figure 50. Electron Micrograph of a Replicated Polished Surface of Specimen 858-AA Showing the Small, Rounded, "Dimpled", Grains

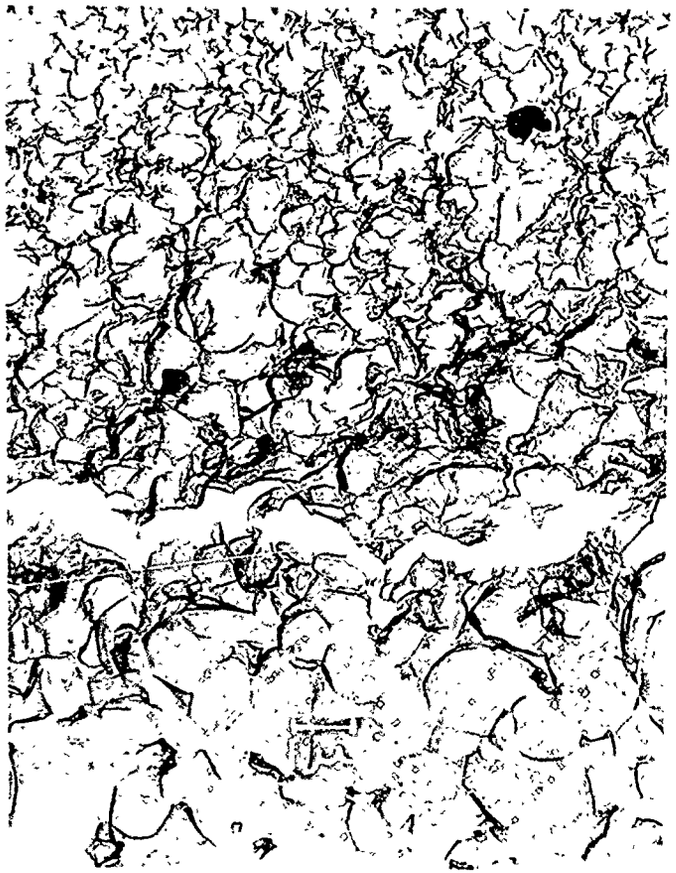

Figure 51. Electron Micrograph of a Replicated Fracture Surface of Specimen 858-A Showing the Microstructure Transition from Small, Rounded Grains to Large, Equiaxed Grains

Figure 52. Electron Micrograph of a Replicated Fracture Surface of Specimen 858-AA Showing the Microstructure Transition from Small, Rounded Grains to Large Equiaxed Grains

Figure 53. Electron Micrograph of a Replicated Fracture Surface of Specimen 858-L Showing the Microstructure Transition from Small, Rounded Grains to Equiaxed Grains

Figure 54. Electron Micrograph of a Replicated Fracture Surface of Specimen 858-L Showing the Large, Elongated Grains as Flat, Featureless Areas

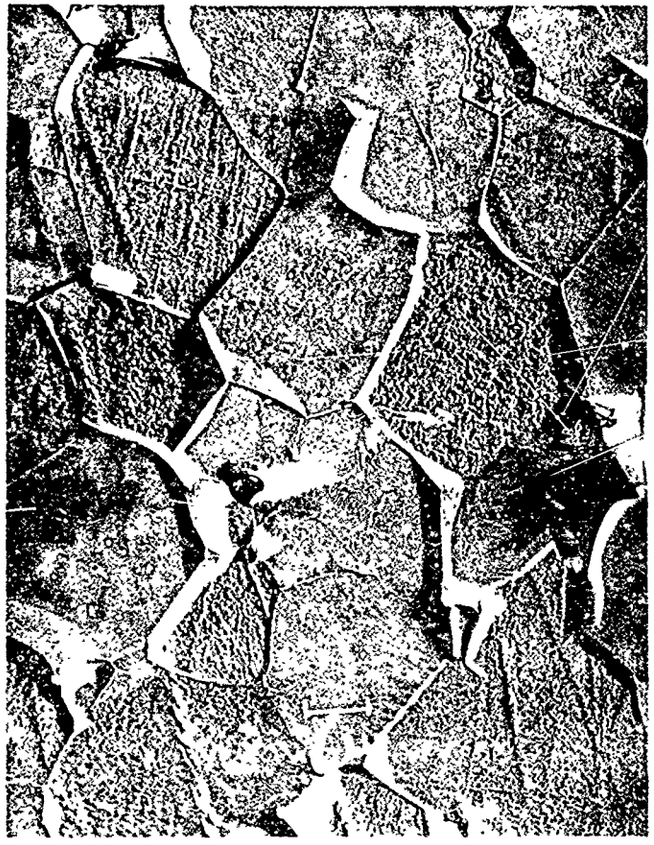

Figure 55. Electron Micrograph of a Replicated Polished Surface of Specimen 826-44A Showing the Equiaxed Grain Structure

Figure 56. Electron Micrograph of a Replicated Fracture Surface of Specimen 826-44A Showing Equiaxed Grain Structure and Intergranular Fracture

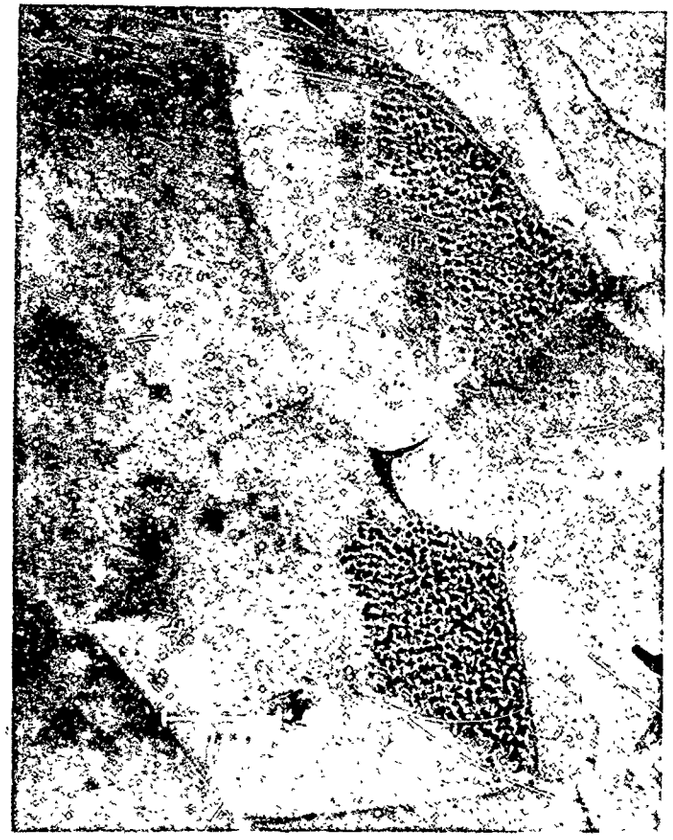

Figure 57. Electron Micrograph of a Replicated Fracture Surface of Specimen 826-44A Showing Intergranular Fracture Surfaces and Microporosity Coalescence

Figure 58. Electron Micrograph of a Replicated Polished Surface of Specimen 806-QA Showing Uniform Grain Structure

Figure 59. Electron Micrograph of a Replicated Fracture Surface of Specimen 806-QA Showing Uniform Grain Structure and Intergranular Fracture Characteristics

Figure 60. Electron Micrograph of a Replicated Fracture Surface of Specimen 806-QA Showing Transgranular and Cleavage Fracture Areas

Figure 61. Electron Micrograph of a Replicated Fracture Surface of Specimen 806-QA Showing Transgranular and Cleavage Fracture Areas

Figure 62. Electron Micrograph of a Replicated Fracture Surface of Specimen 830-13 Showing a Representative White Area

Figure 63. Electron Micrograph of a Replicated Fracture Surface of Specimen 830-13 Showing a Representative Gray Area

Table 1

Ultimate Tensile Strength Values for the Phase I
ATJ Graphite Specimens

Loading Direction	Stress Rate psi/sec	Specimen Number	Bulk Density gm/cc	Ultimate Tensile Strength psi
With Grain	500	1-A-i-I	1.75	4420
With Grain	500	1-E-o-I	1.76	>3900[1]
With Grain	500	1-G-i-I	1.75	3830
With Grain	500	2-B-i-I	1.76	4500
With Grain	500	2-J-o-I	1.77	>3120[2]
		Average	1.76	4250
With Grain	500	1-B-i-II	1.75	3670
With Grain	500	1-H-o-II	1.76	3950
With Grain	500	2-D-i-II	1.75	4170
With Grain	500	2-C-o-II	1.76	3670
With Grain	500	2-F-o-II	1.75	4110
		Average	1.75	3910
With Grain	500	1-A-o-III	1.76	4350
With Grain	500	1-E-i-III	1.75	3520
With Grain	500	1-H-i-III	1.75	3530
With Grain	500	2-B-o-III	1.76	>2470[2]
With Grain	500	2-J-i-III	1.75	4340
		Average	1.75	3940
With Grain	500	1-B-i-IV	1.76	4490
With Grain	500	1-G-o-IV	1.76	3540
With Grain	500	2-C-o-IV	1.74	>3100[1]
With Grain	500	2-F-i-IV	1.75	4300
With Grain	500	2-H-o-IV	1.76	3930
		Average	1.75	4070

Table 1 (continued)

Ultimate Tensile Strength Values for the Phase I
ATJ Graphite Specimens

Loading Direction	Stress Rate psi/sec	Specimen Number	Bulk Density gm/cc	Ultimate Tensile Strength psi
With Grain	500	1-C-o-V	1.76	4110
With Grain	500	1-E-i-V	1.75	3940
With Grain	500	1-H-i-V	1.75	4040
With Grain	500	2-B-i-V	1.75	3650
With Grain	500	2-J-o-V	1.76	3850
		Average	1.75	3920
With Grain	500	1-A-i-VI	1.76	4200
With Grain	500	1-H-o-VI	1.76	–[3]
With Grain	500	2-B-o-VI	1.75	4420
With Grain	500	2-H-i-VI	1.75	>3490[1]
With Grain	500	2-F-i-VI	1.73	3660
		Average	1.75	4090
With Grain	500	1-B-o-VII	1.77	–[4]
With Grain	500	1-C-i-VII	1.76	4470
With Grain	500	1-G-i-VII	1.75	4170
With Grain	500	2-D-i-VII	1.74	4080
With Grain	500	2-H-i-VII	1.74	3920
		Average	1.75	4160
With Grain	500	1-B-o-VIII	1.76	4220
With Grain	500	1-C-i-VIII	1.76	–[4]
With Grain	500	2-D-o-VIII	1.76	4110
With Grain	500	2-F-o-VIII	1.74	3710
With Grain	500	2-J-i-VIII	1.74	–[3]
		Average	1.75	4010

Table 1 (continued)

Ultimate Tensile Strength Values for the Phase I
ATJ Graphite Specimens

Loading Direction	Stress Rate psi/sec	Specimen Number	Bulk Density gm/cc	Ultimate Tensile Strength psi
With Grain	500	1-A-o-IX	1.78	4500
With Grain	500	1-E-o-IX	1.77	4300
With Grain	500	1-G-o-IX	1.77	3690
With Grain	500	2-C-i-IX	1.74	4150
With Grain	500	2-H-o-IX	1.74	3230
		Average	1.76	3970
With Grain	500	1-D-i-X	1.75	3340
With Grain	500	2-A-i-X	1.76	3880
With Grain	500	1-D-i-X	1.76	3420
With Grain	500	2-A-i-X	1.76	3490
		Average	1.76	3532
With Grain	500	1-D-o-XI	1.77	4530
With Grain	500	1-D-o-XI	1.78	4580
With Grain	500	2-A-o-XI	1.77	4490
With Grain	500	2-A-o-XI	1.77	4420
With Grain	500	2-A-o-XI	1.78	4730
		Average	1.77	4550

Notes:

1. Fractured outside of gage section at tool mark – value not used in average.
2. Used to calibrate stress rate. Broke after repeated loadings. Value not used in average.
3. Inadvertently broken in assembly.
4. Broken during machining operations.

Table 2

A Comparison of Parameters for the Phase I ATJ Graphite Specimens

Specimen Type	Average Density gm/cc	Surface Finish rms	Gage Diameter in.	Gage Length in.	Gage Surface Area in.^{2}	Gage Volume in.^{3}	Ratio of Gage Surface Area to Volume in.$^{-1}$	Average Ultimate Tensile Strength psi
I	1.76	80	0.250	0.500	0.393	0.0246	16	4250
II	1.75	400	0.250	1.000	0.785	0.0491	16	3910
III	1.75	80	0.187	0.894	0.525	0.0246	21	3940
IV	1.75	80	0.125	2.000	0.785	0.0246	32	4070
V	1.75	80	0.125	1.000	0.393	0.0123	32	3920
VI	1.75	80	0.125	1.000	0.393	0.0123	32	4090
VII	1.75	80	0.150	1.400	0.660	0.0248	27	4160
VIII	1.75	80	0.094	1.334	0.393	0.0093	42	4010
IX	1.76	35	0.250	1.000	0.785	0.0491	16	3970
X	1.76	10	0.375	2.300	2.709	0.2540	11	3532
XI	1.77	10	0.094	0.188	0.055	0.0013	43	4550

Table 3

Average Percent Theoretical Density and Average Grain Size for the Alumina Tiles

Tile Number	Average Grain Diameter (Microns)	% Theoretical Density
700	3.5	99.0
746	2.0	98.3
758	1.1 to 1.5	99.0 to 99.2
764	1.3 to 2.2	98.2
766	1.4 to 2.9	99.2 to 99.5
768	1.0 to 2.0	99.2
770	1.0 to 2.0	98.2
774	1.6	98.7
788	1.4 to 1.8	97.7
790	1.0 to 2.0	98.5
792	1.0 to 2.0	98.7
794	1.3	99.0
796	1.0 to 2.0	99.0
798	1.7 to 2.7	98.7
800	1.5 to 1.7	98.6
806	1.6	99.2
808	1.7 to 2.0	99.0
810	1.0 to 2.0	98.0
826	1.0 to 2.0	98.0
830	1.0 to 2.0	99.0
832	1.0 to 2.0	98.0
858	1.0 to 2.0	98.2
866	1.0 to 2.0	98.7
870	1.0 to 2.0	98.7

Table 4

Ultimate Tensile Strength Values for the Phase II Alumina Specimens*

Gage Volume in.^{3}	Specimen Number	Ultimate psi
1.33	770-4	35,550[1,7]
	764-12	–[3,7]
	766-8	25,550[7]
	766-18	35,450[1]
	768-6	25,500
	770-6	23,150
	770-14	–[3]
	770-12	33,100[2]
	774-27	35,550[1]
	774-26	34,200
	788-8	32,100[4,8]
	788-5	33,100[4]
	790-B	35,800
	790-H	37,900
	792-W	27,700[8]
	792-T	22,800[8]
	794-22	26,100[2]
	794-28	29,000[2]
	794-25	24,650[2]
	792-0	36,600
	794-24	27,700[2]
	794-31	29,900
	Average=	29,000
	Deviation=	4,920
0.62	830-9	28,300[1,7,6]
	832-38	26,700[8]
	830-7	38,320[7]
	700-8	38,300
	758-7	35,800
	700-1	36,950
	796-6	34,850
	858-N	20,000[4,6,8]

Gage Volume in.^{3}	Specimen Number	Ultimate psi
0.62	832-43	23,390[7]
	800-41	29,780
	798-G	33,890
	866-9	20,650[4,8]
	764-2	33,200[7]
	774-25	40,200
	764-14	32,300
	758-8	30,700[1,2]
	758-1	30,200
	794-26	27,800
	770-3	29,250[2]
	766-10	43,300[8]
	766-7	30,250
	796-2	32,950
	770-2	29,100[1,2]
	774-28	36,600
	770-4	27,800[2]
	806-T	38,300[1,4]
	826-53	34,900
	800-38	34,100
	806-Y	35,600[1,4,7]
	810-31	30,300
	832-40	25,500
	830-8	31,500[8]
	866-10	18,950[4,8]
	858-L	17,050[2,4]
	800-43	37,100[9]
	826-47	23,100
	800-39	32,000
	796-3	29,550
	832-42	25,500
	766-19	31,100[1]
	858-K	19,860[4]
	808-8	37,100[1]
	800-37	35,100[7]

*All specimens were tested at 70°F, with a stress rate of 5000 psi/sec. All specimens had a surface finish on the gage section of 5–10 rms.

Table 4 (continued)

Ultimate Tensile Strength Values for the Phase II Alumina Specimens

Gage Volume in.^{3}	Specimen Number	Ultimate psi
0.62	858-M	19,700[4,7]
	870-2	27,000[4]
	768-9	23,900
	758-5	32,200
	770-5	32,700
	792-X	29,100[2]
	766-21	27,050[7]
	764-1	29,400[9]
	774-22	34,100
	788-4	25,300[4]
	832-41	20,650[2,6]
	792-R	–[5,8]
	794-27	34,700[1,7]
	758-4	31,600
	758-2	37,400
	768-10	27,700
	794-30	38,700[8]
	788-2	37,800[4]
	792-P	34,600[8]
	810-30	34,100
	810-23	35,700
	808-4	40,800
	808-2	31,500[1]
	830-13	31,500
	764-13	34,600[1]
	806-X	34,000[1,4,7]
	810-29	38,800
	764-3	39,900[7]
	826-51	29,900
	796-7	25,900
	810-27	30,400
	810-24	30,500
	758-6	33,200[9]
	766-20	29,500[7]
	792-V	27,600

Gage Volume in.^{3}	Specimen Number	Ultimate psi
0.62	870-1	27,200[4]
	866-5	20,400[4]
	794-29	30,800[1,7]
	810-22	28,450[8]
	798-D	29,200
	830-12	32,300
	806-U	29,700[1,4,7]
	774-24	33,400[7]
	764-15	26,150[1,7]
	858-J	18,150[4,8]
	808-6	27,100[1,7]
	806-Z	35,800[1,4,7]
	798-E	33,400[7]
	808-9	39,600[1,7]
	806-W	32,500[4]
	832-39	23,500[2]
	808-10	40,900
	798-H	28,900
	798-B	27,300
	798-F	27,950
	800-42	30,200[7]
	810-28	33,200[7]
	790-F	34,850[7]
	808-5	33,200[7]
	768-11	21,200
	794-23	33,200[1,9]
	866-7	17,000[4,8]
	826-49	27,900[1,7]
	808-3	31,400[1]
	826-50	28,150[1,7]
	832-37	23,800[8]
	866-4	19,550[4]
	758-9	37,000[1]
	826-52	35,200[1,7]
	790-D	33,000

Table 4 (continued)

Ultimate Tensile Strength Values for the Phase II Alumina Specimens

Gage Volume in.^{3}	Specimen Number	Ultimate psi
0.62	836-8	17,000[4,8]
	808-11	30,400
	830-10	34,800
	810-26	27,700[2,8]
	808-7	36,600[1,7]
	806-V	26,600[2]
	830-11	29,100[1]
	826-48	29,700[1,9]
	Average=	32,000
	Deviation=	4,730
0.25	792-U	–[5,8]
	790-E	33,000
	700-3	40,500
	790-G	33,000[8]
	770-13	31,850[2]
	796-4	33,400[8]
	788-7	27,150[1,7]
	790-C	32,700[1]
	764-4	–[5,7]
	768-8	39,100
	774-23	46,500
	792-S	29,200[8]
	766-22	27,800[1,7]
	768-5	29,750
	796-10	34,850
	796-5	–[5]
	788-6	28,750[1,4,7]
	796-8	39,950[1]
	788-3	28,050[1,4]
	792-Q	30,350[2]
	Average=	35,000
	Deviation=	5,220
0.031	700-1	29,570[8]

Gage Volume in.^{3}	Specimen Number	Ultimate psi
0.031	700-2A	31,810
	700-2B	26,310[8]
	700-5B	29,680
	700-5A	17,300[2,6]
	746-8	–[4,5,6]
	746-2	23,740[4,8]
	746-6B	23,640[1,4,8]
	758-10	–[5]
	770-17A	40,900
	770-17	42,500
	770-16	35,000[2]
	866-3	26,100[4]
	866-1	16,600[2,4]
	866-3A	17,500[2,4]
	858-A	22,700[4]
	858-B	43,900[4]
	858-D	30,000[4]
	858-FA	24,900[4]
	858-F	30,300[4]
	858-H	25,800[4]
	858-I	25,300[4]
	858-HA	27,000[4]
	858-AA	21,600[4]
	788-1	34,300[4]
	788-11	38,000[4]
	788-12	38,000[4]
	788-12A	28,300[4]
	788-10	27,100[4]
	788-10	23,000[4]
	788-9	35,800[2,4]
	788-13	35,100[4]
	788-1	32,000[4]
	808-1B	33,600
	800-31	35,200
	800-33	37,600
	800-32	31,600
	800-34	42,600
	800-31	45,800
	800-33	39,800

Table 4 (continued)

Ultimate Tensile Strength Values for the Phase II Alumina Specimens

Gage Volume in.^{3}	Specimen Number	Ultimate psi
0.031	800-35	41,500
	832-32A	28,000
	832-33	42,800
	832-31	33,000
	832-36	26,300
	832-34A	26,400
	832-34	27,700
	832-31	43,300
	832-36A	28,700
	832-35	25,600[3]
	832-32	32,600[3]
	768-6A	29,300
	768-2	40,000
	768-3	38,500
	768-6	27,600
	764-11	33,000
	764-5	25,610[6]
	764-6	22,620[6]
	764-6A	21,680[6]
	758-11	26,320[6]
	758-3	29,950[6]
	810-21B	25,700
	810-25	37,000
	810-25A	45,800
	810-21	33,000
	794-21	40,100
	794-21	32,300
	792-N	37,200[2]
	798-M	30,800
	798-K1	39,800
	798-K	41,800
	798-L1	34,600
	798-M1	37,500
	798-L	41,300
	798-I	43,000
	826-41	37,800[2]

Gage Volume in.^{3}	Specimen Number	Ultimate psi
0.031	826-44	46,700
	826-44A	43,500
	826-41	31,300
	826-45	40,500
	826-42	47,200
	826-43	31,000
	830-2	45,300
	830-1	36,100
	830-6	50,000
	830-4A	43,700
	830-4	39,000
	830-3A	45,300
	830-5	51,300
	830-1A	33,200
	830-3	37,700
	774-29	37,400
	774-33	32,200
	774-32	48,400
	774-33	41,000
	774-30A	39,900
	774-32	35,300
	790-I	37,500
	790-K	32,000
	790-L	42,800
	790-A	28,600
	790-I	33,600
	790-M	43,000
	790-M	39,900
	790-J	41,300
	790-J	38,300
	806-N	54,000[4]
	806-S	52,400[4]
	806-Q	44,000[4]
	806-O	51,000[4]
	806-SA	48,200[4]
	806-QA	45,800[4]

Table 4 (continued)

Ultimate Tensile Strength Values for the Phase II Alumina Specimens

Gage Volume in.^{3}	Specimen Number	Ultimate psi
0.081	806-OA	53,000[4]
	806-R	46,000[4]
	806-P	47,500[4]
	788-13	36,800[4]
	Average=	37,500
	Deviation=	6,280
0.012	768-7	29,000
	768-4A	39,000
	764-11A	47,300
	764-11B	29,100
	758-12	43,500
	774-31	33,000
	774-21	35,200
	774-31A	40,200
	774-21	44,900
	790-L	53,300
	770-1A	50,200
	770-1	39,000
	766-17A	44,800
	766-17B	43,800
	766-11A	54,900
	Average=	41,800
	Deviation=	7,720

[1]Specimen fractured outside the gage section.
[2]Visible flaw in the fracture.
[3]Specimen slipped in grips because epoxy failed.
[4]Material from which the specimen was machined exhibited lower or higher strengths than did the majority of the materials.
[5]Run was no good because of mechanical difficulties.
[6]Run was made with a flat gas bearing which would not support the load properly.
[7]Flat area in the break located next to the specimen surface indicating the presence of a surface flaw.
[8]Flat area located in the interior of the fracture.
[9]Small surface in the fracture which was perpendicular to the primary fracture surface.

Table 5

Ultimate Tensile Strength and Approximate Flaw Size for Alumina Specimens Containing Visible Flaws

Specimen Type	Specimen Number	Flaw Size in.	Ultimate Tensile Strength psi
I	794-24	$\frac{3}{32}$	27,700
	794-22	$\frac{1}{16}$	26,100
	794-28	Spot[1]	29,000
	770-12	Spot	33,100
	794-25	Spot	24,650
		Average=	28,110
II	758-8	$\frac{1}{32}$	30,700
	806-V	$\frac{1}{32}$	26,600
	770-4	Speck[2]	27,800
	770-3	Speck	29,250
	770-2	Speck	29,100
	858-L	$\frac{3}{32}$	17,050
	792-X	$\frac{1}{32}$	29,100
	832-41	$\frac{1}{32}$	20,650
	832-39	$\frac{1}{64}$	23,500
	810-26	$\frac{1}{16}$	27,700
		Average=	26,100
III	770-13	Speck	31,850
	792-Q	$\frac{1}{32}$	30,350
		Average=	31,100
IV	700-5A		17,300
	770-16	Speck	35,000
	866-1	$\frac{1}{16}$	16,600
	866-3A		17,500
	788-9	Speck	35,800
	832-35	$\frac{1}{32}$	25,600
	832-32		32,600
	792-N	Speck	37,200
	826-41	Speck	37,800
		Average=	28,400

[1]Spot denotes a small circular flaw with a diameter less than $\frac{1}{64}$".

[2]Speck denotes a small inclusion in the material.

Table 6

Average Grain Size and Average Ultimate Strength for Type II Alumina Specimens

Average Grain Size Microns	Average Ultimate Tensile Strength psi	Number of Points in Average
3.5	38,300	1
1.1 - 1.5	37,200	8
1.3 - 2.2	32,600	6
1.4 - 2.9	33,200	5
1.0 - 2.0	27,400	57
1.6	34,300	11
1.4 - 1.8	31,600	2
1.3	33,000	5
1.7 - 2.7	30,100	6
1.5 - 1.7	33,000	6
1.7 - 2.0	34,900	8

Table 7

Fracture Strength Frequency Distribution for Type IV Alumina Specimens
Using Culled Data Only

25,000 to 27,500 psi	27,500 to 30,000 psi	30,000 to 32,500 psi	32,500 to 35,000 psi	35,000 to 37,500 psi	37,500 to 40,000 psi	40,000 to 42,500 psi	42,500 to 45,000 psi	45,000 to 47,500 psi	47,500 to 50,000 psi	50,000 to 52,500 psi
832-36	700-5B	700-2A	808-18	800-31	800-36	770-17A	770-17	800-31	830-6	830-5
832-34A	832-32A	800-32	832-31	810-25	800-33	800-35	800-34	810-25A	774-32	
810-21B	832-34	794-21	764-11	830-1	768-3	768-2	832-33	826-44		
	832-36A	798-M	810-21	774-29	798-K1	794-21	832-31	826-42		
	768-6A	826-41	798-L1	774-32	798-M1	798-K	798-I	830-3A		
	768-6	826-43	830-1A		830-4	798-L	826-44A	830-2		
	790-A	774-33	790-I		830-3	826-46	830-4A			
		790-K			774-30A	774-33	790-L			
					790-I	790-J	790-M			
					790-M					
					790-J					
3	7	3	7	5	11	9	9	6	2	1

Table 8

Average Fracture Stress, Standard Deviation, Coefficient of Variation, and Weibull Material Constants for Subsets of Size N

N	σ_m	a	$\frac{a}{\sigma_m}$	m	σ_u	σ_o
60	32,130	4830	.150	5.91	6000	26,100
	31,950	4810	.151	5.80	6400	25,500
	31,870	4920	.154	4.83	9900	21,800
	32,110	4550	.142	5.41	9500	22,500
	32,620	4580	.141	5.81	8300	24,300
40	31,220	4710	.151	6.66	2000	29,200
	32,300	4540	.141	6.82	3600	28,700
	32,090	4330	.135	4.91	12,000	20,000
	32,000	4540	.142	7.43	0	31,900
	31,700	4310	.136	6.68	4900	26,800
20	32,170	4790	.149	2.86	17,900	13,700
	31,640	4380	.138	7.16	0	31,500
	31,920	4100	.128	7.72	0	31,800
	30,690	4880	.159	6.22	0	30,500
	32,260	4120	.128	2.07	23,200	8,400
15	32,690	3390	.104	8.85	0	32,600
	29,900	5180	.173	2.60	14,800	14,400
	32,240	3920	.121	7.83	0	32,100
	30,360	4620	.152	5.80	2600	27,600
	31,180	4210	.135	7.21	0	31,000
10	32,390	4120	.127	6.76	0	32,200
	31,270	4800	.153	5.58	0	31,000
	33,610	4560	.136	3.53	15,500	17,700
	32,010	5320	.166	5.25	0	31,700
	30,950	5870	.190	2.98	10,800	19,500

Table 9

Physical Properties of Alumina Tensile Specimens
Selected for Fractography

Specimen Number	Average* Grain Size microns	% Theoretical* Density	Gage Volume in.^{3}	Color	Ultimate Tensile Strength psi
858-AA	1.0-2.0	98.2	0.031	Grayish White	21,600
858-A	1.0-2.0	98.2	0.031	White	22,700
858-L	1.0-2.0	98.2	0.620	White	17,000
826-44A	1.0-2.0	97.9	0.031	White	43,500
806-QA	1.6	99.2	0.031	Two-Tone Gray	53,000
830-13	1.0-2.0	99.2	0.620	Gray-White	31,500

*Avco data - Average for entire tile.

UNCLASSIFIED

Security Classification

DOCUMENT CONTROL DATA - R&D

(Security classification of title, body of abstract and indexing annotation must be entered when the overall report is classified)

1. ORIGINATING ACTIVITY (Corporate author) Southern Research Institute 2000 Ninth Avenue South Birmingham, Alabama 35205	2a. REPORT SECURITY CLASSIFICATION UNCLASSIFIED 2b. GROUP

3. REPORT TITLE

AN EXPERIMENTAL STUDY OF THE WEIBULL VOLUME THEORY

4. DESCRIPTIVE NOTES (Type of report and inclusive dates)

Summary Report 28 May 1964 to 31 December 1965

5. AUTHOR(S) (Last name, first name, initial)

Pears, C. D. and Starrett, H. Stuart

6. REPORT DATE March 1967	7a. TOTAL NO. OF PAGES 102	7b. NO. OF REFS 17
8a. CONTRACT OR GRANT NO. AF 33(615)-1690 b. PROJECT NO. 7350 c. TASK NO. 735003 d.	9a. ORIGINATOR'S REPORT NUMBER(S) AFML-TR-66-228 9b. OTHER REPORT NO(S) (Any other numbers that may be assigned this report)	

10. AVAILABILITY/LIMITATION NOTICES This document is subject to special export controls and each transmittal to foreign governments or foreign nationals may be made only with prior approval of the Metals and Ceramics Division (MAM), Air Force Materials Laboratory, Wright-Patterson AFB, Ohio 45433.

11. SUPPLEMENTARY NOTES	12. SPONSORING MILITARY ACTIVITY Metals and Ceramics Division (MAMD) Air Force Materials Laboratory Wright-Patterson AFB, Ohio 45433

13. ABSTRACT

Using a gas-bearing tensile test facility, an experimental program was conducted to provide clarification of Weibull's volume effect theory. The facility provides uniaxial loading with a uniform tensile field thus permitting a study of the Weibull theory in its simplest form. The primary material used for this investigation was hot pressed alumina made by AVCO. Graphite was used to explore effects as a guide to the general program. As a result, quite useful data are available on the graphite as well as alumina.

The program verified the general conclusions of the theory of decreasing strength and standard deviation with increasing volume, but a single set of material constants to describe the total results was not obtained. Criteria are presented that will assist in both material understanding and design with brittle materials with more confidence.

Evidence indicates that sample sizes should include at least 60 coupons for an optimum analysis of material constants and as few as 10 coupons for some values such as average strength.

Strength correlated with density and there was evidence that the fracture location, whether transgranular or in the grain boundaries, is dependent on grain size and/or the structure.

Unfortunately, the strengths between different discs of the material from which the specimens were machined varied more than desired and even more than some of the variables being measured.

DD FORM 1 JAN 64 1473

UNCLASSIFIED

Security Classification

UNCLASSIFIED

Security Classification

14. KEY WORDS	LINK A ROLE	LINK A WT	LINK B ROLE	LINK B WT	LINK C ROLE	LINK C WT

INSTRUCTIONS

1. ORIGINATING ACTIVITY: Enter the name and address of the contractor, subcontractor, grantee, Department of Defense activity or other organization *(corporate author)* issuing the report.

2a. REPORT SECURITY CLASSIFICATION: Enter the overall security classification of the report. Indicate whether "Restricted Data" is included. Marking is to be in accordance with appropriate security regulations.

2b. GROUP: Automatic downgrading is specified in DoD Directive 5200.10 and Armed Forces Industrial Manual. Enter the group number. Also, when applicable, show that optional markings have been used for Group 3 and Group 4 as authorized.

3. REPORT TITLE: Enter the complete report title in all capital letters. Titles in all cases should be unclassified. If a meaningful title cannot be selected without classification, show title classification in all capitals in parenthesis immediately following the title.

4. DESCRIPTIVE NOTES: If appropriate, enter the type of report, e.g., interim, progress, summary, annual, or final. Give the inclusive dates when a specific reporting period is covered.

5. AUTHOR(S): Enter the name(s) of author(s) as shown on or in the report. Enter last name, first name, middle initial. If military, show rank and branch of service. The name of the principal author is an absolute minimum requirement.

6. REPORT DATE: Enter the date of the report as day, month, year; or month, year. If more than one date appears on the report, use date of publication.

7a. TOTAL NUMBER OF PAGES: The total page count should follow normal pagination procedures, i.e., enter the number of pages containing information.

7b. NUMBER OF REFERENCES: Enter the total number of references cited in the report.

8a. CONTRACT OR GRANT NUMBER: If appropriate, enter the applicable number of the contract or grant under which the report was written.

8b, 8c, & 8d. PROJECT NUMBER: Enter the appropriate military department identification, such as project number, subproject number, system numbers, task number, etc.

9a. ORIGINATOR'S REPORT NUMBER(S): Enter the official report number by which the document will be identified and controlled by the originating activity. This number must be unique to this report.

9b. OTHER REPORT NUMBER(S): If the report has been assigned any other report numbers *(either by the originator or by the sponsor)*, also enter this number(s).

10. AVAILABILITY/LIMITATION NOTICES: Enter any limitations on further dissemination of the report, other than those imposed by security classification, using standard statements such as:

(1) "Qualified requesters may obtain copies of this report from DDC."

(2) "Foreign announcement and dissemination of this report by DDC is not authorized."

(3) "U. S. Government agencies may obtain copies of this report directly from DDC. Other qualified DDC users shall request through _____."

(4) "U. S. military agencies may obtain copies of this report directly from DDC. Other qualified users shall request through _____."

(5) "All distribution of this report is controlled. Qualified DDC users shall request through _____."

If the report has been furnished to the Office of Technical Services, Department of Commerce, for sale to the public, indicate this fact and enter the price, if known.

11. SUPPLEMENTARY NOTES: Use for additional explanatory notes.

12. SPONSORING MILITARY ACTIVITY: Enter the name of the departmental project office or laboratory sponsoring *(paying for)* the research and development. Include address.

13. ABSTRACT: Enter an abstract giving a brief and factual summary of the document indicative of the report, even though it may also appear elsewhere in the body of the technical report. If additional space is required, a continuation sheet shall be attached.

It is highly desirable that the abstract of classified reports be unclassified. Each paragraph of the abstract shall end with an indication of the military security classification of the information in the paragraph, represented as *(TS)*, *(S)*, *(C)*, or *(U)*.

There is no limitation on the length of the abstract. However, the suggested length is from 150 to 225 words.

14. KEY WORDS: Key words are technically meaningful terms or short phrases that characterize a report and may be used as index entries for cataloging the report. Key words must be selected so that no security classification is required. Identifiers, such as equipment model designation, trade name, military project code name, geographic location, may be used as key words but will be followed by an indication of technical context. The assignment of links, rules, and weights is optional.

UNCLASSIFIED

Security Classification